

SURFACE MODIFICATION OF TITANIUM DIOXIDE  
AND SYNTHESIS OF NON-ELECTROACTIVE  
COATINGS BY ELECTROCHEMICAL POLYMERIZATION

by

Rathnapala S. Vithanage

Dissertation Submitted to the Faculty of  
Virginia Polytechnic Institute and State University  
in Partial Fulfillment of the  
Requirement for the degree of

DOCTOR OF PHILOSOPHY

in

Chemistry

Approved:

---

H. O. Finklea

---

H. M. Bell

---

R. E. Dessy

---

J. G. Mason

---

L. T. Taylor

Blacksburg, Virginia

May 1985

MSM  
2/4/86

SURFACE MODIFICATION OF  $TiO_2$  AND SYNTHESIS OF NON-ELECTROACTIVE  
COATINGS BY ELECTROCHEMICAL POLYMERIZATION

(ABSTRACT)

by

Rathnapala S. Vithanage

The objective of this project was the modification of  $TiO_2$  electrodes with various silanes in order to evaluate the stability of modified layers when they are used on photoelectrodes in SEMICONDUCTOR LIQUID-JUNCTION SOLAR CELLS (SLJSC). To determine the nature of the reactivity of surface hydroxyl groups towards different silanes, a surface IR study was carried out on  $TiO_2$  powders. The powder ( $TiO_2$ ) was pressed into a pellet and subjected to reactions with various silanes under different reaction conditions. All of these reactions were carried out in a vacuum line under very anhydrous conditions in order to prevent polymerization of the silanes. This study provided an understanding of the reactivity of different silanes towards surface hydroxyl groups of  $TiO_2$  and the best reaction conditions for this purpose.

With this information in hand we studied the  $TiO_2$  (rutile) single crystal electrodes. These electrodes were subjected to reaction with silanes under the same conditions as the powders. Then the modified surface was studied using ESCA. These electrodes were subsequently subjected to photoelectrochemical conditions (photocurrent generation) and were reexamined using ESCA in order to evaluate the stability of

the modified layer. A reaction scheme which was devised to induce crosslinking in the modified layer was shown to enhance the stability of the surface bound silane during the photocurrent generation.

In order to form more homogeneous modified surfaces electrochemically derived polymer coatings were synthesized from divinylbenzene, 4-vinylpyridine, N-methyl-4-vinylpyridinium salts, and phenol. Except for polymers formed from N-methyl-4-vinyl pyridinium salts, other coatings were shown to be neutral. An anomalous pre-wave, and potential-induced polymer swelling and shrinking phenomena were observed in these coatings.

The photocorrosion of small bandgap n-type semiconductor electrodes is a serious impediment to the development of efficient and durable conversion (photoelectrochemical) devices. Our objective in this investigation was to develop newer modified surfaces that are useful for the inhibition of this photocorrosion, and enhance the performance of n-type small bandgap semiconductors in the photoelectrochemical systems.

This dissertation is  
dedicated to my late Father  
and beloved Family.

## ACKNOWLEDGEMENTS

I would like to express my gratitude to the following persons for their support:

To Dr. Harry O. Finklea for his encouragement and guidance, which greatly helped me complete this work in a relatively short period of time.

To my colleagues and friends,  
, , and for their cooperation.

To the department of chemistry at VPI and Diamond Shamrock Corporation for their financial support during the period of study.

To for typing the original draft, and Mrs. Harris for the typing of the final draft.

Finally, to the members of my family for their love, patience, understanding and moral support during these long and trying years.

## TABLE OF CONTENTS

	Page
ABSTRACT.....	ii-iii
DEDICATION. ....	iv
ACKNOWLEDGEMENT.....	v
TABLE OF CONTENTS.....	vi-viii
LIST OF TABLES.....	ix
LIST OF FIGURES.....	x-xii
Chapter 1. INTRODUCTION .....	1-3
Chapter 2. INFRARED SPECTROSCOPY OF SILANE MODIFIED TiO <sub>2</sub> .....	4-83
2.I Introduction .....	4
2.II.A Literature Review .....	6
2.II.B Reactions of silane with silica .....	10
2.III.A Experimental .....	14
2.III.B Synthesis .....	16
2.IV Data and Interpretation .....	17
2.IV.A Reactions of TiO <sub>2</sub> with silanes .....	21
2.IV.B Reactions with trimethylchlorosilane .....	22
2.IV.C Reactions of DMCS and TCMS with TiO <sub>2</sub> .....	27
2.IV.D Steric reasons against trifunctional reactions with TCMS .....	36
2.IV.E Reactions of SiCl <sub>4</sub> .....	37
2.IV.F Reactions of methoxysilanes with TiO <sub>2</sub> .....	38
2.IV.G Reactions of HMDS with TiO <sub>2</sub> .....	58
2.IV.H Reactions of HCl with TiO <sub>2</sub> .....	66
2.IV.I Reactions of methanol with TiO <sub>2</sub> .....	67
2.IV.J Reactions of NH <sub>3</sub> with TiO <sub>2</sub> .....	70
2.IV.K Summary of percentage OH loss .....	76
2.IV.L Surface coverage .....	79
2.V Conclusion .....	81
Chapter 3. PHOTOELECTROCHEMICAL SYSTEMS .....	84-139
3.I Introduction .....	84
3.II Semiconductors .....	86
3.III Doping .....	88
3.IV Band bending in semiconductors .....	88
3.V Energy scales .....	91
3.VI Semiconductor/electrolyte interface .....	93
3.VI.A Equilibrium in the dark .....	94
3.VI.B Illumination .....	96
3.VII Blocking behavior of semiconductors .....	99

TABLE OF CONTENTS (Continued)

	Page
3.VIII Efficient PEC systems .....	99
3.VIII.A Bandgap .....	99
3.VIII.B Bandgap location .....	99
3.VIII.C Stability .....	100
3.VIII.D Doping level .....	100
3.VIII.E Redox couple .....	101
3.IX Problems associated with the PEC devices .....	101
3.X Survey of chemically modified semiconductor electrodes ...	103
3.XI Experimental .....	111
3.XI.A Electrode preparation .....	111
3.XI.B Silanization .....	111
3.XI.C Electrochemistry .....	112
3.XI.D X-ray photoelectron spectroscopy .....	112
3.XII Results and Discussion .....	114
3.XII.A XPS of modified TiO <sub>2</sub> .....	114
3.XII.B Photocurrent generation process .....	118
3.XII.C Criteria for silane layer stability .....	119
3.XII.D Direct silanization .....	122
3.XII.E Crosslinking scheme .....	128
3.XII.F Stability of crosslinked modified layers .....	130
3.XII.G Silane decomposition mechanisms .....	132
3.XIII Conclusion .....	139
 Chapter 4. ELECTROCHEMICAL POLYMERIZATION .....	 140-194
4.I Introduction .....	140
4.II Review of previous work .....	145
4.II.A Characteristics of surface bound redox species ...	154
4.III Experimental .....	156
4.III.A Synthesis .....	156
4.III.B Electrochemistry .....	156
4.IV Results and discussion .....	158
4.IV.A Vinyl polymerization .....	158
4.IV.B Polymerization of phenol .....	161
4.IV.C Stability of electrochemically formed radicals ...	164
4.IV.D Polymerization of DVB .....	165
4.IV.E Coated electrodes in ferrocene electrolytes .....	172
4.IV.F 4-vinylpyridine .....	181
4.IV.G Phenol .....	184
4.IV.H N-methyl-4-vinylpyridinium salts .....	184
4.IV.I Diffusion of solutes at rotating disk electrode ..	188
4.V Conclusion .....	194
 Chapter 5. CONCLUSION .....	 195-196
REFERENCES .....	197-203
APPENDIX .....	204-205

TABLE OF CONTENTS (continued)

page

VITA .....206



## LIST OF TABLES

Table		Page
I	Infrared band assignments of surface OH groups of TiO <sub>2</sub> .....	8
II	IR data of TiO <sub>2</sub> and D <sub>2</sub> O exchange .....	18
III	Reaction of TiO <sub>2</sub> with trimethylchlorosilane .....	24
IV - V	Reaction of TiO <sub>2</sub> with trimethylchlorosilane .....	28-29
VI - VII	Reaction of TiO <sub>2</sub> with dimethyldichlorosilane .....	30-32
IX - XI	Reaction of TiO <sub>2</sub> with trichloromethylsilane .....	33-35
XII - XIV	Reaction of TiO <sub>2</sub> with tetrachlorosilane .....	39-41
XV - XVII	Reaction of TiO <sub>2</sub> with trimethylmethoxysilane .....	46-48
XVIII - XX	Reaction of TiO <sub>2</sub> with dimethyldichlorosilane .....	49-51
XXI - XXIII	Reaction of TiO <sub>2</sub> with methyltrimethoxysilane .....	52-54
XXIV - XXVI	Reaction of TiO <sub>2</sub> with tetramethoxysilane .....	55-57
XXVII - XXIX	Reaction of TiO <sub>2</sub> with hexamethyldisilazane .....	60-65
XXX - XXXI	Reaction of TiO <sub>2</sub> with hydrogen chloride .....	67-68
XXXII - XXXIV	Reaction of TiO <sub>2</sub> with methanol .....	70-72
XXXV - XXXVI	Reaction of TiO <sub>2</sub> with ammonia .....	74-75
XXXVIIa,b	Percentage OH peak attenuation after chemical modification .....	76-77
XXXVIII	Surface coverage data .....	81
XXXIX	XPS data of a control electrode .....	121
XXXX	Redox potentials of aromatic monomers .....	160

LIST OF FIGURES

	Page
Figure (1): Rutile crystal structure .....	10
Figure (2): IR Spectra of clean TiO <sub>2</sub> and D <sub>2</sub> O exchanged TiO <sub>2</sub> .....	19
Figure (3): IR spectra of TiO <sub>2</sub> reacted with dimethyl- dichlorosilane .....	22
Figure (4): IR spectra of TiO <sub>2</sub> reacted with silicon tetrachloride	38
Figure (5): Contrast of chlorosilane modification vs. methoxysilane modification .....	43
Figure (6): Contrast of tetramethoxysilane-reacted TiO <sub>2</sub> at different reaction stages .....	44
Figure (7): IR spectra of TiO <sub>2</sub> modified with HMDS .....	59
Figure (8): Energy level diagram for an intrinsic semiconductor .	87
Figure (9): Doped semiconductors .....	89
Figure (10): Band bending situation of a semiconductor .....	90
Figure (11): Positions of conduction and valence band edges of semiconductors at pH = 1 .....	92
Figure (12): Regenerative SLJSC using a n-type semiconductor .....	95
Figure (13): Energy situation in a SLJSC .....	97
Figure (14): Photoelectrochemical experimental setup .....	113
Figure (15): XPS- traces of TiO <sub>2</sub> before and after derivatization [O(1s) and Ti(2p) peaks] .....	116
Figure (16): XPS- traces of TiO <sub>2</sub> before and after derivatization [C(1s) and Si(2p) peaks] .....	117
Figure (17): Cyclic voltammetric curve of TiO <sub>2</sub> photoanode in 0.5M H <sub>2</sub> SO <sub>4</sub> .....	120
Figure (18): Bar graphs of SiCl <sub>4</sub> -derivatized TiO <sub>2</sub> electrodes before and after photocurrent generation .....	123
Figure (19): Bar graphs of Me <sub>2</sub> SiCl <sub>2</sub> -derivatized TiO <sub>2</sub> electrodes ..	124
Figure (20): Bar graphs of MeSiCl <sub>3</sub> -derivatized TiO <sub>2</sub> electrodes ...	125

LIST OF FIGURES (Continued)

	Page
Figure (21): Crosslinking scheme for TiO <sub>2</sub> modification .....	129
Figure (22): Bar graphs of SiCl <sub>4</sub> /Me <sub>2</sub> SiCl <sub>2</sub> -derivatized [crosslinked] TiO <sub>2</sub> electrodes .....	131
Figure (23): Bar graphs of MeSi(OMe) <sub>3</sub> -derivatized [crosslinked] TiO <sub>2</sub> electrodes .....	133
Figure (24): Bar graphs of Si(OMe) <sub>4</sub> -derivatized [double crosslinked] TiO <sub>2</sub> electrodes .....	134
Figure (25): Bar graphs of MeSiCl <sub>3</sub> -derivatized [double crosslinked] TiO <sub>2</sub> electrodes .....	135
Figure (26): Bar graphs of MeSi(OMe) <sub>3</sub> -derivatized [double crosslinked] TiO <sub>2</sub> electrodes .....	136
Figure (27): Electrochemical deposition of DVB (10 mM) in the presence of ferrocene .....	166
Figure (28): Electrochemical deposition of DVB (10 mM) .....	168
Figure (29): Electrochemical deposition of DVB (80 mM) .....	169
Figure (30): Cyclic voltammetry of poly-DVB coated electrode (10 mM) in ferrocene and nitrobenzene .....	170
Figure (31): Cyclic voltammetry of a poly-DVB coated electrode (100 mM) in ferrocene .....	173
Figure (32): Contrast of cyclic voltammetric behavior of a poly- DVB coated electrode (100 mM) in 10 mM Fe <sup>2+</sup> /0.5M sulfuric acid .....	178
Figure (33): Cyclic voltammetry of Br <sup>-</sup> trapped in a poly-DVB coated electrode .....	180
Figure (34): Electrochemical deposition in 100 mM 4-vinylpyridine.	182
Figure (35): Cyclic voltammetry of a poly 4-vinylpyridine coated electrode in 1 mM hydroquinone .....	183
Figure (36): Electrochemical deposition of phenol .....	185
Figure (37): Cyclic voltammetry of a poly-phenol coated electrode in 2 mM ferrocene .....	186

LIST OF FIGURES (Continued)

	Page
Figure (38): Electrochemical deposition of N-methyl-4-vinylpyridinium $\text{BF}_4^-$ .....	187
Figure (39): Cyclic voltametry of electrostatically bound $\text{Fe}(\text{CN})_6^{4-}$ on poly-N-methyl-4-vinylpyridinium-coated electrode .....	189
Figure (40): Scan rate study of electrostatically-bound $\text{Fe}(\text{CN})_6^{4-}$ on poly-N-methyl-4-vinylpyridinium coated electrode .	190
Figure (41): Rotating disk voltammetric plots of clean Pt and DVB-coated electrodes in the presence of 1 mM ferrocene .	193

Chapter 1  
INTRODUCTION

Chemical modification of electrodes is a relatively new research area in electrochemistry. The interest in attachment of molecules onto electrode surfaces is due to several reasons; most importantly attachment of molecules of known properties can bring about interesting changes in the properties of the electrode, in a more predictable, and externally controllable manner. There are several different approaches which have been successfully employed in the modification of electrode surfaces:

(a) chemisorption: Some species tend to strongly adsorb onto the electrode surface; e.g., organic molecules containing double bonds which are hydrophobic, on surfaces such as C, Pt, from aqueous solutions (1).

(b) The reaction of oxidized metal oxides with silane reagents, (2a). This process yields a monolayer of silane on the electrode surface. The chemical functionalities present in the modified layer may be subject to further modifications, which in turn induces additional changes of electrode properties.

(c) Coating of electrode with polymer layers (2b), by either (i) simple dip coating, which results a multilayer of polymer on the electrode surface, or (ii) formation of polymers in-situ, i.e. polymerization can be induced by electrochemical or other (rf plasma) means.

These electrodes may be characterized by several different methods.

As the amount of substance on the modified electrode is very small, rather sensitive techniques are required to detect its presence as well as to evaluate its chemical and physical properties. Electrochemical methods are very simple and present adequate sensitivity in order to detect redox active species on the surface. Non-redox active species may be detected by an indirect electrochemical means. Electron spectroscopic methods can be used to detect and identify the elements present on the electrode surface and to a certain extent their chemical nature as well. More detailed molecular level information can be obtained by UV, IR, visible and Raman spectroscopic methods either in transmission mode or reflection mode depending on the nature of the substrate.

The modified electrodes have several different interesting applications in electrochemistry: a) these modified surfaces can act as a catalyst, by mediating the electron transfer between the electrode and the solution species, including a chemical reaction which would not take place at the naked electrode; b) modified electrodes in the cells can be used as display devices if the immobilized molecules change color or emit light when they are electrically excited; c) the immobilized species with a charge can be employed to preferentially extract solution species, and subsequently be detected electrochemically. They may have some ion-selective properties which may be used in potentiometric applications. Presently, there are several reports in the literature indicating the applications of modified electrodes as "proton" sensors, d) these modified surfaces have been shown to be very useful in the prevention of photocorrosion

in photoelectrochemical cells. Both the covalently attached surfaces as well as polymer modified surfaces have been employed in this regard with a reasonable success.

There are a number of research groups who are actively pursuing these goals and more and more interesting applications of modified electrode surfaces will be uncovered in the foreseeable future.

As it has been already indicated, our objective in this investigation was to develop newer surfaces which are useful in small bandgap semiconductor (n-type) photoelectrochemical systems. In the first part of this project we have studied the reactivity of different silanes towards the surface hydroxyl groups of  $\text{TiO}_2$  by infra-red spectroscopy. Secondly,  $\text{TiO}_2$  single crystal surfaces were modified with these silanes and the stability of these modified layers has been studied by X-ray photoelectron spectroscopy. In the final part of the project electrochemical polymerization techniques have been employed as a means to synthesize homogeneous modified layers.

## Chapter 2

### INFRARED SPECTROSCOPY OF SILANE MODIFIED TiO<sub>2</sub>

#### 2.1 Introduction

The importance of the characterization of surface structure has been recognized for decades, in order to understand the adsorption processes that take place at interfaces. In the late fifties and early sixties, due to lack of the development of suitable techniques, surface structure was understood imperfectly on a molecular level and the progress was slow. But in the last 10-15 years due to the advent of newer techniques this area of research has enjoyed a reasonably fast growth. The study of the gas-solid interface has drawn the interest of both industrial and academic scientists because of the tremendous potential of the "Surface Catalytic Process". The capability of surfaces to selectively accelerate favorable chemical reactions is the basis for many industrial chemical processes. Therefore, understanding of the adsorption, kinetics, and chemical reactions taking place at surfaces at molecular or atomic level is absolutely important. The application of infrared spectroscopy in surface studies has aided scientists to understand many surface reactions, to identify adsorbed reaction intermediates, and to propose mechanisms. During the last decade or so it has had a tremendous impact in the enhancement of knowledge and understanding of "Surface Processes". This is amply demonstrated by the vast number of papers that have been published in



this field (3,4,5). The characteristic vibrations of molecules can be used to study the structure and bonding of surface-bound species. Primarily transmission mode studies has been employed at the earlier stages of these studies. Lately the application of FTIR and reflection-absorption methods have considerably enhanced the potential of this technique (6,7). The surfaces carry only very small amount of sample. Therefore, it is a challenge to obtain sufficient sensitivity to extract adequate information on surface-bound species. This problem has been overcome by employing substrates with high surface area which are transparent to infra-red radiation.

During physisorption, the bond between the surface and the adsorbed species is a weak one (Van-der-Waal type), and hence the changes in the absorption spectra of gaseous physisorbed species is minimal. In the second type of interaction, chemisorption, adsorbates undergo strong interaction with the surface. They may be dissociated, non-dissociated or reactive, thereby sometimes causing substantial changes in the absorption spectrum of the species concerned. This enables one to differentiate between chemisorption and physisorption at a surface in many instances.

Infra-red spectroscopy yields several advantages over electron spectroscopic techniques, in surface characterization (6):

1. It provides detailed atomic and molecular level information.
2. Samples are not subjected to destruction or alteration in the process of obtaining information.
4. It is relatively inexpensive compared to most other surface techniques.

Our objective in this portion of the project was to obtain detailed molecular level information of the gaseous phase surface reactions of silanes with  $\text{TiO}_2$ . The information sought by these studies is:

1. The reactivity of different types of OH groups on the surface.
2. The reactivity of different silane reagents towards surface OH groups.
3. The extent of surface coverage obtained.
4. The thermal and hydrolytic stability of modified layers.
5. The effect of reaction variables on the final modified surface.

#### 2.II.A Literature Review

Infra-red spectroscopy has been employed extensively in the characterization of the properties of oxide surfaces. In the past there has been considerable interest in the surface properties of alumina and silica, most probably due to their catalytic properties. The interest in surface properties of  $\text{TiO}_2$  is due to a) its use as an adsorbant with regenerative surface properties, and b) the photosensitivity of  $\text{TiO}_2$  electrodes. But the literature on surface characterization studies of  $\text{TiO}_2$  is relatively small compared to other oxides (e.g., silica, alumina). There are several British research groups who have independently carried out detailed studies on surface characterization of  $\text{TiO}_2$ .

Jackson and Parfitt (8) have studied three different types of rutile surfaces with the objective of understanding their thermal dehydration and rehydration properties, and also they have attempted to correlate the observed properties to the interaction of gaseous  $\text{H}_2\text{O}$

molecules with the underlying crystallographic cleavage surface. It is assumed that low index crystallographic planes dominate the surface of polycrystalline powders because in these planes the titanium ions remain maximally coordinated. One such plane on rutile is the (110) plane. The (110) cleavage plane of rutile results in loss of coordination of both  $Ti^{4+}$  and  $O^{2-}$  ions, yielding sites for adsorption of water molecules. The water molecules dissociate to leave OH groups at metal ion sites and protons at oxide ion sites. The OH groups at metal ion sites have monodentate attachment (terminal groups), whereas oxide sites are considered bidentate OH's (bridging type). The IR assignments of the OH bands have been based on the observed thermal properties of these groups, which are presented in Table I.

Jones and Hockey (9) also have conducted a detailed study of rutile surfaces with the objectives of understanding the covalent and ionic nature of surface OH species and coordination properties of surface cations. They have observed seven absorption bands due to hydroxyl and adsorbed  $H_2O$  species, six of them being in the  $3000-4000\text{ cm}^{-1}$  region and the seventh around  $1600\text{ cm}^{-1}$ . The IR absorption assignments are shown in Table I.

In the subsequent report, Jones and Hockey (10) attempted to correlate observed surface OH bands to interactions of  $H_2O$  molecules with surface planes of rutile. The authors have chosen (110), (101), and (100) as likely cleavage planes of rutile. The reasons for selection of these planes as surface planes for rutile powder is

(a) Rutile is known to crystallise so that the majority (98%) of the crystal surface is composed of the planes (110), (101) and (100), with

Table I

Infrared Absorption Band Assignment of Surface Hydroxyl Groups of  $\text{TiO}_2$ 

Sample	Terminal Isolated OH, $\text{cm}^{-1}$	Bridged OH, $\text{cm}^{-1}$	Adsorbed $\text{H}_2\text{O}$ , $\text{cm}^{-1}$	Hydrogen-Bonding $\text{cm}^{-1}$	Reference
Rutile	3670	3700	3615 3530 3400 1600 (bending)	3429	9
			3680 3610 3550 1610 (bending)		10, 11
Anatase	3715 3675		1605 (bending)		12
Rutile	3680	3410	1610 (bending)		12
Anatase	3715			3665	14
Rutile	3665			3685 3410	14
Rutile	3700 3660 3655 3610	3410	3400 1610 (bending)	3520	15

the (110) plane being 60% of the total area and the latter two planes (101), (100), equally 20% each (11).

(b) Electron micrographic studies of crystalline rutile powders that were used in this work (10) showed morphological resemblance to large rutile crystals.

(c) For energetic reasons crystal cleavage occurs so that the surface cations have coordination numbers as close as that in the bulk of the crystal. In the case of  $\text{TiO}_2$ , Ti ions have a co-ordination number six. In the (101) and (100) planes the surface cations have a co-ordination number of five with respect to oxide ions and in the (110) plane equal number of cations have co-ordination numbers five and four with respect to oxide anions.

Dissociative addition of a water molecule forms a terminal OH ion above row A/ $\text{Ti}^{4+}$  ions and forms a bridging OH between pairs of cations on row B. The pentacoordinate Ti ions on the planes (101) and (100) have been identified as sites for terminal OH groups.

Yates (12) and Primet et al. (13) also have attempted to identify surface hydroxyl groups of both rutile and anatase. These band assignments are given in Table I.

In the above discussion it is evident that in some instances there is some inconsistency in the band assignment by different authors (8,9,12,13). To overcome this problem, Griffiths and Rochester (14) have conducted a very detailed study of water adsorption of the rutile surface. They have identified nine absorption bands due to adsorbed  $\text{H}_2\text{O}$  and surface OH groups. These bands are at 3725, 3700, 3680, 3655, 3610, 3520, 3410, 3400 (broad) and  $1620 \text{ cm}^{-1}$ . The correlation of these

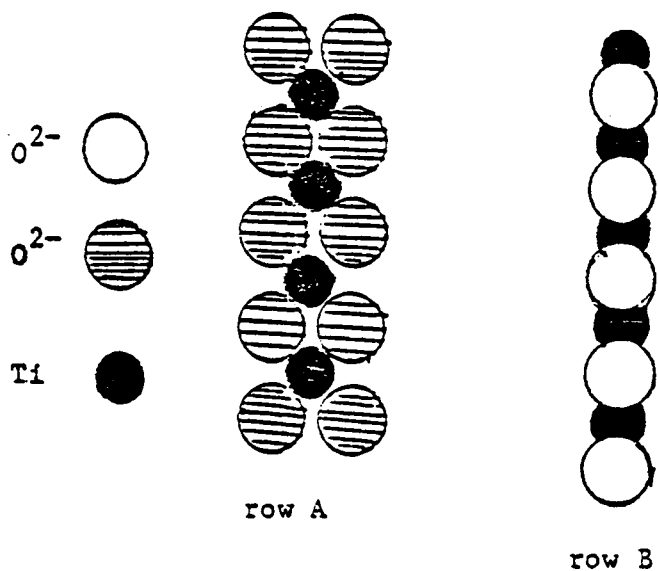


Figure 1: (110) plane of rutile. The terminal OH groups are generated by dissociative adsorption of water molecules at row A Ti ions.

The bridging OH are formed by the dissociative adsorption of water molecules at row B  $O^{2-}$  ions.

bands to the hydroxylated  $\text{TiO}_2$  surface is presented in Table I. Our assignments of  $\text{TiO}_2$  OH bands are given in the discussion section.

The studies of the interaction of  $\text{NH}_3$  and pyridine by Parfitt et al. (15,16) have further confirmed the presence of two different adsorption sites on the rutile surface, which would be the molecular water adsorption sites on a hydroxylated rutile surface. Herrmann and Boehm (17) have reported that adsorption of ammonia on anatase yields  $\text{NH}_4^+$  species as a result of surface 'OH' groups.

#### 2.II.B Reactions of silanes with silica

The interest in reactions of oxides with silane reagents is due to several reasons. In general, silanization provides a way to deactivate active sites on surfaces. In gas chromatography, before the glass (silica) columns are packed, they are treated with silane reagents to form an inert surface in order to prevent peak tailing. The used GC columns are treated with silanes in order to block the active sites formed by 'column bleeding' during the operation. Silane reagents with hydrolytically unstable bands and with various organic functionalities are used to form bonded column packing materials (stationary phase). Therefore, due to the wide interest of these silanization reactions, knowledge of the mechanistic aspects of these reactions is likely to enhance the understanding of these processes. There are only a very few reports (18,19), on the silanization of  $\text{TiO}_2$  in the literature. But these studies have not carried out with the objective of studying kinetics or mechanistic aspects of the derivatization process.

Hair and Hertl (20,21,22,23) have published a series of reports on

the kinetics of gaseous phase silanization of the silica surface with both the chloro- and methoxysilanes. In the reaction of trimethoxymethylsilane with silica (20), they observe that the reaction by-product, methanol, also reacts with the surface. Quantitative experiments show that for every molecule of siloxane present, 0.36 molecules of methanol react with the surface. The variation of bands at  $3745\text{ cm}^{-1}$  (Si - OH) and  $2850\text{ cm}^{-1}$  (C - H) are used to plot the reaction curve. During the reaction, they observe the appearance of a broad band at  $3350\text{ cm}^{-1}$ , which is assigned to the interaction of unreacted OMe groups with the surface OH species. This accounts for 10-15% removal of surface OH groups during the reaction. The reaction is shown to follow 3rd order kinetics with respect to surface OH species up to about 80% of the reaction. The third order kinetics indicate that for every molecule of siloxane reacted with the surface, 3 OH groups are removed from the surface. This does not necessarily mean that the siloxane reacts trifunctionally. A mass balance calculation shows that 40% of the siloxane molecule reacts monofunctionally and 60% of it difunctionally. The study indicates that the chemisorption reaction is preceded by the physisorption of siloxane onto the surface. The dependence of reaction rate being 3rd order with respect to the free surface OH species as well as 3rd order with respect to the fraction of absorbed (siloxane) OH groups shows that the configuration of the siloxane molecule in physisorption and chemisorption somewhat similar.

In the subsequent report Hair and Hertl (21) present the results of the silica reaction with mono- and dimethoxymethylsilanes. As in the



previous case the hydrogen-bonded OH species do not react with the silane molecule. The rate-determining step for this process is suggested to be the formation of Si - O - Si bonds from the physisorbed molecules. The reaction curve is plotted in a similar manner to the previous report. These data yield linear kinetic plots with orders of 1.6 for monomethoxy- and 2.2 for dimethoxysilanes. From the mass balance equation it is determined that 60% of the dimethoxysilanes react monofunctionally and 40% difunctionally.

In contrast to methoxysilane reactions, the by-product HCl formed during the chlorosilane reactions ( $\text{SiCl}_4$ ,  $\text{MeSiCl}_3$ ,  $\text{Me}_2\text{SiCl}_2$  and  $\text{Me}_3\text{SiCl}$ ) (22) does not show any significant reaction towards silanol groups of silica. As in the previous reports (20,21) the reaction curve is obtained from the variation of absorbance for bands at 3745 ( $\text{SiOH}$ ) and  $2850 \text{ cm}^{-1}$ . The orders of respective reactions are obtained by a curve-fitting technique on a variable-order rate equation. As expected, monofunctional chlorosilane has a 1st order rate with respect to surface OH species, whereas all three other silanes have an order of 1.5 (approximately). This corresponds to 50% of the silane reacting monofunctionally and 50% difunctionally. Analysis of reacted samples reveals the presence of chlorine in reasonable amounts, which is unexpected. The initial fast reaction is attributed to direct replacement of OH by Cl, as shown in equation 1.



The activation energies calculated for all of the chlorosilane

reactions are about the same (22 cal/mole). This indicates the similarity of the reaction mechanisms. In contrast to the reactions of methoxysilanes, the reactions of chlorosilanes have shown to be pressure-independent in the 15-80 torr range.

In a similar study of reactions of HMDS with silica surface (24), the rate of the reaction is second order with respect to surface OH concentration and 1.74 order with respect to fraction of surface OH covered by adsorbed (physically) silane. This indicates that the 70% of adsorbed species are at two sites and 30% are at a single site.

This review has covered the literature on surface band assignment of  $\text{TiO}_2$  and the kinetics of silane reactions with silica surface.

#### 2.III.A Experimental

$\text{TiO}_2$  (P-25) powder was obtained from Degussa Corporation. According to the specifications provided by the manufacturer, the mean particle size was  $0.03 \mu$  and silicon content was less than 0.2% by weight. An X-ray powder diffraction study on this powder has shown that this is indeed a mixture of anatase and rutile (85:15).

Before the experiment the powder was subjected to two different heat treatments in order to remove the impurities: a) heat to  $400^\circ\text{C}$  to remove carbonaceous matter; b) press into a pellet (60 mg of powder was pressed in a 13 mm die at a pressure of 80-100 MPa); c) fire pellet at  $500^\circ\text{C}$  for 7-8 hours in order to remove organic impurities.

The surface area, measured by the BET method, was  $51.2 \text{ m}^2/\text{g}$  before step (a),  $48.6 \text{ m}^2/\text{g}$  after step (b), and  $31.5 \text{ m}^2/\text{g}$  after step (c). This may be due to sintering and particle-particle contact in the pressed

pellet. After the pellet was burned in the oven, it was allowed to cool to room temperature, and was stored in a humid atmosphere to achieve maximum surface rehydroxylation. This was found to eliminate carbon dioxide adsorption onto the pellet.

All the reactions were carried out on a 'greaseless' vacuum line containing Teflon stopcocks and #15 O-ring joints. Vacuum conditions were achieved by mechanical and oil diffusion pumps, which were isolated from the reaction area by two liquid nitrogen traps. The pressure of the vacuum line was monitored by two Hastings Vacuum gauges, which were pre-calibrated. The vacuum line was capable of sustaining dynamic pressure below 0.001 torr.

The pellet was held in the IR-cell with the help of a 8-mm diameter Teflon holder. The IR-cell consisted of three 15 O-ring joints. Two of them were colinear and the third was used to connect the whole cell to the vacuum line. The  $\text{CaF}_2$  windows were sealed at the colinear O-ring joints with Teflon O-rings. The cell and the windows were held together by two clamping plates. Heating was achieved by wrapping a heating tape around the body of the cell. The adjustment of the heating control unit, a 'HexAcon' solid state control device, was pre-calibrated using a thermometer. The Teflon stopcock adaptor of the IR-cell allowed it to be sealed or connected to the vacuum line. The clamping plates helped to hold the IR-cell in the light path of IR-spectrometer as well. All the IR-spectra were recorded on a Perkin-Elmer 283B Spectrophotometer. The reference beam was attenuated with an empty vacuum IR-cell.

### 2.III.B Synthesis

All the silanes (Petrach) used were distilled and degassed by two freeze-pump-thaw cycles. These were stored under vacuum in flasks with Teflon stopcocks until use. After the pellet was carried through the cleaning steps, it was mounted in the IR-cell, dried under vacuum (0.001 torr) at 150°C for 2 hrs., and an IR-spectrum of the sample was obtained. The IR-cell was reinstalled in the vacuum line and the pellet was exposed to silane vapour. The vapour pressure of the silane was controlled by thermostating the flask containing the silane reagent, which was open to the vacuum line. The pellet was allowed to react with the silane for one hour. The silane was pumped away for about 15-20 min., the IR-cell was sealed under vacuum and the second IR-spectrum of the sample was obtained.

For each silane reagent three different reactions were carried out on separate pellets.

A) After drying the pellet at 150°C for 2 hrs., the pellet was reacted at room temperature while the liquid silane temperature was controlled at 0°C. After the reaction (1 hr.) the excess silane was pumped out and the IR-spectrum of the reacted pellet was obtained. Then the IR-cell was reinstalled in the vacuum line, and heated at 150°C for 2 hrs. under vacuum (0.001 torr); the third spectrum was then obtained. The pellet was then exposed to humid air for 3 hrs. under a large beaker. The saturated water vapour pressure within the beaker was achieved by inserting a smaller beaker filled with water. This pellet was reinstalled in the vacuum line and dried at 150°C under vacuum (0.001 torr) for 2 hrs., and the final IR-spectrum of the pellet

was recorded.

B) The same reaction procedure was followed as in (A), except the pellet was at 150°C, and the silane was at 0°C, during the derivatization reaction.

C) Same as (B), except the silane was held at 15°C in order to obtain higher vapour pressure.

#### 2.IV Data and Interpretation

The IR spectrum of TiO<sub>2</sub>, dried at 150°C under vacuum conditions as shown in Table II, shows a range of peaks due to OH stretching vibrations in the 3000-4000 cm<sup>-1</sup> range. In this table and in the rest of the infrared data tables (II + XXXIX) the peak heights have been measured with respect to the immediately adjacent base line. There are two weak bands which appear in the 2800-3000 cm<sup>-1</sup> range and a broad band at 1620 cm<sup>-1</sup>. This spectrum is shown in Figure 2A as well.

When this pellet is exposed to D<sub>2</sub>O, all the bands in the 3000-4000 cm<sup>-1</sup> region are displaced to a lower frequency region. The ratio of  $\nu_{OH}/\nu_{OD}$  is about 1.36 for all three of these bands, which is close to the theoretical value expected for a deuterium shift of OH to OD. This shows the -OH nature associated with all bonds in that region. Further the quantitative exchange shows that the surface -OH groups are accessible to gaseous reagents. This has been confirmed by Jones and Hockey (9), who noted that some -OH groups are not exchangeable with D<sub>2</sub>O; these OH groups may lie in grain boundaries or particle contact points. The bands which appear in the 2800-3000 cm<sup>-1</sup> region correspond to C-H stretching vibrations of hydrocarbons. We have observed three

Table II  
 IR Data of  $\text{TiO}_2^{\text{a}}$  and  $\text{D}_2\text{O}$  Exchange<sup>b</sup>.

Step A		Step B	
Peak ( $\text{cm}^{-1}$ )	Abs.	Peak ( $\text{cm}^{-1}$ )	Abs.
3725	0.10	—	—
3642	0.20	3641	0.02
3412	0.19	3415	0.02
2953	0.10	2953	0.13
2924	0.12	2922	0.12
2851	0.06	2849	0.06
2831	0.05	—	—
—	—	2741	0.06
—	—	2525	0.16
—	—	2450	0.13
1620	0.06	—	—
1560	0.11	1556	0.09

a) Dried at  $150^\circ\text{C}$  for two hours under vacuum.

b) Exposure to  $\text{D}_2\text{O}$  (9-10 torr) for 30 min. and dried at  $150^\circ\text{C}$  for 30 min.

In all the infra-red data tables the peak heights have been measured with respect to the immediately adjacent base line.

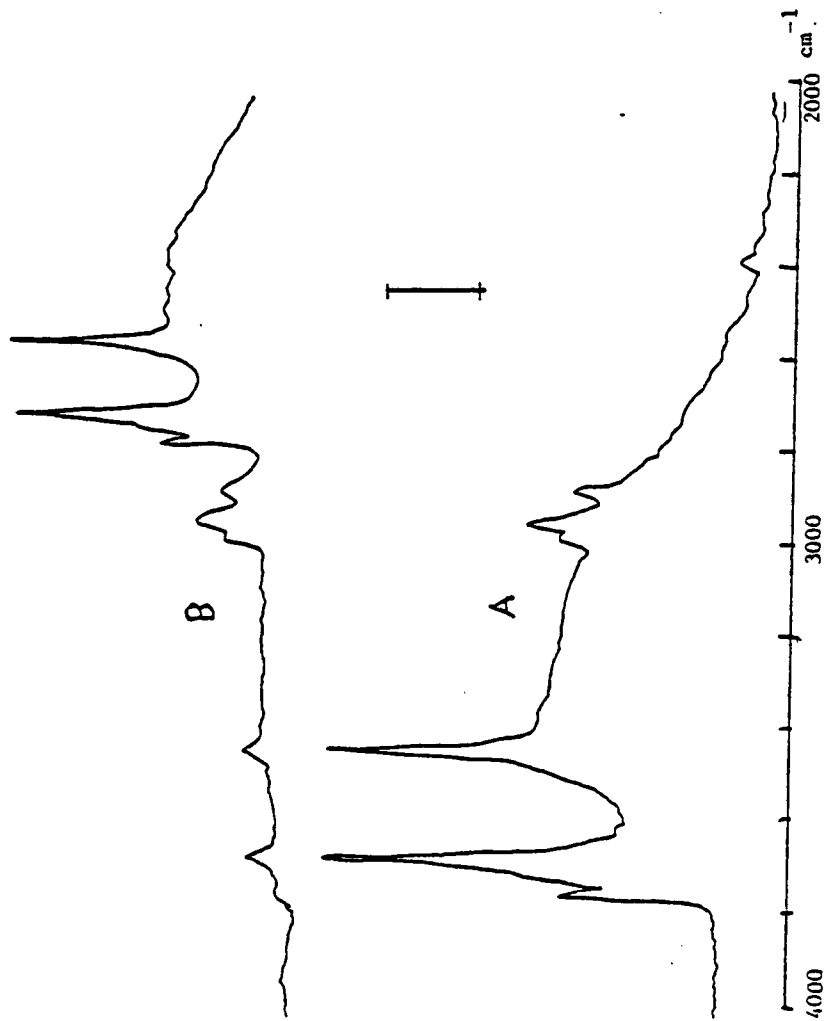


Figure 2: IR spectra of (A) clean pellet after heating under vacuum for 2hrs. (B) after exposing to D<sub>2</sub>O vapour(5 torr) followed by drying as in A. Bar = 0.15 abs. units.

distinct bands at 3730, 3650 and 3420  $\text{cm}^{-1}$  and a shoulder at 3680  $\text{cm}^{-1}$  in the IR-spectrum of vacuum dried  $\text{TiO}_2$  [150°C]. As it has been shown above, the deuterium exchange has confirmed the hydroxylic nature of these bands. As the P-25 was a mixture of anatase and rutile, it is expected that the hydroxyl groups due to both of these components are present in the IR-spectrum. In previous rutile spectra, the terminal OH species is assigned to the bands at 3680, 3655  $\text{cm}^{-1}$  (14), 3665  $\text{cm}^{-1}$  (13), 3680 (12), 3650 (9,10) and 3670 (8) (Table I). Therefore the 3650  $\text{cm}^{-1}$  band and the 3680  $\text{cm}^{-1}$  shoulder observed is most likely to be due to terminal OH species of rutile component. The bridging OH species has been previously assigned to the 3410  $\text{cm}^{-1}$  band (9,10,14) (Table I) for rutile.

Anatase spectra show a terminal OH band at 3715  $\text{cm}^{-1}$  (12,13) (Table I). Therefore, the peak observed at 3730  $\text{cm}^{-1}$  we believe is due to the anatase component of P25. The 3650  $\text{cm}^{-1}$  is thought to be due to the overlap of 3665  $\text{cm}^{-1}$  of anatase (13) and 3650  $\text{cm}^{-1}$  (9,10) and 3655  $\text{cm}^{-1}$  (14) of rutile components. The bands which appear in the 2800-3000  $\text{cm}^{-1}$  region correspond to C-H stretching vibrations of hydrocarbons. We have observed weak absorption bands in this region throughout this series of experiments. We believe these bands are due to sample contamination caused by the hydrocarbon leachants from the 'O' rings used in the vacuum line. The broad envelope centered around 3400  $\text{cm}^{-1}$  has been assigned to hydrogen-bonded OH of adsorbed water. Jackson and Parfitt (8) have shown the sensitivity of this band to the extent of water present on the surface.

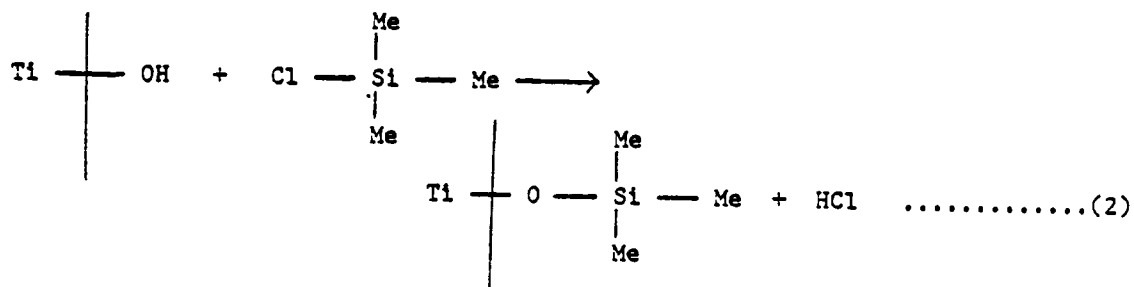
The broad band at 1620  $\text{cm}^{-1}$  is assigned to molecular water.



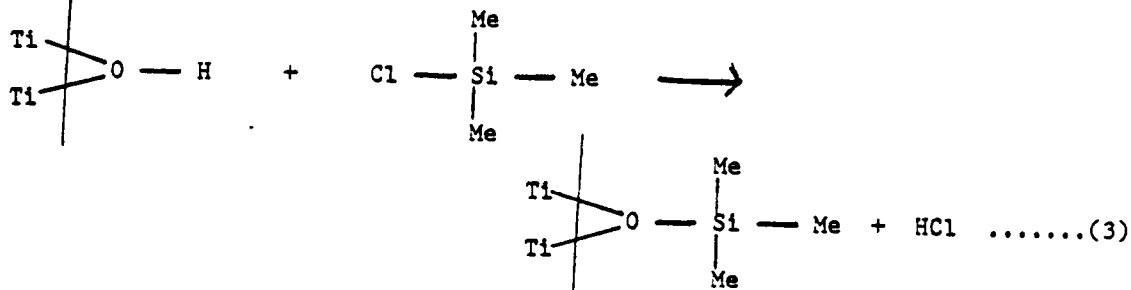
### 2.IV.A Reactions of TiO<sub>2</sub> with Silanes

The surface hydroxyl groups, both the terminal and the bridging on the TiO<sub>2</sub> surface, react with gaseous silane reagents to form derivatized TiO<sub>2</sub> surfaces. The reactions may be visualized as shown equations 2 and 3.

Terminal OH:



Bridged OH:



In these reactions, the reaction by-products of chloro- and methoxy-silanes, and HMDS [hexamethyldisilazane], are HCl, MeOH, and NH<sub>3</sub>, respectively.

### 2.IV.B. Reactions with trimethylchlorosilane

The IR spectra of TiO<sub>2</sub> before and after the reaction with dimethyldichlorosilane are shown in Figure 3. The changes that take

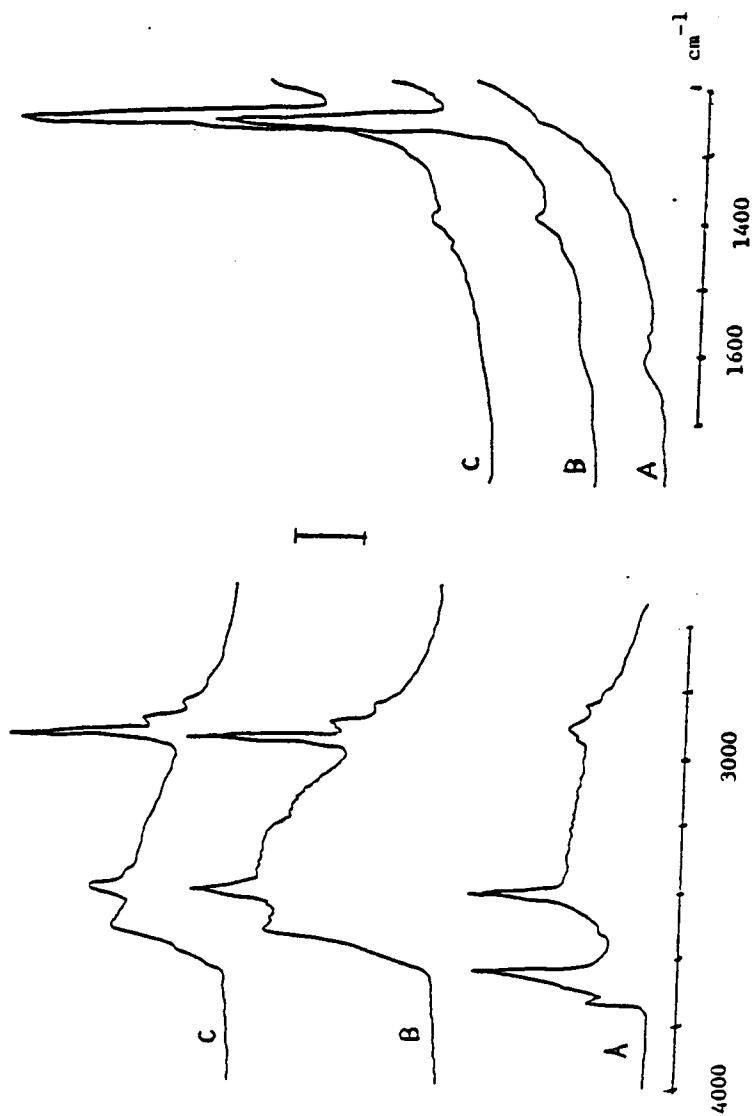


Figure 3: IR spectra of  $\text{TiO}_2$  reacted with  $\text{Me}_2\text{SiCl}_2$  using regime 1: (A) clean  $\text{TiO}_2$  pellet (b) after reaction with the silane(V.P.41 torr), (C) after evacuation at  $150^\circ\text{C}$  for 2 hrs. Bar 0.2(L.H.S.), 0.4(R.H.S.) abs.

place on a  $\text{TiO}_2$  surface after the reaction with trimethylchlorosilane are very much similar to those observed for dimethyldichlorosilane. The respective IR data are given in Table III. The sample was at  $150^\circ\text{C}$ , and the liquid silane v.p. was 63 torr. The main differences in spectra A and B are that the intensity of the surface terminal hydroxyl groups at  $3730$  and  $3650\text{ cm}^{-1}$  are drastically reduced and the bridging groups at  $3425\text{ cm}^{-1}$  are considerably attenuated due to the derivatization reaction. The attenuation of terminal OH groups is 86% and the bridging OH is 64%. This shows that terminal groups are more reactive toward a chlorosilane than the bridging OH. The bridging OH groups are under the influence of two titanium ions in the (110) plane of  $\text{TiO}_2$  whereas the terminal OH's are under the influence of only one titanium ion. Jones and Hockey (10) have proposed that a) the basicity of the bridging OH group is much higher than that of the terminal OH, hence the higher polarity of the bridging OH species makes them more reactive in hydrolytic reactions, and b) the bridging OH group is closer to the (110) surface than the terminal OH group. It may be that the silane reagent first approaches and reacts with the terminal OH groups as they extend further away from the surface than the bridging OH groups. Once the reaction occurs at terminal groups, the bulky trimethylsilyl group hinders the approach of the next reagent molecule towards the bridged OH groups.

The presence of the trimethylsilyl group is evident due to the enhancement of absorption at  $2960$  and  $2927\text{ cm}^{-1}$  which is assigned to C-H stretching vibrations. Further, there is a very strong absorption band at around  $1259\text{ cm}^{-1}$  which is due to the Si-C stretching mode. A

Table III

Reaction of  $\text{TiO}_2$  with Trimethylchlorosilane<sup>a</sup>.

Peak ( $\text{cm}^{-1}$ )	Step I*		Step II**		Step III***	
	Abs.	Peak ( $\text{cm}^{-1}$ )	Abs.	Peak ( $\text{cm}^{-1}$ )	Abs.	Peak ( $\text{cm}^{-1}$ )
3733	0.11	3733	—	3733	—	3733
3650	0.30	3640	0.04	3640	0.04	3640
—	—	3549	0.20	3549	0.12	3545
3418	0.21	3425	0.08	3425	0.04	3423
—	—	2960	0.39	2960	0.33	2960
2927	0.25	2927	0.24	2927	0.21	2927
—	—	2904 (s)	0.17	2904 (s)	0.16	2906 (s)
2855	0.15	2856	0.12	2856	0.09	2866
1620	0.05	—	—	—	—	—
—	—	1410	0.05	1410	—	—
—	—	1259	str. abs.	1259	str. abs.	1260
—	—	—	—	—	—	str. abs.

a) Sample at room temperature, silane vapor pressure 63 torr.

\* After heating at 150°C for two hours.

\*\* After reaction with TMCS.

\*\*\* After heating at 150°C for two hours.

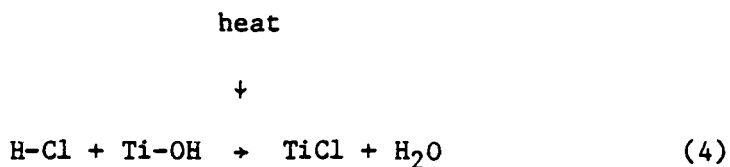
C-H bending vibration appears at  $1410\text{ cm}^{-1}$ . A solution containing  $\text{Me}_2\text{SiCl}_2$  in  $\text{CCl}_4$  produces absorption bands at 2978, 2914, 1407, and  $1260\text{ cm}^{-1}$ . Similar peaks have been observed for all silanized  $\text{TiO}_2$  surfaces.

The other processes that would be responsible for attenuation of surface OH groups are a) thermal dehydroxylation and b) physical adsorption of reagent and by-product. Heating of a clean  $\text{TiO}_2$  pellet overnight at  $150^\circ\text{C}$  under vacuum causes only a 10% reduction of the terminal peak intensity and an 8% reduction of the bridging OH peak intensity. Therefore, contribution to the peak attenuation of OH groups by this mechanism would be minimal during the one hour reaction at  $150^\circ\text{C}$ .

Table III shows the IR data obtained after heating the sample at  $150^\circ\text{C}$  for two hours after the excess silane reagent is removed from the reaction system. It shows that after the thermal treatment, both the  $2900\text{--}3000\text{ cm}^{-1}$  and  $1260\text{ cm}^{-1}$  absorption bands remain at almost the same intensity. This indicates that if there is any physical adsorption of chlorosilane, it is minimal.

After reaction with any chlorosilane, we have observed a new band around  $3545\text{ cm}^{-1}$ . A similar band appears when clean  $\text{TiO}_2$  is exposed to HCl (see below). There are two observed properties of this peak: a) it exchanges with  $\text{D}_2\text{O}$  with a peak shift ratio  $\nu_{\text{OH}}/\nu_{\text{OD}}$  close to 1.35 and b) the effect of heating the pellet is more drastic on this peak (Table III) than on the surface OH groups of  $\text{TiO}_2$ . Hair and Hertl (22) in their study of the reaction of chlorosilanes with silica, found that their type of silica did not adsorb HCl; no corresponding new peak was

observed on their samples. We believe that this peak is due to OH groups which are hydrogen-bonding to adsorbed HCl. The sharpness of this peak indicates a well-defined orientation of the hydrogen-bond. Both Jones (9) and Jackson (8) have shown that acceleration of dehydration of  $TiO_2$  is due to the presence of  $Cl^-$ . The enhanced thermal attenuation of this peak may be due to its association with HCl and under thermal treatment, the following dehydration reaction is possible.



Also, after silanization there is a drastic reduction in the bending mode of adsorbed water at  $1620\text{ cm}^{-1}$ . This peak has been assigned to  $H_2O$  which acts as on ligands at bare  $Ti^{4+}$  sites. Parfitt et al. (8,16;17) have shown that during the  $NH_3$  and pyridine adsorption experiments, the adsorbed water is being replaced by these molecules. But in this reaction with silane, there is hardly any species available which would be a good ligand that would replace adsorbed  $H_2O$ . We therefore conclude that the water is being removed by reaction with excess silane.

Table III shows the room temperature reaction of  $TiO_2$  with  $SiMe_3Cl$  at 63 torr. The terminal hydroxy groups have attenuated 92% and the bridging OH about 38%. Under the same vapour pressure at  $150^\circ C$  the peak attenuation observed for these OH groups of  $TiO_2$  are 86% and 21%, respectively (Table IV). So in these reactions, the temperature of the reaction and vapor pressure of silane do not show definite trends on

the reactivity of the terminal OH and the reactivity of the bridging OH groups. We suggest that reactions have essentially ceased within the 1 hour reaction time.

Table V shows the IR data for  $\text{TiO}_2$  ( $150^\circ\text{C}$ ) modified with trichloromethylsilane, keeping the liquid silane at  $15^\circ\text{C}$  (v.p. 143 torr). The only difference between these reaction conditions and the previous ones (Table III and IV) is the silane vapor pressure, 63 torr and 143 torr, respectively. But the attenuation of the terminal OH is almost the same (92% compared to 86%). The reactivity of the bridging OH groups exhibits a considerable difference (41% to 21%). This indicates that the silane vapor pressure does not have any large effect on the derivatization reaction. Hair and Hertl (22) have shown that a variation of chlorosilane vapor pressure between 15 and 80 torr does not effect the kinetics of their reaction with silica.

#### 2.IV.C Reactions of Dimethyldichlorosilane [DMCS] and Trichloromethylsilane [TCMS] with $\text{TiO}_2$

The tables VI-VIII and IX-XI show the IR data obtained for the reactions of  $\text{TiO}_2$  with  $\text{Me}_2\text{SiCl}_2$  and  $\text{MeSiCl}_3$ . The reactivity of the terminal hydroxyl groups are essentially quantitative whereas the bridging groups show a definite trend in reactivities in contrast to TMCS reactivity. The extent of reaction of this OH species increases with both the vapor pressure of silane and the temperature of the reaction. In spite of the fact that these silanes have lower vapor pressure at  $15^\circ\text{C}$  than TMCS, the attenuation of OH peaks is comparable or higher at  $150^\circ\text{C}$  reactions (19b). This may be due to the fact that

Table IV.  
Reaction of  $\text{TiO}_2$  with Trimethylchlorosilane<sup>a</sup>.

Peak ( $\text{cm}^{-1}$ )	Step A*		Step B**		Step C***	
	Abs.	Peak ( $\text{cm}^{-1}$ )	Abs.	Peak ( $\text{cm}^{-1}$ )	Abs.	Peak ( $\text{cm}^{-1}$ )
3733	0.11	—	—	—	—	—
3650	0.30	3640	0.04	3640	0.04	3640
—	—	3549	0.20	3545	0.12	3545
3418	0.21	3425	0.08	3423	0.04	3423
—	—	2960	0.34	2960	0.33	2960
2927	0.25	2927	0.24	2927	0.21	2927
2855	0.15	2856	0.12	2866	0.09	2866
1670	0.05	—	—	—	—	—
—	—	1259	str. abs.	1260	str. abs.	1260

a)  $\text{TiO}_2$  at 150 C and silane vapor pressure 63 torr.

\* Heating at 150 C for two hours under vacuum.

\*\* Reaction with silane.

\*\*\* Heating at 150 C for two hours under vacuum.



Table V

Reaction of  $\text{TlO}_2$  with Trimethylchlorosilane<sup>a</sup>.

Peak ( $\text{cm}^{-1}$ )	Step I*		Step II**		Step III***	
	Abs.	Peak ( $\text{cm}^{-1}$ )	Abs.	Peak ( $\text{cm}^{-1}$ )	Abs.	Peak ( $\text{cm}^{-1}$ )
3729	0.18	—	—	—	—	—
3684	0.23	—	—	—	—	—
3650	0.42	3641	0.03	3639	0.11	3639
—	—	3551	0.26	3551	0.18	3551
3417	0.26	3422	0.12	3422	0.16	3422
2964	0.04	2960	0.39	2960	0.32	2960
2924	0.08	2924	0.12	2924	—	—
—	—	2904 (s)	0.14	2905	0.10	2905
—	—	2851	0.05	2854	0.04	2854
1620	0.11	1622	0.02	1620	0.06	1620
—	—	1411	0.08	—	—	—
—	—	1268	str. abs.	1265	str. abs.	1265

a)  $\text{TlO}_2$  at  $150^\circ\text{C}$ , silane vapor pressure 143 torr.

\* Heating  $\text{TlO}_2$  at  $150^\circ\text{C}$  for two hours under vacuum.

\*\* Reaction with Trimethylchlorosilane.

\*\*\* Exposed to  $\text{H}_2\text{O}$  vapor for three hours and heated at  $150^\circ\text{C}$  for two hours.

Table VI

Reaction of  $\text{TiO}_2$  with Dimethyldichlorosilane<sup>a</sup>.

Peak ( $\text{cm}^{-1}$ )	Step I*		Step II**		Step III***		Step IV****	
	Abs.	Peak ( $\text{cm}^{-1}$ )	Abs.	Peak ( $\text{cm}^{-1}$ )	Abs.	Peak ( $\text{cm}^{-1}$ )	Abs.	Peak ( $\text{cm}^{-1}$ )
3731	0.16	—	—	—	—	—	—	—
3650	0.85	3650	—	—	—	—	3617	0.27
—	—	3537	0.11	3541	0.14	3542	0.32	—
3418	0.29	3425	0.23	3423	0.12	3424	0.19	—
—	—	2965	0.53	—	—	2962	0.52	—
2961	0.05	2963	0.11	2963	0.53	—	—	—
2925	0.08	—	—	2927	0.14	2928	0.11	—
—	—	2908	0.18	2908	0.15	2907	0.13	—
2854	0.06	2856	0.04	2855	0.05	2858	0.04	—
1615	0.07	—	—	—	—	—	—	—
—	—	1408	0.11	1405	0.07	—	—	—
—	—	1260	str. abs.	1260	str. abs.	1259	str. abs.	—

a)  $\text{TiO}_2$  at room temperature, silane vapor pressure 41 torr.\* Heating at  $150^\circ\text{C}$  for two hours under vacuum.

\*\* Reaction with DMCS.

\*\*\* Heating for two hours under vacuum at  $150^\circ\text{C}$ .\*\*\*\* Exposure to moisture for three hours and heated for two hours at  $150^\circ\text{C}$ .

Table VII

Reaction of  $\text{TiO}_2$  with Dimethyldichlorosilane<sup>a</sup>.

Peak ( $\text{cm}^{-1}$ )	Step A*		Step B**		Step C***		Step D****	
	Abs.	Peak ( $\text{cm}^{-1}$ )	Abs.	Peak ( $\text{cm}^{-1}$ )	Abs.	Peak ( $\text{cm}^{-1}$ )	Abs.	Peak ( $\text{cm}^{-1}$ )
3735	0.13	—	—	—	—	—	—	—
3650	0.36	3608	0.08	—	—	—	—	3620 0.07
—	—	3550	0.16	3512	0.04	3544	0.17	—
3418	0.33	3424	0.12	3421	0.06	3424	0.14	—
2959	0.12	2964	0.33	2964	0.28	2962	0.39	—
2927	0.13	2928	0.09	2929	0.09	2927	0.12	—
—	—	2910	0.12	2908	0.11	2909	0.13	—
2855	0.17	2857	0.03	2855	0.03	2856	0.04	—
1618	0.04	—	—	—	—	—	—	—
—	—	1529	0.03	1527	0.09	—	—	—
—	—	1407	0.04	1406	0.05	1413	0.04	—
—	—	1260	str. abs.	1260	str. abs.	1260	str. abs.	—

a)  $\text{TiO}_2$  at  $150^\circ\text{C}$  and silane vapor pressure 41 torr.\* Heating at  $150^\circ\text{C}$  for two hours under vacuum.

\*\* Reaction with DMCS.

\*\*\* Heating at  $150^\circ\text{C}$  for two hours under vacuum.\*\*\*\* Exposed to  $\text{H}_2\text{O}$  vapor for three hours and heated for two hours at  $150^\circ\text{C}$ .

Table VIII

Reaction of  $\text{TiO}_2$  with Dimethyldichlorosilane<sup>a</sup>.

Peak ( $\text{cm}^{-1}$ )	Step A*		Step B**		Step C***	
	Abs.	Peak ( $\text{cm}^{-1}$ )	Abs.	Peak ( $\text{cm}^{-1}$ )	Abs.	Peak ( $\text{cm}^{-1}$ )
3733	0.10	—	—	—	—	—
3650	0.33	3603	0.04	3619	0.03	3619
—	—	3547	0.14	3545	0.10	3545
3418	0.31	3423	0.09	2424	0.08	2424
2956	0.08	2966	0.26	2965	0.24	2965
2931	0.14	2927	0.08	2934	0.06	2934
—	—	2910	0.08	2908	0.07	2908
2854	0.06	2855	0.03	2858	0.01	2858
1617	0.05	—	—	—	—	—
1565	0.02	—	—	—	—	—
—	—	1407	0.06	—	—	—
—	—	1264	str. abs.	1262	str. abs.	1262

a)  $\text{TiO}_2$  at  $150^\circ\text{C}$  and silane vapor pressure 84 torr.

\* Heating at  $150^\circ\text{C}$  for two hours under vacuum.

\*\* Reaction with DMCS.

\*\*\* Exposure to  $\text{H}_2\text{O}$  vapor for three hours and heated for two hours

Table IX

Reaction of  $\text{TiO}_2$  with Trichloromethylsilane<sup>a</sup>.

Peak ( $\text{cm}^{-1}$ )	Step A *		Step B **		Step C ***		Step D ****	
	Abs.	Peak ( $\text{cm}^{-1}$ )	Abs.	Peak ( $\text{cm}^{-1}$ )	Abs.	Peak ( $\text{cm}^{-1}$ )	Abs.	Peak ( $\text{cm}^{-1}$ )
3731	0.09	—	—	—	—	—	—	—
3683	0.11	—	—	—	—	—	—	—
3649	0.14	—	—	—	—	—	—	—
—	—	3545	0.23	3550	0.12	3550	0.10	3550
3420	0.09	3423	0.06	3422	0.03	3421	0.04	3421
2956	0.06	2960	0.07	2963	0.10	2967	0.10	2967
2928	0.10	2927	0.09	2927	0.13	2928	0.11	2928
2855	0.04	2855	0.03	2855	0.05	2856	0.05	2856
2835	0.03	—	—	—	—	—	—	—
1620	0.01	1622	0.45	—	—	—	—	—
—	—	1271	0.45	1270	0.55	1272	0.53	1272

a)  $\text{TiO}_2$  at room temperature, silane vapor pressure 54 torr.

\* Heat at  $150^\circ\text{C}$  for two hours under vacuum.

\*\* Reaction with TCMS.

\*\*\* Heating for two hours at  $150^\circ\text{C}$  under vacuum.

\*\*\*\* Exposed to  $\text{H}_2\text{O}$  vapor for three hours and heated at  $150^\circ\text{C}$  for two hours under vacuum.

Table X

Reaction of  $\text{TiO}_2$  with Trichloromethylsilane<sup>a</sup>.

Peak ( $\text{cm}^{-1}$ )	Step A*		Step B**		Step C***	
	Abs.	Peak ( $\text{cm}^{-1}$ )	Abs.	Peak ( $\text{cm}^{-1}$ )	Abs.	Peak ( $\text{cm}^{-1}$ )
3731	0.17	—	—	3729	0.01	—
3678	0.22	—	—	—	—	—
3650	0.43	—	—	3640	0.07	—
—	—	3540	0.08	3556	0.10	—
3414	0.16	3423	0.06	3422	0.15	—
2956	0.05	2959	0.10	2972	0.27	—
2922	0.12	2922	0.13	2914	0.05	—
2852	0.07	2853	0.06	—	—	—
1618	0.07	—	—	1612	0.28	—
—	—	1406	0.06	1416	0.07	—
—	—	1270	str. abs.	1271	str. abs.	—

a)  $\text{TiO}_2$  at  $150^\circ\text{C}$ , silane vapor pressure 54 torr.\* Heat at  $150^\circ\text{C}$  for two hours under vacuum.

\*\* Reaction with TCMS.

\*\*\* Exposed to  $\text{H}_2\text{O}$  vapor for three hours and heated at  $150^\circ\text{C}$  for two hours under vacuum.

Table XI

Reaction of  $\text{TiO}_2$  with Trichloromethylsilane<sup>a</sup>.

Peak ( $\text{cm}^{-1}$ )	Step A <sup>*</sup>		Step B <sup>**</sup>		Step C <sup>***</sup>	
	Abs.	Peak ( $\text{cm}^{-1}$ )	Abs.	Peak ( $\text{cm}^{-1}$ )	Abs.	Peak ( $\text{cm}^{-1}$ )
3732	0.09	—	—	—	—	—
3680	0.13	—	—	—	—	—
3651	0.20	—	—	—	—	—
—	—	3544	0.11	3551	0.12	3551
3420	0.13	3422	0.04	3424	0.06	3424
2955	0.03	2968	0.08	2971	0.09	2971
2924	0.05	2921	0.05	2918	0.05	2918
2854	0.02	2852	0.02	2850	0.02	2850
1621	0.03	—	—	1617	0.02	1617
—	—	1271	0.60	1273	0.62	1273

a)  $\text{TiO}_2$  at  $150^\circ\text{C}$  and silane vapor pressure 101 torr.

\* Heat at  $150^\circ\text{C}$  for two hours under vacuum.

\*\* Reaction with TCMS.

\*\*\* Exposed to  $\text{H}_2\text{O}$  vapor for three hours and heated for two hours at  $150^\circ\text{C}$  under vacuum.

both the DMCS and TCMS are able to form silane bridges as they have two or more hydrolytically unstable Si-Cl bonds in each molecule. It is possible that after these molecules undergo the hydrolytic reaction with one of the terminal or bridging OH groups, the proximity of the second Si-Cl bond with a second OH group facilitates the subsequent bridging. Due to the interatomic layer distance on the (10) plane of  $TiO_2$ , it is more likely that bridged silane bonds form between the bridging OH species in the layer B than the interlayer (AB) bridges (10).

#### 2.IV.D Steric reasons against trifunctional reactions with Trichloromethylsilanes

According to the surface hydroxylation model proposed by Jones and Hockey (9) (p. 9), the distance between the hydroxyl groups on the same row (A-A or B-B) is 2.9 Å and between hydroxyl groups on the adjacent rows (A-B), 3.6 Å. The approximate value for Si-Cl covalent distance is 2.0 Å (in  $SiCl_3H$ ) and by taking the bond angle as  $109^\circ$ , the calculated distance between two Cl atoms on the base of a tetrahedral pyramid is 3.26 Å. If one considers any three adjacent hydroxyl groups on the (110) plane of rutile, they are in a geometry corresponding to a right angle triangle, with the sides 2.96 Å (A-A or B-B), 3.6 Å (A-B), and 4.6 Å (A-B, diagonal). Two bonds can be readily formed between any two surface oxygens and the Si atom, but simple geometry shows that the formation of a third Si-O bond creates considerable strain on all the Si-O bonds.

In this experiment with DMCS and TCMS, we have never observed free Si-OH ( $3730\text{ cm}^{-1}$ ) (derived from unreacted SiCl bonds) after the



complete reaction sequence. It may be that Si-OH groups condense with similar groups in the surroundings during the thermal activation after exposure to water vapor (step D of the reaction sequence). To examine if there are any free SiOH groups on the surface, an IR spectrum was recorded after the hydrolysis of the TCMS-derivatized TiO<sub>2</sub> pellet after a couple of hours of evacuation at room temperature (no heating). There is only a very weak absorption (0.02 absorbance units) band in the 3730 cm<sup>-1</sup> region. But there is a broad and strong absorption band in the region 3750 - 2500 cm<sup>-1</sup> due to excessive adsorbed water present on the surface. It may be that most of the Si-OH groups are hydrogen-bonded with surface-adsorbed water, and the corresponding free Si-OH band is hidden in the broad absorption band.

#### 2.IV.E Reactions of SiCl<sub>4</sub>

There are several striking differences in the reactivity of tetrachlorosilane compared to the other three chlorosilanes. First, it shows a strong dependence on silane vapor pressure. At 150°C under 152 torr v.p. 100% of both the terminal and bridging OH groups have reacted, whereas at the same temperature and under 83 torr, only 66% and 1% react, respectively. Compared to SiCl<sub>4</sub>, all the other chlorosilanes that have been used in our experiments have lower vapour pressures at both 0°C and 15°C. In spite of this fact, they have been shown to cause much higher attenuation of OH species of TiO<sub>2</sub> than SiCl<sub>4</sub> (19b).

The experimental data observed for SiCl<sub>4</sub> reactions is given in Tables XII-XIV. These data as well as Figure 4 show that a relatively

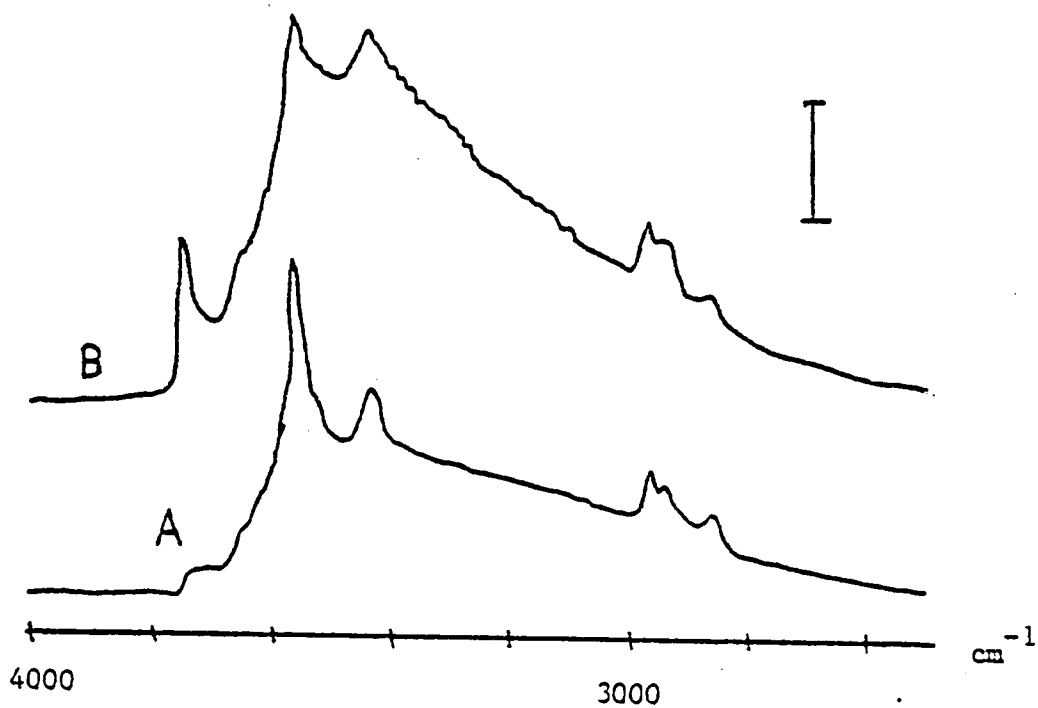


Figure 4: IR spectra of titanium dioxide reacted with silicon tetrachloride (regime 2, V.P. 83 torr)

(A) evacuation for 2 hrs at  $150^{\circ}\text{C}$ , after reaction.

(B) after exposure to moisture (10 torr) and heating at  $150^{\circ}\text{C}$ , for 2 hrs.

Table XII

Reaction of  $\text{TiO}_2$  with Tetrachlorosilane<sup>a</sup>.

Peak ( $\text{cm}^{-1}$ )	Step A*		Step B**		Step C***		Step D****	
	Abs.	Peak ( $\text{cm}^{-1}$ )	Abs.	Peak ( $\text{cm}^{-1}$ )	Abs.	Peak ( $\text{cm}^{-1}$ )	Abs.	Peak ( $\text{cm}^{-1}$ )
3732	0.14	3731 (s)	0.02	3731	0.07	3740	0.17	—
3680	0.19	—	—	—	—	—	—	—
3650	0.39	3646	0.09	3647	0.06	3646	0.03	—
—	—	3546	0.30	2549	0.03	3554	0.25	—
3417	0.26	3423	0.23	3422	0.03	3428	0.07	—
2958	0.05	2960	0.60	2961	0.05	2960	0.07	—
2927	0.12	2928	0.09	2928	0.07	2929	0.11	—
2853	0.05	2854	0.05	2855	0.04	2853	0.06	—
2832	0.06	—	—	—	—	—	—	—
1620	0.06	—	—	—	—	1601	0.06	—
—	—	1268	0.08	—	—	1266	weak abs.	—

a)  $\text{TiO}_2$  at room temperature and silane vapor pressure 82 torr.\* Heat at  $150^\circ\text{C}$  for two hours under vacuum.\*\* Reaction with  $\text{SiCl}_4$ .\*\*\* Heat at  $150^\circ\text{C}$  for two hours under vacuum.\*\*\*\* Exposed to  $\text{H}_2\text{O}$  vapor for three hours and heated at  $150^\circ\text{C}$  for two hours under vacuum.

Table XIII

Reaction of  $\text{TiO}_2$  with Tetrachlorosilane<sup>a</sup>.

Peak ( $\text{cm}^{-1}$ )	Step A *		Step B **		Step C ***		Step D ****	
	Abs.	Peak ( $\text{cm}^{-1}$ )	Abs.	Peak ( $\text{cm}^{-1}$ )	Abs.	Peak ( $\text{cm}^{-1}$ )	Abs.	Peak ( $\text{cm}^{-1}$ )
3731	0.14	3734 (s)	0.04	3733	0.05	3740	0.36	
3650	0.38	3644 (s)	0.10	3644	0.08	3643	0.06	
—	—	3550	0.64	3550	0.54	3551	0.36	
3419	0.32	3424	0.29	3425	0.15	3427	0.14	
2955	0.10	2959	0.13	2959	0.12	2960	0.15	
2928	0.19	2926	0.12	2927	0.09	2931	0.12	40
2830	0.09	2857	0.05	2857	0.05	2856	0.02	
1619	0.14	1626	0.04	1613	0.03	1600	0.06	
—	—	1260	weak abs.	—	—	1265	0.18	

a)  $\text{TiO}_2$  at 150 C and silane vapor pressure 83 torr.

\* Heat at 150 C for two hours under vacuum.

\*\* Reaction with  $\text{SiCl}_4$ .

\*\*\* Heat at 150 C for two hours under vacuum.

\*\*\*\* Exposed to  $\text{H}_2\text{O}$  vapor for three hours and heated at 150 C for two hours under vacuum.

Table XIV

Reaction of  $\text{TiO}_2$  with Tetrachlorosilane<sup>a</sup>.

Peak ( $\text{cm}^{-1}$ )	Step A *		Step B **		Step C ***	
	Abs.	Peak ( $\text{cm}^{-1}$ )	Abs.	Peak ( $\text{cm}^{-1}$ )	Abs.	Peak ( $\text{cm}^{-1}$ )
3736	0.12	—	—	3741	0.29	—
3675	0.21	—	—	—	—	—
3653	0.25	—	—	—	—	—
—	—	3546	0.09	3554	0.31	—
3419	0.14	—	—	3421	0.03	—
2958	0.06	2961	0.03	2962	0.09	—
2926	0.09	2931	0.04	2930	0.10	—
2855	0.03	2855	0.01	2859	0.02	—
1622	0.02	1605	0.02	1620	0.05	—
—	—	—	—	1266	weak abs.	—

a)  $\text{TiO}_2$  at  $150^\circ\text{C}$  and silane vapor pressure 152 torr.

\* Heating for two hours at  $150^\circ\text{C}$  under vacuum.

\*\* Reaction with  $\text{SiCl}_4$ .

\*\*\* Exposed to  $\text{H}_2\text{O}$  vapor for three hours and heated at  $150^\circ\text{C}$  for two hours under vacuum.

strong Si-OH band at  $3730\text{ cm}^{-1}$  is present after the reaction sequence. This band is not observed in the reactions with mono-, di-, and trichlorosilanes. According to the previous discussion, the multifunctional silanes are less likely to form more than two bonds with the  $\text{TiO}_2$  surface, and it is argued that the third Si-Cl could be condensed with the neighboring Si-OH groups under thermal activation to form Si-O-Si crosslinks. But in the case of  $\text{SiCl}_4$ , there is a fourth Si-Cl bond after the reaction, most probably perpendicular to the  $\text{TiO}_2$  surface, being directed away from any reactive groups. This fourth Si-Cl group is then hydrolyzed to form the free SiOH. In some orientations,  $\text{SiCl}_4$  may undergo total reaction with the four functionalities forming two bonds with the surface and two siloxane bridges with neighboring silane molecules.

#### 2.IV.F Reactions of Methoxy Silanes with $\text{TiO}_2$ surface

As in the case of chlorosilanes, the presence of silane on the surface after the reaction is evident by the enhancement of bands in the C-H stretching region and a strong absorption band in the  $1250\text{ cm}^{-1}$  region. But an infrared spectrum of methoxysilane-reacted  $\text{TiO}_2$  shows several differences compared to the corresponding chlorosilane-reacted sample (20). The disturbed OH peak ( $3540\text{ cm}^{-1}$ ) region is not evident, (Figure 5). Further, this is in contrast with the methoxysilane reactions with silica surfaces reported by Hertl (20,21). The IR spectrum of methoxysilane-reacted  $\text{TiO}_2$  does not show any bands in the  $3350\text{ cm}^{-1}$  region (Figure 6B), whereas silica samples show a broad band in this region, which has been assigned to hydrogen-bonding

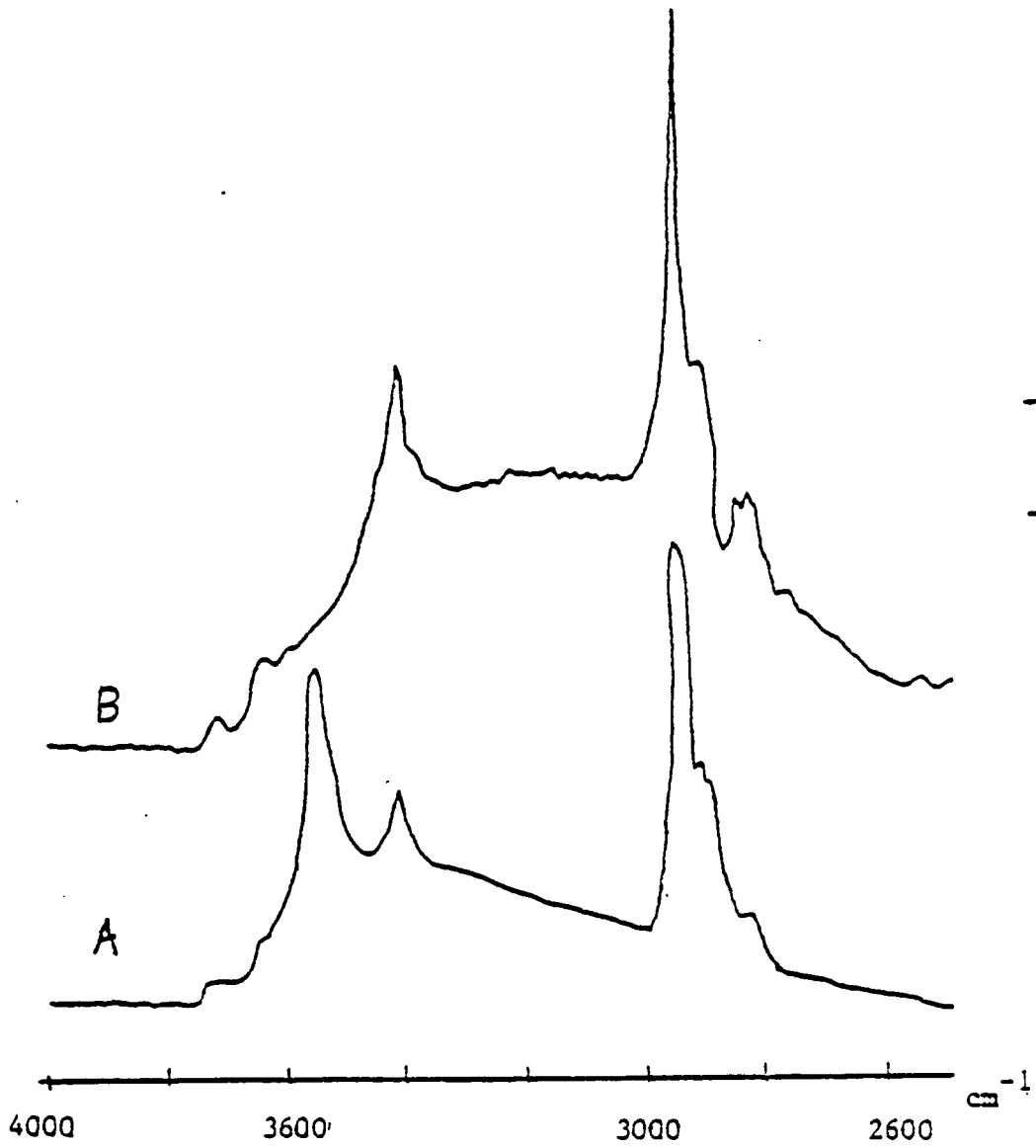


Figure 5: The contrast of chlorosilane( $\text{MeSiCl}$ ) modification (curve A) vs methoxysilane( $\text{MeSi(OMe)}$ ) modification (curve B)

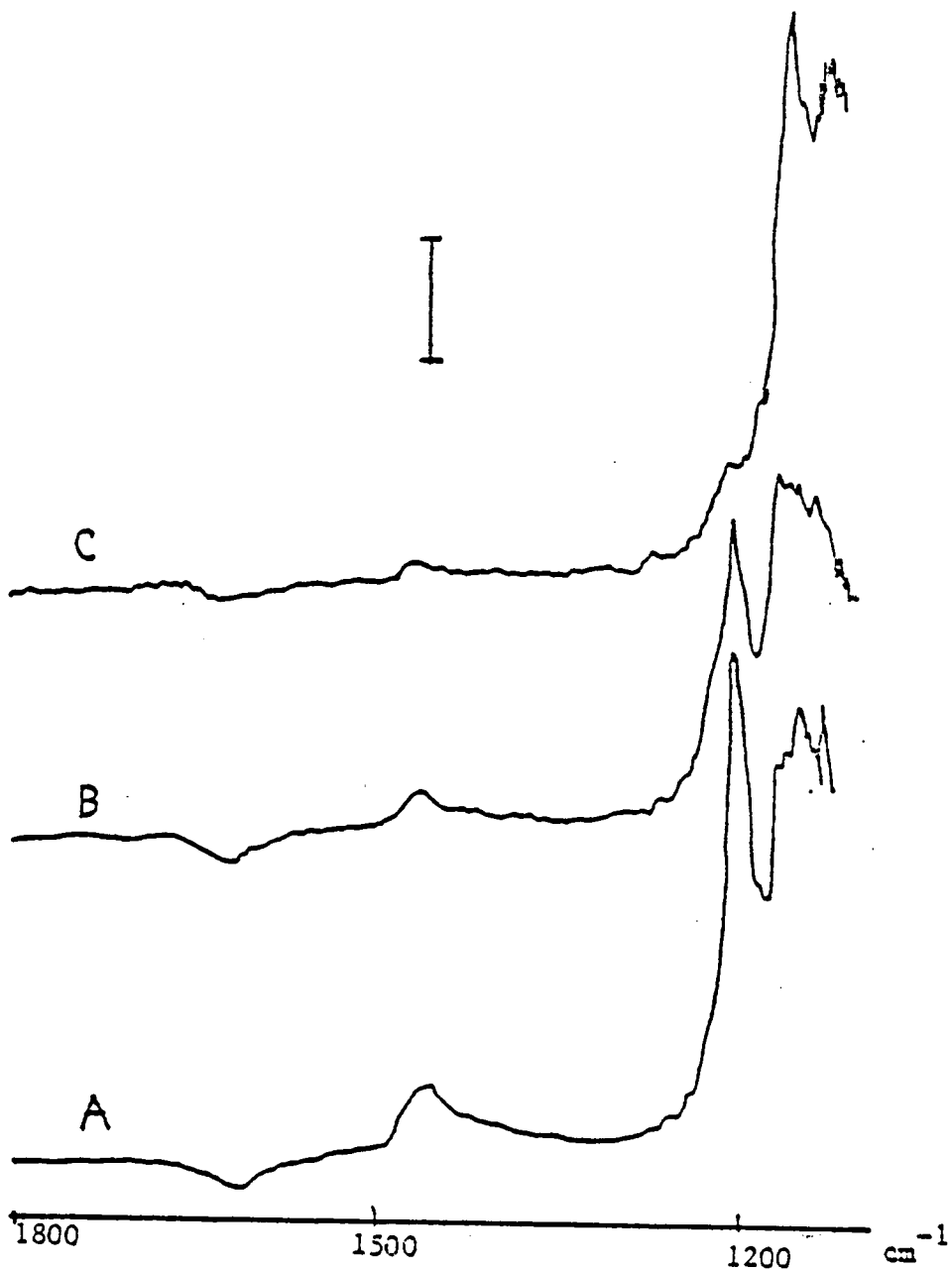


Figure 6: Difference spectra of tetramethoxysilane reacted titanium dioxide, (regime 1). (a) after reaction, (b) after evacuation the pellet at  $150^{\circ}\text{C}$  for 2 hrs, (C) after exposing the sample to moisture for 2 hrs followed by heating under vacuum at  $150^{\circ}\text{C}$  for 2 hrs.



interactions of unreacted MeOH groups with surface OH groups. Next, there is a relatively strong band around the  $2840\text{ cm}^{-1}$  region, in addition to the bands observed in the  $2900\text{--}3000\text{ cm}^{-1}$  region. Similar bands have been observed by Hertl (20,21) after reaction of methoxysilanes with silica. We have tentatively assigned this  $2850\text{ cm}^{-1}$  band to  $\text{Ti-O-CH}_3$ . But the lower intensity observed in this band in the chlorosilane reactions is not quite clear from the extent of peak attenuation in the derivatization reaction. The byproduct HCl reacts with the surface of  $\text{TiO}_2$ , and methanol [byproduct] also reacts with the surface of  $\text{TiO}_2$ . Examination of Tables II-XIV and XV-XXVI reveals that, after the complete reaction sequence, in methoxysilane-reacted surfaces, the regeneration of both the terminal and bridging OH species is more extensive than in the case of chlorosilane reactions. This may be due to the fact that adsorbed methanol is removed from the surface much more easily than adsorbed HCl. [Results of byproduct adsorption will be addressed in a later section.] The reaction of tetramethoxysilane is somewhat parallel to that of tetrachlorosilane, as we have observed residual Si-OH groups after the complete reaction sequence.

In the case of chlorosilanes, the unreacted Si-Cl bands ( $550 - 610\text{ cm}^{-1}$ ) are not observable spectroscopically on  $\text{TiO}_2$ . The methoxysilanes show a characteristic band at  $1190 - 1195\text{ cm}^{-1}$  which is assigned to the Si-O-C moiety. This band is clearly evident in  $\text{Si}(\text{OMe})_4$  reactions (Figure 6A), but not in the methanol adsorption reactions, and it is thermally stable (Figure 6B) and strongly attenuated when the pellet is exposed to water vapor (Figure 6c). All of these facts are consistent

Table XV

Reaction of  $\text{TiO}_2$  with Trimethylmethoxysilane<sup>a</sup>.

Peak ( $\text{cm}^{-1}$ )	Step A*		Step B**		Step C***		Step D****	
	Abs.	Peak ( $\text{cm}^{-1}$ )	Abs.	Peak ( $\text{cm}^{-1}$ )	Abs.	Peak ( $\text{cm}^{-1}$ )	Abs.	Peak ( $\text{cm}^{-1}$ )
3732	0.21	3716	0.05	3731	0.06	3724	0.05	
3676	0.44	—	—	—	—	—	—	—
3651	0.61	3634	0.08	3646	0.14	3647	0.14	
3417	0.32	3417	0.33	3418	0.36	3418	0.36	
—	—	2956	1.39	2956	1.14	2956	0.91	
2922	0.04	2915 (s)	0.44	2901 (s)	0.29	2901	0.19	
2853	0.02	2841	0.15	2847	0.05	2849	0.06	
—	—	2823	0.17	2827	0.24	2828	0.16	
1620	0.20	1621	0.04	1620	0.03	1620	0.06	
—	—	1251	str. abs.	1251	str. abs.	1252	str. abs.	

a)  $\text{TiO}_2$  at room temperature and silane vapor pressure 70 torr.\* Heat at  $150^\circ\text{C}$  for two hours under vacuum.\*\* Reaction with  $\text{Si}(\text{OMe})\text{Me}_3$ .\*\*\* Heat at  $150^\circ\text{C}$  for two hours under vacuum.\*\*\*\* Exposed to  $\text{H}_2\text{O}$  vapor and heated for two hours under vacuum.

Table XVI

Reaction of  $\text{TiO}_2$  with Trimethylmethoxysilane<sup>a</sup>.

Peak ( $\text{cm}^{-1}$ )	Step A *		Step B **		Step C ***		Step D ****	
	Abs.	Peak ( $\text{cm}^{-1}$ )	Abs.	Peak ( $\text{cm}^{-1}$ )	Abs.	Peak ( $\text{cm}^{-1}$ )	Abs.	Peak ( $\text{cm}^{-1}$ )
3731	0.20	3718	0.02	3717	0.02	3718	0.02	3718
3650	0.61	3645	0.14	3646	0.16	3646	0.16	3646
3417	0.46	3417	0.36	3417	0.44	3419	0.48	3419
2952	0.01	2956	0.78	2956	0.64	2957	0.62	2957
2922	0.03	2933 (s)	0.37	2930	0.35	2931	0.25	2931
—	—	2900 (s)	0.24	2902	0.20	2900	0.14	2900
2852	0.02	2846	0.05	—	—	2853	0.02	2853
—	—	2826	0.16	2826	0.16	2829	0.06	2829
1619	0.12	1625	0.02	—	—	1621	0.05	1621
—	—	1252	str. abs.	1252	str. abs.	1251	str. abs.	1251

a)  $\text{TiO}_2$  at  $150^\circ\text{C}$  and silane vapor pressure 70 torr.\* Heat at  $150^\circ\text{C}$  for two hours under vacuum.\*\* Reaction with  $\text{Si}(\text{OMe})\text{Me}_3$ .\*\*\* Heat at  $150^\circ\text{C}$  for two hours under vacuum.\*\*\*\* Exposed to  $\text{H}_2\text{O}$  vapor for three hours and heated at  $150^\circ\text{C}$  for two hours under vacuum.

Table XVII

Reaction of  $\text{TiO}_2$  with Trimethylmethoxysilane<sup>a</sup>:

Peak ( $\text{cm}^{-1}$ )	Step A*		Step B**		Step C***	
	Abs.	Peak ( $\text{cm}^{-1}$ )	Abs.	Peak ( $\text{cm}^{-1}$ )	Abs.	Peak ( $\text{cm}^{-1}$ )
3731.	0.18	3716	0.02	3729	0.02	3729
3650	0.42	3646	0.07	3647	0.16	3647
3418	0.41	3417	0.40	3417	0.33	3417
2957	0.06	2956	0.65	2957	0.46	2957
2925	0.10	2930	0.42	2930	0.22	2930
2854	0.06	2843	0.04	2852	0.03	2852
—	—	2823	0.18	2979	0.08	2979
1620	0.08	—	—	1621	0.03	1621
—	—	1250	0.59	1251	0.45	1251

a)  $\text{TiO}_2$  at  $150^\circ\text{C}$  and silane vapor pressure 140 torr.\* Heat at  $150^\circ\text{C}$  for two hours under vacuum.\*\* Reaction with  $\text{Si}(\text{OMe})\text{Me}_3$ .\*\*\* Exposed to  $\text{H}_2\text{O}$  vapor for three hours and heated for two hours at  $150^\circ\text{C}$  under vacuum.

Table XVIII

Reaction of  $\text{TiO}_2$  with Dimethyldimethoxysilane<sup>a</sup>.

Peak ( $\text{cm}^{-1}$ )	Step A*		Step B**		Step C***		Step D****	
	Abs.	Peak ( $\text{cm}^{-1}$ )	Abs.	Peak ( $\text{cm}^{-1}$ )	Abs.	Peak ( $\text{cm}^{-1}$ )	Abs.	Peak ( $\text{cm}^{-1}$ )
3731	0.30	3715	0.03	3721	0.03	3722	0.03	3722
3652	0.56	3602	0.06	3648	0.06	3646	0.07	3646
3418	0.38	3421	0.25	3421	0.18	3419	0.21	3419
2955	0.05	2960	0.54	2963	0.34	2963	0.29	2963
2928	0.10	2918	0.39	2928	0.15	2933	0.17	2933
2854	0.04	—	—	—	—	—	—	—
2836	0.04	2838	0.07	—	—	2830	0.06	2830
—	—	2820	0.17	—	—	—	—	—
1620	0.06	—	—	—	—	—	—	—
—	—	1258	str. abs.	1258	str. abs.	1259	str. abs.	1259

a)  $\text{TiO}_2$  at room temperature and silane vapor pressure 24 torr.\* Heat at  $150^\circ\text{C}$  for two hours under vacuum.

\*\* Reaction with silane.

\*\*\* Heat at  $150^\circ\text{C}$  for two hours under vacuum.\*\*\*\* Exposed to  $\text{H}_2\text{O}$  vapor for three hours and heated at  $150^\circ\text{C}$  for two hours under vacuum.

Table XIX

Reaction of  $\text{TiO}_2$  with Dimethyldimethoxysilane<sup>a</sup>.

Peak ( $\text{cm}^{-1}$ )	Step A *		Step B **		Step C ***		Step D ****	
	Abs.	Peak ( $\text{cm}^{-1}$ )	Abs.	Peak ( $\text{cm}^{-1}$ )	Abs.	Peak ( $\text{cm}^{-1}$ )	Abs.	Peak ( $\text{cm}^{-1}$ )
3733	0.17	3725	0.02	3718	0.02	3721	0.02	3721
3681	0.24	—	—	—	—	—	—	—
3652	0.35	3618	0.02	3621	0.02	3644	0.03	3644
3418	0.15	3423	0.13	3424	0.11	3423	0.13	3423
2958	0.03	2962	0.65	2962	0.66	2962	0.37	2962
2925	0.05	2928	0.61	2928	0.53	2932	0.20	2932
—	—	2910	0.63	2909	0.54	2911	0.13	2911
2855	0.02	—	—	—	—	—	—	—
—	—	2822	0.43	2823	0.37	2829	0.10	2829
—	—	2807	0.29	2809	0.23	—	—	—
1618	0.06	—	—	—	—	—	—	—
—	—	1258	str. abs.	1254	str. abs.	1259	str. abs.	1259

a)  $\text{TiO}_2$  at  $150^\circ\text{C}$  and silane vapor pressure 24 torr.\* Heat at  $150^\circ\text{C}$  for two hours under vacuum.

\*\* Reaction with silane.

\*\*\* Heat at  $150^\circ\text{C}$  for two hours under vacuum.\*\*\*\* Exposed to  $\text{H}_2\text{O}$  vapor for three hours and heated at  $150^\circ\text{C}$  for two hours under vacuum.

Table XX  
Reaction of  $\text{TiO}_2$  with Dimethyldimethoxysilane<sup>a</sup>

Peak ( $\text{cm}^{-1}$ )	Step A <sup>*</sup>		Step B <sup>**</sup>		Step C <sup>***</sup>	
	Abs.	Peak ( $\text{cm}^{-1}$ )	Abs.	Peak ( $\text{cm}^{-1}$ )	Abs.	Peak ( $\text{cm}^{-1}$ )
3731	0.09	3715	0.01	3719	0.01	0.01
3648	0.20	3605	0.01	3648	0.05	0.05
3419	0.11	3423	0.08	3421	0.08	0.08
2958	0.05	2961	0.44	2962	0.29	0.29
2926	0.12	2927	0.38	2929	0.19	0.19
2854	0.05	—	—	2855	0.07	0.07
—	—	2821	0.18	2830	0.04	0.04
1618	0.08	—	—	1625	0.02	0.02
—	—	1258	str. abs.	1259	str. abs.	str. abs.

a)  $\text{TiO}_2$  at  $150^\circ\text{C}$  and silane vapor pressure 50 torr.

\* Heat at  $150^\circ\text{C}$  for two hours under vacuum.

\*\* Reaction with silane.

\*\*\* Exposed to  $\text{H}_2\text{O}$  vapor for three hours and heated at  $150^\circ\text{C}$  for two hours under vacuum.

Table XXI

Reaction of  $\text{TiO}_2$  with Methyltrimethoxysilane<sup>a</sup>.

Peak ( $\text{cm}^{-1}$ )	Step A*		Step B**		Step C***		Step D****	
	Abs.	Peak ( $\text{cm}^{-1}$ )	Abs.	Peak ( $\text{cm}^{-1}$ )	Abs.	Peak ( $\text{cm}^{-1}$ )	Abs.	Peak ( $\text{cm}^{-1}$ )
3729	0.12	3716	0.02	3721	0.03	3733	0.03	3733
3650	0.29	3623	0.06	3642	0.06	3646	0.07	3646
3417	0.24	3418	0.23	3417	0.16	3417	0.13	3417
2957	0.04	2963	0.31	2967	0.17	2970	0.10	2970
—	—	2948	0.47	2946	0.21	—	—	—
2925	0.07	2925	0.34	2916	0.23	2925	0.11	2925
2853	0.03	2840	0.26	2841	0.10	2852	0.03	2852
—	—	2817	0.12	2823	0.13	2828	0.05	2828
1619	0.05	—	—	—	—	—	—	—
—	—	1263	str. abs.	1264	str. abs.	1267	str. abs.	1267

a)  $\text{TiO}_2$  at room temperature and silane vapor pressure 7 torr.\* Heat at  $150^\circ\text{C}$  for two hours under vacuum.

\*\* Reaction with silane.

\*\*\* Heat at  $150^\circ\text{C}$  for two hours under vacuum.\*\*\*\* Exposed to  $\text{H}_2\text{O}$  vapor for three hours and heated at  $150^\circ\text{C}$  for two hours under vacuum.



Table XXII

Reaction of  $\text{TiO}_2$  with Methyltrimethoxysilane<sup>a</sup>.

Step A *		Step B **		Step C ***		Step D ****	
Peak ( $\text{cm}^{-1}$ )	Abs.	Peak ( $\text{cm}^{-1}$ )	Abs.	Peak ( $\text{cm}^{-1}$ )	Abs.	Peak ( $\text{cm}^{-1}$ )	Abs.
3731	0.15	3732	0.02	3719	0.02	3728	0.03
3680	0.20	—	—	—	—	—	—
3649	0.38	3625	0.02	—	—	3642	0.04
3416	0.27	3420	0.02	3419	0.15	3420	0.17
2956	0.05	2965	0.41	2966	0.36	2970	0.17
—	—	2943	0.55	2944	0.43	—	—
2924	0.10	2920	0.52	2915	0.45	2925	0.18
2852	0.06	2839	0.37	2840	0.24	2850	0.06
—	—	2821	0.25	2821	0.24	2828	0.08
1618	0.05	—	—	—	—	1624	0.02
—	—	1261	str. abs.	1262	str. abs.	1266	str. abs.

a)  $\text{TiO}_2$  at  $150^\circ\text{C}$  and silane vapor pressure 7 torr.

\* Heat at  $150^\circ\text{C}$  for two hours under vacuum.

\*\* Reaction with silane.

\*\*\* Heat at  $150^\circ\text{C}$  for two hours under vacuum.

\*\*\*\* Exposed to  $\text{H}_2\text{O}$  vapor for three hours and heated at  $150^\circ\text{C}$  for two hours under vacuum.

Table XXIII

Reaction of  $\text{TiO}_2$  with Methyltrimethoxysilane<sup>a</sup>

Peak ( $\text{cm}^{-1}$ )	Step A *		Step B **		Step C ***	
	Abs.	Peak ( $\text{cm}^{-1}$ )	Abs.	Peak ( $\text{cm}^{-1}$ )	Abs.	Peak ( $\text{cm}^{-1}$ )
3730	0.15	3716	0.01	3727	0.02	3727
3649	0.35	3612	0.04	3644	0.02	3644
3415	0.27	3420	0.18	3420	0.15	3420
2956	0.05	2944	0.48	2971	0.17	2971
2924	0.12	2915	0.46	2926	0.17	2926
2854	0.06	2840	0.34	2850	0.06	2850
—	—	2821	0.22	2829	0.07	2829
1619	0.04	—	—	1634	0.01	1634
—	—	1265	str. abs.	1268	str. abs.	1268

a)  $\text{TiO}_2$  at  $150^\circ\text{C}$  and silane vapor pressure 16 torr.\* Heat at  $150^\circ\text{C}$  for two hours under vacuum.

\*\* Reaction with silane.

\*\*\* Exposed to  $\text{H}_2\text{O}$  vapor for three hours and heated at  $150^\circ\text{C}$  for two hours under vacuum.

Table XXIV

Reaction of  $\text{TiO}_2$  with Tetramethoxysilane<sup>a</sup>.

Step A *		Step B **		Step C ***		Step D ****	
Peak ( $\text{cm}^{-1}$ )	Abs.	Peak ( $\text{cm}^{-1}$ )	Abs.	Peak ( $\text{cm}^{-1}$ )	Abs.	Peak ( $\text{cm}^{-1}$ )	Abs.
3731	0.12	—	—	3722	0.02	3735	0.25
3651	0.29	3628	0.02	3641	0.03	3649	0.05
3417	0.18	3421	0.15	3416	0.09	3419	0.12
2960	0.04	2942	0.70	2950	0.47	2955	0.14
2926	0.08	—	—	2930	0.27	2931	0.16
2855	0.05	2845	0.65	2844	0.39	2853	0.10
—	—	—	—	2826	0.12	2832	0.08
1618	0.05	—	—	—	—	1622	0.03
—	—	1458	0.10	1459	0.06	1458	0.04

a)  $\text{TiO}_2$  at room temperature and silane vapor pressure 1 torr.

\* Heat at  $150^\circ\text{C}$  for two hours under vacuum.

\*\* Reaction with silane.

\*\*\* Heat at  $150^\circ\text{C}$  for two hours under vacuum.

\*\*\*\* Exposed to  $\text{H}_2\text{O}$  vapor for three hours and heated at  $150^\circ\text{C}$  for two hours under vacuum.

Table XXV

Reaction of  $\text{TiO}_2$  with Tetramethoxysilane<sup>a</sup>.

Peak ( $\text{cm}^{-1}$ )	Step A *		Step B **		Step C **		Step D ****		
	Abs.	Peak ( $\text{cm}^{-1}$ )	Abs.	Peak ( $\text{cm}^{-1}$ )	Abs.	Peak ( $\text{cm}^{-1}$ )	Abs.	Peak ( $\text{cm}^{-1}$ )	
3733	0.13	—	—	—	—	—	—	3734	0.31
3652	0.28	—	—	—	—	—	—	3645	0.02
3417	0.25	3421	0.14	3420	0.08	—	—	3421	0.12
2958	0.03	2949	0.79	—	—	—	—	2954	0.15
2948	0.03	—	—	2949	0.68	—	—	—	—
2927	0.06	2925 (s)	0.36	2925 (s)	0.32	—	—	—	—
2856	0.03	2845	0.20	2846	0.58	—	—	2851	0.09
—	—	2826 (s)	0.14	2824 (s)	0.13	—	—	2831	0.06
1620	0.05	—	—	—	—	—	—	1618	0.03
—	—	1460	0.12	1457	0.11	—	—	1451	0.03

a)  $\text{TiO}_2$  at  $150^\circ\text{C}$  and silane vapor pressure 1 torr.\* Heat at  $150^\circ\text{C}$  for two hours under vacuum.

\*\* Reaction with silane.

\*\*\* Heat at  $150^\circ\text{C}$  for two hours under vacuum.\*\*\*\* Exposed to  $\text{H}_2\text{O}$  vapor for three hours and heated at  $150^\circ\text{C}$  for two hours under vacuum.

Table XXVI

Reaction of  $\text{TiO}_2$  with Tetramethoxysilane<sup>a</sup>.

Peak ( $\text{cm}^{-1}$ )	Step A*		Step B**		Step C***	
	Abs.	Peak ( $\text{cm}^{-1}$ )	Abs.	Peak ( $\text{cm}^{-1}$ )	Abs.	Peak ( $\text{cm}^{-1}$ )
3731	0.11	—	—	3735	0.28	—
3651	0.30	—	—	3646	0.03	—
3419	0.21	3423	0.15	3423	0.12	—
2954	0.04	2450	0.81	2954	0.19	—
2928	0.07	2927 (s)	0.38	2931	0.13	—
2854	0.04	—	—	2852	0.09	—
—	—	—	—	2830	0.04	—
1618	0.06	—	—	1623	0.02	—
—	—	1458	0.14	—	—	—

a)  $\text{TiO}_2$  at  $150^\circ\text{C}$  and silane vapor pressure 6 torr.\* Heat at  $150^\circ\text{C}$  for two hours under vacuum.

\*\* Reaction with silane.

\*\*\* Exposure to  $\text{H}_2\text{O}$  vapor for three hours and heated at  $150^\circ\text{C}$  for two hours under vacuum.

with the assignment of this band to the Si-O-C moiety. Pellets reacted with  $\text{MeSi(OMe)}_3$  and  $\text{Si(OMe)}_4$  show this peak, but it is not distinguishable on a pellet reacted with  $\text{Me}_2\text{Si(OMe)}_2$  or  $\text{Me}_3\text{Si(OMe)}$ .

The infrared data obtained for methoxysilane reactions are presented in the Tables XV to XXVI.

#### 2.IV.G TiO<sub>2</sub> Reaction with HMDS

The attenuation of the terminal OH band during this reaction shows that hexamethyldisilazane (HMDS) is almost as good as chlorosilanes in surface derivatization and is a more potent reagent than methoxysilanes. It is difficult to determine the fate of bridging OH groups due to the strong overlap of N-H absorption bands in this region ( $3100\text{--}3850\text{ cm}^{-1}$ ) (Figure 7). The presence of the  $-\text{Si(Me)}_3$  group after the reaction sequence is evident due to the enhancement of the absorption bands in the  $2900\text{--}3000\text{ cm}^{-1}$  region and strong absorption in the  $1250\text{ cm}^{-1}$  region.

#### 2.IV.H Reactions of HCl with TiO<sub>2</sub> surfaces

All the derivatization reactions with chlorosilanes yield the by-product HCl. In our work as well as other workers (8,9), we have shown that HCl adsorption causes attenuation of both terminal and bridging OH species, and the appearance of absorption bands at  $3550\text{ cm}^{-1}$  and  $1600\text{ cm}^{-1}$  region, accompanied with enhancement of the broad envelope due to hydrogen-bonded OH species. The latter two observations suggest the formation of water adsorbed on the surface during the reaction. Jones

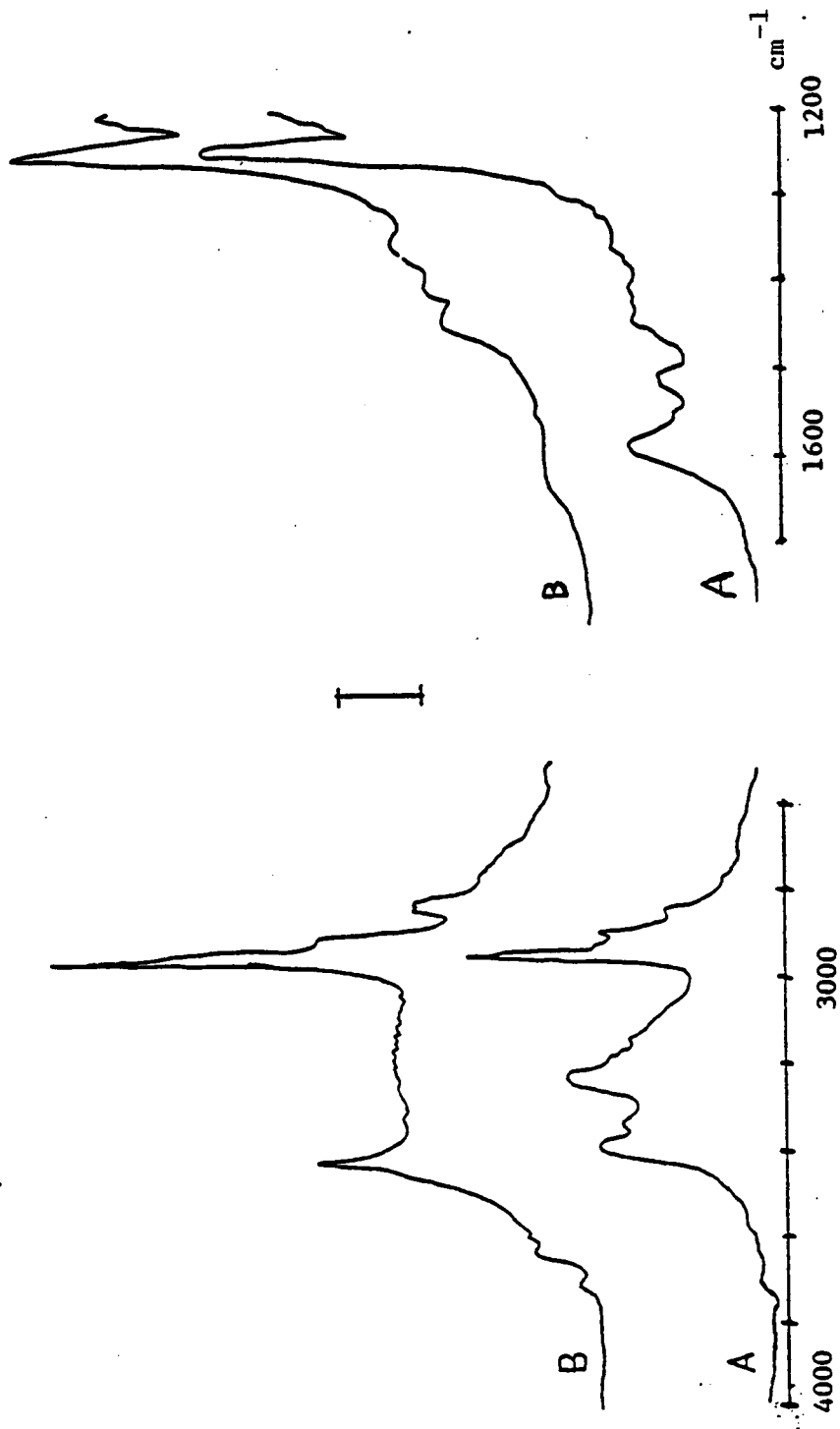


Figure 7: IR spectra of TiO<sub>2</sub> modified with HMDS and Me<sub>3</sub>SiOMe using regime 1:  
(A) HMDS (V.P. 1 torr), (B) Me<sub>3</sub>OMeSi (V.P. 70 torr), Bar 0.3 abs.

Table XXVII-A

Reaction of  $TiO_2$  with Hexamethyldisilazane<sup>a</sup>

Step A*		Step B**		Step C***	
Peak ( $cm^{-1}$ )	Abs.	Peak ( $cm^{-1}$ )	Abs.	Peak ( $cm^{-1}$ )	Abs.
3737	0.14	3714	0.02	3722	0.02
3677	0.19	—	—	—	—
3652	0.31	—	—	3640	0.03
3417	0.18	—	—	3424	0.13
—	—	3396	0.19	3380	0.03
—	—	3344	0.09	3346	0.02
—	—	3239	0.29	—	—
—	—	3152	0.09	3156	0.03
2959	0.06	2954	0.55	2957	0.46
2927	0.13	2927	0.25	—	—
—	—	2900	0.25	2901	0.17
2854	0.04	2854	0.11	—	—
2836	0.05	—	—	—	—
—	—	1595	0.18	1598	0.10



Table XXVII-F

Reaction of  $\text{TiO}_2$  with Hexamethyldisilazane<sup>a</sup>

Step A	Step B	Step C
Peak ( $\text{cm}^{-1}$ )	Peak ( $\text{cm}^{-1}$ )	Peak ( $\text{cm}^{-1}$ )
—	1520	1510
—	1455	1453
—	1415	1415
—	1258	1260
Abs.	Abs.	Abs.
—	0.06	weak abs.
—	weak abs.	weak abs.
—	weak abs.	weak abs.
—	str. abs.	str. abs.

a)  $\text{TiO}_2$  at room temperature and silane vapor pressure 1 torr.

\* Heat at  $150^\circ\text{C}$  for two hours under vacuum.

\*\* Reaction with HMDS.

\*\*\* Exposed to  $\text{H}_2\text{O}$  vapor for three hours and heated at  $150^\circ\text{C}$  for two hours under vacuum.

Table XXVIII-A

Reaction of  $TiO_2$  with Hexamethyldisilazane<sup>a</sup>

Step A <sup>*</sup>		Step B <sup>**</sup>		Step C <sup>***</sup>	
Peak ( $cm^{-1}$ )	Abs.	Peak ( $cm^{-1}$ )	Abs.	Peak ( $cm^{-1}$ )	Abs.
3739	0.06	—	—	—	—
3646	0.09	—	—	—	—
3417	0.24	3420	0.09	3422	0.11
—	—	—	—	3359	0.01
—	—	3242	0.03	3243	0.03
—	—	3156	0.01	3162	0.01
—	—	3145	0.03	—	—
2952 (s)	0.14	2953	0.47	2955	0.50
2927	0.34	2928	0.23	2928	0.24
2899 (s)	0.06	2898	0.19	2900	0.20
2850 (s)	0.09	—	—	—	—
2829	0.25	2826	0.10	2829	0.08
—	—	1598	0.10	1595	0.07
—	—	1520	weak abs.	—	—

Table XVIII-D

Reaction of  $\text{TiO}_2$  with Hexamethyldisilazane<sup>a</sup>

Step A*	Step B**	Step C***
Peak ( $\text{cm}^{-1}$ )	Peak ( $\text{cm}^{-1}$ )	Peak ( $\text{cm}^{-1}$ )
Abs. —	Abs. weak abs.	Abs. weak abs.
1450	1410	1449
1410	1251	1410
1251	str. abs.	1251
—	—	str. abs.

a)  $\text{TiO}_2$  at  $150^\circ\text{C}$  and silane vapor pressure 1 torr.

\* Heat at  $150^\circ\text{C}$  for two hours under vacuum.

\*\* Reaction with silane.

\*\*\* Heat at  $150^\circ\text{C}$  for two hours under vacuum.

Table XXIX-A

Reaction of  $\text{TiO}_2$  with Hexamethyldisilazane<sup>a</sup>

Step A *		Step B **		Step C ***		Step D ****	
Peak ( $\text{cm}^{-1}$ )	Abs.	Peak ( $\text{cm}^{-1}$ )	Abs.	Peak ( $\text{cm}^{-1}$ )	Abs.	Peak ( $\text{cm}^{-1}$ )	Abs.
3731	0.15	3712	0.01	—	—	—	—
3681	0.21	—	—	—	—	—	—
3649	0.35	3630	0.01	—	—	3640	0.06
3416	0.23	3421	0.06	3421	0.02	3425	0.13
—	—	3379	0.03	3376	0.02	—	—
—	—	3346	0.02	—	—	—	—
—	—	—	—	3232	0.02	3245	0.02
—	—	3152	0.03	3143	0.01	—	—
2955	0.11	2955	0.65	2957	0.49	2958	0.51
2927	0.21	2927	0.22	—	—	—	—
—	—	2900	0.27	2901	0.19	2902	0.18
2854	0.12	2857	0.07	2855	0.06	2855	0.06
2836	0.09	—	—	—	—	—	—
1619	0.07	—	—	1600	0.06	—	—

Table XXIX-B

Reaction of  $\text{TiO}_2$  with Hexamethyldisilazane<sup>a</sup>

Peak ( $\text{cm}^{-1}$ )	Step A *		Step B **		Step C ***		Step D ****	
	Abs.	Peak ( $\text{cm}^{-1}$ )	Abs.	Peak ( $\text{cm}^{-1}$ )	Abs.	Peak ( $\text{cm}^{-1}$ )	Abs.	Peak ( $\text{cm}^{-1}$ )
—	—	1598	0.17	—	—	1595	0.03	—
—	—	1517	weak abs.	—	—	—	—	—
—	—	1453	weak abs.	1451	weak abs.	1446	weak abs.	—
1419	0.02	1409	0.07	1406	0.04	1408	0.04	—
—	—	1251	str. abs.	1254	str. abs.	1258	str. abs.	—

a)  $\text{TiO}_2$  at  $150^\circ\text{C}$  and silane vapor pressure 6 torr.

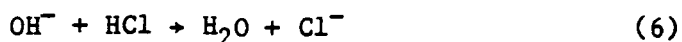
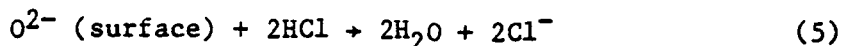
\* Heat at  $150^\circ\text{C}$  for two hours under vacuum.

\*\* Reaction with silane.

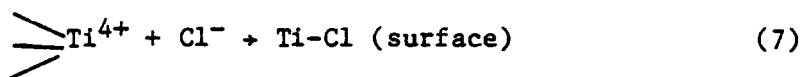
\*\*\* Heat at  $150^\circ\text{C}$  for two hours under vacuum.

\*\*\*\* Exposed to  $\text{H}_2\text{O}$  vapor for three hours and heated at  $150^\circ\text{C}$  for two hours under vacuum.

and Hockey (9) have proposed the following reaction schemes to account for this observation:



The coordinatively unsaturated  $\text{Ti}^{4+}$  ions generated in these reactions in turn can capture  $\text{Cl}^-$  as shown in the following reaction:



Repeated attempts to regenerate the original surface by hydrolysis (exposure to moisture) and dehydroxylation (thermal treatment  $150^\circ\text{C}$ ) was a failure. The observed intensity of both terminal and bridging OH groups is only a fraction of what they were originally. This can be explained by the surface dehydroxylation and Ti-Cl formation as shown in the equations. Further, it may be that Ti-Cl bonds are resistant to hydrolysis under moderate conditions.

The observed data on the HCl adsorption process are presented in Tables XXX and XXXI. The examination of OH absorption bands, in these tables, before and after the reaction scheme, indicates that the surface perturbation caused by HCl adsorption/reaction is rather severe and due to this reason it is more difficult to regenerate the original surface.

Table XXX

Reaction of  $\text{TiO}_2$  with Hydrogen Chloride<sup>a</sup>.

Peak ( $\text{cm}^{-1}$ )	Step A *		Step B **		Step C ***		Step D ****	
	Abs.	Peak ( $\text{cm}^{-1}$ )	Abs.	Peak ( $\text{cm}^{-1}$ )	Abs.	Peak ( $\text{cm}^{-1}$ )	Abs.	Peak ( $\text{cm}^{-1}$ )
3732	0.19	3745	0.04	3734	0.06	3731	0.04	
3651	0.43	3649	0.11	3650	0.16	3650	0.10	
—	—	3553	0.46	3553	0.24	—	—	
3418	0.33	3417	0.08	3419	0.29	3422	0.10	
2957	0.08	2959	0.05	2959	0.05	2957	0.04	
2927	0.16	2926	0.08	2929	0.09	2932	0.08	
2854	0.08	2855	0.04	2855	0.04	2853	0.04	
1615	0.04	1601	0.20	1600	0.12	1611	0.04	

a)  $\text{TiO}_2$  at room temperature under HCl vapor pressure of 85 torr.\* Heat at  $150^\circ\text{C}$  for two hours under vacuum.

\*\* Reaction with HCl.

\*\*\* Heat at  $150^\circ\text{C}$  for two hours under vacuum.\*\*\*\* Heat two hours at  $150^\circ\text{C}$  under vacuum.

Table XXXI

Reaction of  $\text{TiO}_2$  with Hydrogen Chloride<sup>a</sup>.

Peak ( $\text{cm}^{-1}$ )	Step A *		Step B **		Step C ***		Step D ****	
	Abs.	Peak ( $\text{cm}^{-1}$ )	Abs.	Peak ( $\text{cm}^{-1}$ )	Abs.	Peak ( $\text{cm}^{-1}$ )	Abs.	Peak ( $\text{cm}^{-1}$ )
3730	0.17	3742	0.02	3734	0.03	3728	0.05	—
3678	0.19	—	—	—	—	—	—	—
3650	0.41	—	—	—	—	3643 (s)	0.06	—
—	—	3552	0.54	3553	0.34	3556	0.11	—
3417	0.38	—	—	—	—	—	—	—
2958	0.02	2958	0.06	2959	0.06	2960	0.05	—
2927	0.05	2938	0.04	2933	0.05	2932	0.08	—
2854	0.02	2853	0.02	2856	0.03	2838	0.03	—
1618	0.07	—	—	1601	0.12	1600	0.19	—
—	—	1598	0.13	—	—	—	—	—

a)  $\text{TiO}_2$  at  $150^\circ\text{C}$  and  $\text{HCl}$  vapor pressure 152 torr.

\* Heat at  $150^\circ\text{C}$  for two hours under vacuum.

\*\* Reaction with  $\text{HCl}$ .

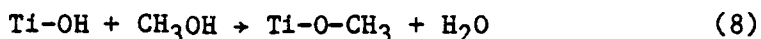
\*\*\* Heat at  $150^\circ\text{C}$  for two hours under vacuum.

\*\*\*\* Exposed to  $\text{H}_2\text{O}$  vapor for three hours and heated at  $150^\circ\text{C}$  for two hours under vacuum.



#### 2.IV.I Reaction of Methanol with TiO<sub>2</sub> Surface

The byproduct of methoxy-silane reactions, MeOH, also reacts with TiO<sub>2</sub> surfaces. In our studies of methanol adsorption on the TiO<sub>2</sub> surface, we have observed a multitude of C-H stretching bands at 2980, 2890, and 2820 cm<sup>-1</sup>. These peaks are stable even after heating the reacted surface at 150°C. This may be due to the chemisorption reaction of methanol with surface OH species as shown in the following equation.



But in contrast to the case of HCl adsorption, neither the band around 1600 cm<sup>-1</sup> nor the hydrogen-bonding envelope in the 3500 cm<sup>-1</sup> region show any enhancement of intensity. In fact, the 1610 cm<sup>-1</sup> band attenuation shows some loss of adsorbed water which is on the surface. But this seems to be a reversible phenomenon since when the methanol-adsorbed sample is exposed to moisture for a couple of days, and re-evacuated at 150°C, the original surface is produced almost completely. Therefore, the methanol adsorption does not cause irreversible effects on TiO<sub>2</sub> surface as it does by HCl adsorption. The pertinent data on MeOH adsorption is presented in Tables XXXII to XXXIV.

#### 2.IV.J Reaction of NH<sub>3</sub> with TiO<sub>2</sub> surface

The reaction byproduct in HMDS reactions is NH<sub>3</sub>. In the subsequent experiments we have observed that NH<sub>3</sub> also can undergo reactions with surface OH groups, though to a lesser extent than HCl or MeOH. The

Table XXXII

Reaction of  $\text{TiO}_2$  with Methanol<sup>a</sup>.

Peak ( $\text{cm}^{-1}$ )	Step A *		Step B **		Step C ***		Step D ****	
	Abs.	Peak ( $\text{cm}^{-1}$ )	Abs.	Peak ( $\text{cm}^{-1}$ )	Abs.	Peak ( $\text{cm}^{-1}$ )	Abs.	Peak ( $\text{cm}^{-1}$ )
3729	0.15	3721	0.04	3723	0.05	3729	0.07	3729
3650	0.44	3647	0.17	3648	0.19	3649	0.18	3649
3417	0.40	3416	0.48	3417	0.34	3419	0.38	3419
—	—	2947	0.54	2948	0.27	2953	0.18	2953
2925	0.04	2923	0.57	2923	0.46	2928	0.34	2928
2854	0.02	2843	0.14	2847	0.07	2850	0.05	2850
—	—	2817	0.44	2823	0.40	2829	0.23	2829
1620	0.07	1625	0.04	—	—	1624	0.03	1624
—	—	1436	weak abs.	1435	weak abs.	1439	weak abs.	1439
—	—	1359	weak abs.	1359	weak abs.	1365	weak abs.	1365

a)  $\text{TiO}_2$  at room temperature and methanol vapor pressure 36 torr.\* Heat at  $150^\circ\text{C}$  for two hours under vacuum.

\*\* Reaction with methanol.

\*\*\* Heat at  $150^\circ\text{C}$  for two hours under vacuum.\*\*\*\* Exposed to  $\text{H}_2\text{O}$  vapor for three hours and heated at  $150^\circ\text{C}$  for two hours under vacuum.

Table XXXIII

Reaction of  $\text{TiO}_2$  with Methanol<sup>a</sup>.

Peak ( $\text{cm}^{-1}$ )	Step A*		Step B**		Step C***		Step D****	
	Abs.	Peak ( $\text{cm}^{-1}$ )	Abs.	Peak ( $\text{cm}^{-1}$ )	Abs.	Peak ( $\text{cm}^{-1}$ )	Abs.	Peak ( $\text{cm}^{-1}$ )
3725	0.15	3731	0.01	3726	0.02	3729	0.12	—
3676	0.18	—	—	—	—	—	—	—
3645	0.34	3646	0.16	3648	0.15	3648	0.29	—
3413	0.27	3417	0.32	3416	0.27	3416	0.03	—
2955	0.03	2945	0.45	2945	0.32	2956	0.08	—
2921	0.06	2923	0.63	2924	0.55	2930	0.16	—
2868	0.02	2887	0.19	2892	0.14	—	—	—
2850	0.03	2841	0.15	2842	0.11	2855	0.06	—
—	—	2817	0.51	2821	0.47	2832	0.08	—
1619	0.05	—	—	—	—	1623	0.03	—
—	—	1460	weak abs.	1440	weak abs.	—	—	—
—	—	1352	weak abs.	1364	weak abs.	—	—	—

a)  $\text{TiO}_2$  at  $150^\circ\text{C}$  and methanol vapor pressure 73 torr.

\* Heat at  $150^\circ\text{C}$  for two hours under vacuum.

\*\* Reaction with methanol.

\*\*\* Heat at  $150^\circ\text{C}$  for two hours under vacuum.

\*\*\*\* Exposed to moisture for two days and evacuated at  $150^\circ\text{C}$  for two hours.

Table XXXIV

Reaction of  $\text{TiO}_2$  with Methanol<sup>a</sup>.

Step A *		Step B **		Step C ***		Step D ****	
Peak ( $\text{cm}^{-1}$ )	Abs.	Peak ( $\text{cm}^{-1}$ )	Abs.	Peak ( $\text{cm}^{-1}$ )	Abs.	Peak ( $\text{cm}^{-1}$ )	Abs.
3732	0.18	3733	0.02	3731	0.02	3730	0.08
3680	0.26	—	—	—	—	—	—
3650	0.40	3647	0.08	3646	0.06	3645	0.07
3418	0.23	3419	0.23	3421	0.21	3422	0.30
2955	0.08	2946	0.54	2948	0.37	2954	0.21
2925	0.15	2925	0.77	2927	0.83	2929	0.45
—	—	2882	0.30	2894	0.23	2900	0.14
2854	0.09	2844	0.20	2848	0.18	2852	0.14
—	—	2822	0.68	2825	0.64	2830	0.23
1618	0.08	—	—	—	—	1621	0.13
—	—	1450	0.08	—	—	1440	weak abs.
—	—	1360	weak abs.	—	—	1360	weak abs.

a)  $\text{TiO}_2$  at  $150^\circ\text{C}$  and methanol vapor pressure 50 torr.

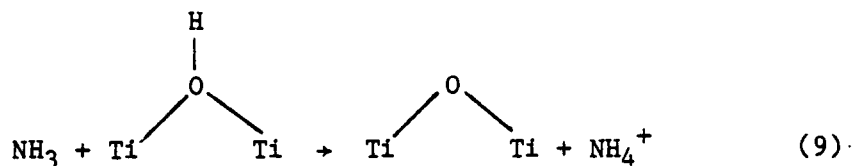
\* Heat at  $150^\circ\text{C}$  for two hours under vacuum.

\*\* Reaction with methanol.

\*\*\* Heat at  $150^\circ\text{C}$  for two hours under vacuum.

\*\*\*\* Sample was heated for one hour at  $150^\circ\text{C}$  under water vapor pressure of 12 torr.

infrared data on these reactions are presented in Tables XXXV-XXVI. We observed four bands (3396, 3344, 3239, and 3152  $\text{cm}^{-1}$ ) after the reaction with HMDS which are believed to be due to N-H stretching vibrations. Parfitt et al. (16) have studied adsorption of ammonia on rutile surface, and they have reported bands at 3400, 3350, 3200, and 3250  $\text{cm}^{-1}$ . These bands have been assigned to adsorption of ammonia on two different Lewis acid sites (10) present on the surface. Peri (24) also has observed bands at 3400 and 3350  $\text{cm}^{-1}$  during ammonia adsorption on alumina. The adsorption bands that are present in the lower frequency range are more puzzling. There are four bands: 1595, 1520, 1453, and 1415  $\text{cm}^{-1}$ .  $\text{NH}_4^+$  ions adsorbed on rutile surface produces bands at 1410, 3050, and 3150  $\text{cm}^{-1}$  (3,24b). The bands at 1595 and 1520  $\text{cm}^{-1}$  are close to the bending modes of H-N-H groups. These two bands may be assigned to bending modes of  $\text{NH}_3$  molecules adsorbed on Lewis sites on the  $\text{TiO}_2$  surface, while the weak 1453 and 1415  $\text{cm}^{-1}$  bands are assigned to  $\text{NH}_4^+$  due to some proton transfer process that takes place on the surface.



#### 2.IV.K Summary of Percentage OH Loss

Tables XXXVII a, and b present the losses of both terminal and bridging OH intensities after reaction of  $\text{TiO}_2$  with different silanes

Table XXXV.  
Reaction of  $\text{TiO}_2$  with Ammonia<sup>a</sup>.

Step A <sup>*</sup>		Step B <sup>**</sup>		Step C <sup>***</sup>		Step D <sup>****</sup>	
Peak ( $\text{cm}^{-1}$ )	Abs.	Peak ( $\text{cm}^{-1}$ )	Abs.	Peak ( $\text{cm}^{-1}$ )	Abs.	Peak ( $\text{cm}^{-1}$ )	Abs.
3731	0.17	3730	0.07	3728	0.08	3730	0.10
3677	0.20	—	—	—	—	3682	0.07
3652	0.39	3643	0.11	3649	0.17	3650	0.21
3414	0.20	3412	0.22	3414	0.18	3415	0.16
—	—	—	—	3386	0.08	3386	0.05
—	—	3352	0.07	3345	0.02	3349	0.02
—	—	3255	0.19	3264	0.05	3250	0.04
—	—	3148	0.07	3147	0.05	3152	0.03
2957	0.05	2953	0.09	2956	0.06	2957	0.08
2924	0.09	2923	0.15	—	—	2927	0.14
2856	0.05	2855	0.06	2851	0.05	2853	0.06
—	—	2822	0.05	2827	0.06	2830	0.05
1619	0.05	—	—	1602	0.09	1601	0.06
—	—	1597	0.15	—	—	—	—

a)  $\text{TiO}_2$  at room temperature and  $\text{NH}_3$  vapor pressure 5 torr.

\* Heat at 150 C for two hours under vacuum.

\*\* Reaction with  $\text{NH}_3$ .

\*\*\* Heat at 150 C for two hours under vacuum.

\*\*\*\* Exposed to  $\text{H}_2\text{O}$  vapor for three hours and heated at 150 C for two hours under vacuum.

Table XXXVI  
Reaction of  $\text{TiO}_2$  with Ammonia<sup>a</sup>.

Peak ( $\text{cm}^{-1}$ )	Step A *		Step B **		Step C ***		Step D ****	
	Abs.	Peak ( $\text{cm}^{-1}$ )	Abs.	Peak ( $\text{cm}^{-1}$ )	Abs.	Peak ( $\text{cm}^{-1}$ )	Abs.	Peak ( $\text{cm}^{-1}$ )
3733	0.19	3729	0.11	3729	0.10	3731	0.11	3731
3682	0.24	3686	0.10	3687	0.08	3686	0.10	3686
3651	0.43	3648	0.21	3650	0.20	3650	0.21	3650
3416	0.23	3415	0.26	3417	0.21	3414	0.27	3414
—	—	3392	0.14	3388	0.09	3391	0.12	3391
—	—	3345	0.06	3342	0.03	3344	0.05	3344
—	—	3253	0.15	3242	0.08	3256	0.10	3256
—	—	3150	0.06	3152	0.06	3154	0.06	3154
2958	0.03	2958	0.04	2953	0.05	2956	0.09	2956
2926	0.05	2925	0.10	2926	0.12	2926	0.16	2926
2855	0.03	2847	0.04	—	—	2854	0.08	2854
—	—	—	—	2829	0.05	2828	0.05	2828
1620	0.06	1600	0.16	1602	0.13	1600	0.13	1600

a)  $\text{TiO}_2$  at  $150^\circ\text{C}$  and  $\text{NH}_3$  vapor pressure of 5 torr.

\* Heat at  $150^\circ\text{C}$  for two hours under vacuum.

\*\* Reaction with  $\text{NH}_3$ .

\*\*\* Heat at  $150^\circ\text{C}$  for two hours under vacuum.

\*\*\*\* Exposed to  $\text{H}_2\text{O}$  vapor for three hours and heated at  $150^\circ\text{C}$  for two hours under vacuum.

Table XXXVII-A

Percentage Loss of Ti-O-H Intensity after Chemical Modification

Silane	(b.p.) <sup>a</sup>	Silane <sup>a</sup> Temper- ature	Silane <sup>b</sup> Vapor Pressure	Pellet <sup>a</sup> Temper- ature	Pellet Number	% Terminal <sup>c</sup> O-H Loss	% Bridging O-H Loss
Me <sub>3</sub> SiCl	(58°)	0°	63	RT <sup>d</sup>	TI 24	100%	47%
		0°	63	RT	TI 26	100%	38%
		0°	63	150°	TI 27	100%	40%
		0°	63	150°	TI 30	100%	41%
		15°	143	150°	TI 66	100%	21%
Me <sub>2</sub> SiCl <sub>2</sub>	(71°)	0°	41	RT	TI 23	100%	7%
		0°	41	RT	TI 34	100%	2%
		0°	41	150°	TI 35	100%	44%
		15°	84	150°	TI 38	100%	61%
MeSiCl <sub>3</sub>	(67°)	0°	54	RT	TI 44	100%	32%
		0°	54	150°	TI 45	100%	25%
		0°	54	150°	TI 68	100%	42%
		15°	101	150°	TI 46	100%	65%
SiCl <sub>4</sub>	(52°)	0°	82	RT	TI 39	75%	2%
		0°	83	150°	TI 40	66%	1%
		15°	152	150°	TI 41	100%	100%
Me <sub>3</sub> SiOMe	(58°)	0°	70	RT	TI 47	73%	0%
		0°	70	150°	TI 48	84%	0%
		15°	140	150°	TI 49	77%	0%
Me <sub>2</sub> Si(OMe) <sub>2</sub>	(82°)	0°	24	RT	TI 51	86%	31%
		0°	24	150°	TI 52	94%	3%
		15°	50	150°	TI 53	91%	34%



Table XXXVII-B

Silane	(b.p.) <sup>a</sup>	Silane <sup>a</sup> Temper- ature	Silane <sup>b</sup> Vapor Pressure	Pellet <sup>a</sup> Temper- ature	Pellet Number	% Terminal <sup>c</sup> O-H Loss	% Bridging O-H Loss
MeSi(OMe) <sub>3</sub>	(103°)	0°	7	RT	TI 54	83%	0%
		0°	7	150°	TI 55	95%	23%
		0°	7	150°	TI 69	100%	32%
		15°	16	150°	TI 54	96%	27%
Si(OMe) <sub>4</sub>	(122°)	0°	1	RT	TI 59	100%	40%
		0°	1	150°	TI 58	98%	0%
		15°	6	150°	TI 57	100%	27%
HMDS	(127°)	0°	1	RT	TI 31	86%	e
		0°	1	150°	TI 32	96%	e
		15°	6	150°	TI 33	98%	e
HCl		--	85	RT	TI 62	62%	69%
		--	152	150°	TI 61	100%	100%
MeOH	(65°)	0°	36	RT	TI 50	68%	0%
		0°	75	150°	TI 60	81%	f
		15°	50	150°	TI 63	90%	f
NH <sub>3</sub>		--	5	RT	TI 64	59%	e
		--	5	150°	TI 65	57%	e

(a) All temperatures in °C; (b) vapor pressures in torr; (c) peak areas above the absorption envelope due to hydrogen-bonding; (d) RT = room temperature, typically 20-25°C; (e) peak area not available due to strong overlap with a byproduct peak (NH<sub>3</sub>); (f) peak area actually increased slightly. Reaction times were one hour.

and their reaction byproducts. But these observed peak attenuations cannot be interpreted in terms of the reactivity of OH groups towards different silanes, due to several reasons. As has been discussed before (p. 25), the peak attenuations are mainly due to:

- a) Reaction of silanes with  $TiO_2$  surfaces,
- b) Adsorption of silanes on  $TiO_2$  surfaces,
- c) Reaction of reaction byproducts with  $TiO_2$  surfaces.

In addition to that in the case of chlorosilanes, a disturbed peak, which is OH in nature, has also been observed. This, in fact, further complicates the interpretation of results that have been observed for chlorosilane reactions. Due to these reasons it is difficult to reach a conclusion as to (a) if the terminal OH species are more reactive than the bridging OH species, (b) if the temperature and vapour pressure of silane have any effect on the reaction equilibrium. But on the basis of peak attenuations observed for methoxysilanes, it appears that terminal OH species are more reactive than bridging OH species.

#### 2.IV.L Surface Coverage

Quantitative determinations by infrared spectroscopy in the liquid phase are not a widely used technique in analytical chemistry. This is mainly due to the availability of other more sensitive techniques for this purpose. Even in the liquid phase the extinction coefficient for certain absorption bands varies with concentration, polarity of solvents, etc. This has been attributed to intermolecular interactions of the species concerned (25). The quantitative determinations of

adsorbed species on solids by infrared spectroscopy is a considerably more complicated task. The major reason is the empirical nature of variation of the extinction coefficient of infrared bands of the adsorbed species (26,27). The extinction coefficient is a function of adsorbate/substrate interaction; Folman and Yates (26) have observed an exponential decrease in the extinction coefficient of N-H stretching band (adsorption of  $\text{NH}_3$  on porous glass) and increase of C-H stretching (adsorption of  $(\text{CH}_3)_2\text{CO}$  and  $\text{CH}_2\text{Cl}_2$  on porous glass) with increasing surface coverage. Further, the extinction coefficients of infrared bands of the adsorbed species are different from that observed for similar species in the liquid phase. Hoffmann and Brindly (3) have reported values of 18.6 and 37.3 for extinction coefficients of  $\text{CH}_2$  symmetrical stretching vibrations of 2,5-hexadione and 2,5,8-nonanetrione adsorbed on Ca-montmorillonite, respectively. The extinction coefficients for the same vibrations in solution are 27.4 and 54.0 respectively. Further, both increase and decrease of extinction coefficients with different surface coverages are also reported in the literature. L.H. Little (28) has reported a decrease in the extinction coefficient of ethylene chemisorbed on  $\text{NiO}$  and an increase after chemisorption on  $\text{CuO}$  with increasing surface coverage.

Therefore, the extinction coefficient of the absorption bands of adsorbed species may be higher or lower than that of liquid phase species, once again depending on the nature of specific interactions present in the system concerned. The literature available on infrared extinction coefficients of adsorbed species is limited and also there are not any theoretical models that have been developed in order to

calculate the same or their variations.

Due to the above indicated complexity as well as the limitations, it is quite difficult to obtain accurate surface coverage information on silane-reacted  $\text{TiO}_2$  surfaces. Therefore we have carried out approximate calculations of silane surface coverage based on the available data and other necessary information using the following equation.

$$\Gamma = 10^3 \left( \frac{A}{\epsilon} \right) \frac{\pi r^{2*}}{a\omega} \quad (10)$$

The derivation is based on the application of the Beer-Lambert law for surface-adsorbed species and the calculations are based on the absorption coefficient values which have been determined for solution species.

On the basis of results presented in Table XXXVIII the following trends are observed.

(a) Surface coverage obtained for trimethyl, dimethyl and monomethyl increase in that order. This may be due to two reasons, (i) trimethyl groups are sterically larger than the other two groups, hence

---

\* Derivation is presented in Appendix I (p. 204 ).

Table XXVIII

## Surface Coverage Data

Pellet	Reagent	Reaction regime	Silane pressure	Absorbance	Pellet weight	$\Gamma$
T130	Me <sub>3</sub> SiCl	2	63T	0.59	0.0569	1.84
T166	Me <sub>3</sub> SiCl	3	143T	1.16	0.0721	2.8
T134	Me <sub>2</sub> SiCl <sub>2</sub>	1	41T	1.49	0.0790	4.9
T135	Me <sub>2</sub> SiCl <sub>2</sub>	2	41T	1.50	0.0792	4.9
T138	Me <sub>2</sub> SiCl <sub>2</sub>	3	84T	1.37	0.1127	3.2
T144	MeSiCl <sub>3</sub>	1	54T	0.44	0.0399	5.8
T168	MeSiCl <sub>3</sub>	2	54T	0.915	0.0597	8.0
T147	Me <sub>3</sub> SiOMe <sup>***</sup>	1	70T	0.81	0.0995	3.5
T148	Me <sub>3</sub> SiOMe <sup>***</sup>	2	70T	0.55	0.1045	1.0
T149	Me <sub>3</sub> SiOMe <sup>***</sup>	3	140T	0.64	0.0878	1.0
T154	MeSi(OMe) <sub>3</sub> <sup>*</sup>	1	7T	0.47	0.0627	3.9
T169	MeSi(OMe) <sub>3</sub> <sup>*</sup>	2	7T	1.15	0.0683	8.8
T156	MeSi(OMe) <sub>3</sub> <sup>*</sup>	3	16T	0.99	0.0681	7.8
T131	HMDS <sup>***</sup>	1	1T	0.480	0.0611	1.3
T170	HMDS <sup>***</sup>	2	1T	0.785	0.0669	2.0
T133	HMDS <sup>***</sup>	3	6T	1.42	0.0762	3.2
T152	Me <sub>2</sub> Si(OMe) <sub>2</sub> <sup>**</sup>	2	24T	1.32	0.827	5.0
T153	Me <sub>2</sub> Si(OMe) <sub>2</sub> <sup>**</sup>	3	50T	0.68	0.0423	4.2

<sup>\*</sup> monomethylsilane c-80, <sup>\*\*</sup> dimethylsilane c-160,

<sup>\*\*\*</sup> trimethylsilane, c-240

lower surface coverage results due to steric reasons, (ii)  $\epsilon$  observed for trimethyl moiety is the largest in the liquid phase. The  $\epsilon$  for adsorbed species is unknown, and the error in using the liquid phase  $\epsilon$  values in surface coverage calculations is unknown.

(b) Taking into account that all the surface coverage calculations were made on the basis of some set of assumptions, reactivity of all three types of silanes (chloro, methoxy and HMDS), appears to be the same. But, these data do not provide any information of the reactivities of terminal and bridging OH species.

(c) These surface coverage data do not show any strong trends with respect to reaction parameters, ie. temperature and vapour pressure.

## 2.V Conclusion

1. On the basis of data on attenuation of surface OH species during the reactions with silanes (p. 76, 78) it is difficult to determine as to what extent surface OH species react with silane reagents, due to the presence of several different mechanisms which cause OH peak attenuation. Further it is uncertain as to whether there is a difference in reactivities of bridging and terminal OH species toward silanes..
2. Surface coverage calculations show near monolayer\* coverage in the reactions with almost all the silane reagents. Further, it does not show any remarkable difference of reactivity among different silane reagents (ie. chloro, methoxy, and HMDS) as potential

---

\* Monolayer coverage for the TMS group is  $4 \mu\text{mol}/\text{m}^2$ .

surface derivatization agents, or strong trends in reactivity with respect to temperature or pressure.

3. Surface perturbations caused by reaction byproducts is most severe with chlorosilanes. The by-products of the other two types of silanes induce only temporary changes in  $TiO_2$  surface.
4. Even though from the bond distance data, only two bonds with the surface are sterically permissible per silane molecule, only the tetrafunctional silanes show free Si-OH groups after the complete reaction scheme.

## Chapter 3

### PHOTOELECTROCHEMICAL SYSTEMS

#### 3.1 Introduction

The conversion of solar energy into more practically usable forms of energy is an attractive idea. The prevalent energy crisis, which is due to the depletion of natural resources, and the increasing cost of production, and also the availability of solar radiation at no cost are added incentives to explore solar energy conversion as a dependable source for future energy needs. The goal of this venture is to develop stable and durable systems that are capable of converting solar energy into usable forms with reasonably high efficiency. The conversion may be either directly to electrical energy or to storable chemical energy such as hydrogen, oxygen, etc. (29). The former is for direct usage or application and the latter may be transported or stored as circumstances demand. Another advantage of these systems compared to the present systems, such as petroleum, natural gas, etc., is that they are essentially non-polluting. The other criterion for the success of this newer energy source is its economic viability. It should be either comparable or less costly compared to presently existing or alternative sources of energy.

The other advantage of solar energy conversion is its abundance and its inexhaustible nature (29). This will spare the other sources of energy such as coal, fuels, and natural gases, which are exhaustible,



for their unique needs such as the synthesis of fabrics, plastics, and other uses. In addition to that, solar energy is a more attractive alternative compared to nuclear energy and fossil fuels for safety reasons and cleanliness, respectively.

Plant photosynthesis, which has probably existed for millions of years, is an excellent example of conversion and storage of solar energy (30). In this process atmospheric carbon dioxide and moisture are converted to organic matter with the help of solar radiation. The organic matter that is formed in the photochemical process is storable energy which can be utilized subsequently (wood, biomass), or may be converted to other sources of energy such as gaseous and liquid fuels by biological or chemical means.

There are two types of photoelectric conversion devices. The first is the solid state system known as the photovoltaic device (29) which is capable of converting solar radiation directly to electricity. The second is the interfacial device consisting of a semiconductor/electrolyte, which is known as a photoelectrochemical system. The latter system is capable of converting solar radiation either directly to electricity or to storable chemical fuels such as  $O_2$ ,  $H_2$ , etc. In the following discussion, the fundamentals and other pertinent aspects of a photoelectrochemical device will be discussed.

Photoelectrochemically-induced electrolysis of water has several advantages. Hydrogen, which is a chemical fuel (31), can be stored much more easily than either heat or electricity. It is non-polluting, renewable, inexhaustible, and may be converted into other forms of energy such as heat (by combustion) and electricity (via fuel cells).

Also it may be used in the synthesis of ammonia, which is a chemical feed stock in very high demand.

### 3.II Semiconductors

It is impossible to begin an introduction on photovoltaic devices or photoelectrochemical systems without referring to the band model of solids. In atoms and molecules we refer to atomic and molecular orbitals respectively. But in the formation of a solid lattice of a metal (e.g. Cu, Si) or an oxide ( $\text{TiO}_2$ ,  $\text{SrTiO}_3$ ), due to the overlap of very large numbers of orbitals, the bonding and anti-bonding orbitals are very closely spaced (31). This essentially forms bands of bonding (filled) and antibonding (vacant) orbitals (Fig. 8A). The highest filled and lowest vacant bands are known as the valence band and conduction band, respectively.  $E_v$  marks the upper edge of the valence band, and  $E_c$  the lower edge of the conduction band. In semiconductors these bands are separated by an energy,  $E_{bg}$ , which is known as the bandgap, and is an intrinsic property of the semiconductor.

If the semiconductor is provided with energy greater than  $E_{bg}$  by thermal or optical means a valence band electron can be excited into the conduction band. The fundamental principle of both the photovoltaic devices and the photoelectrochemical systems is based on the photoexcitation of the valence band electrons to the conduction band and efficient separation of photo-produced electrons and holes; the latter is a mobile positive charge in the valence band formed by the removal of an electron.

The Fermi level ( $E_f$ ) represents the chemical potential of an

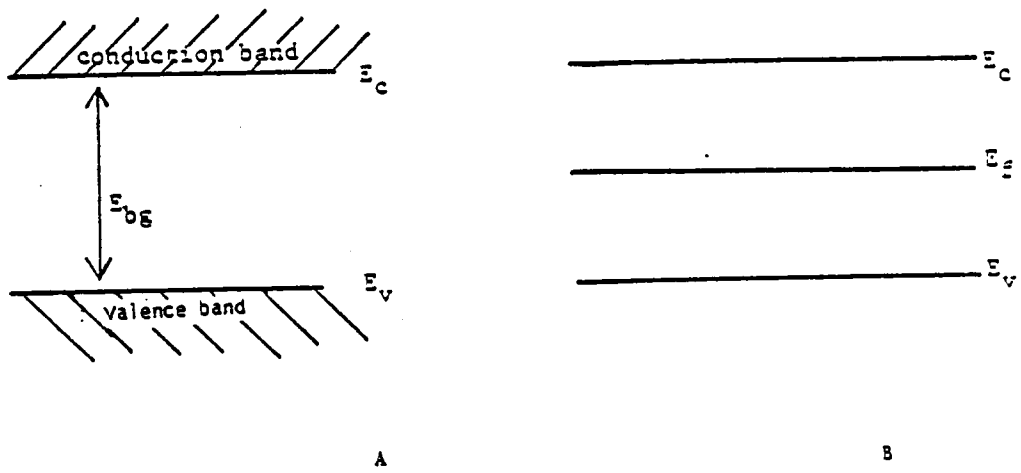


Figure 8: Energy level diagram for an intrinsic semiconductor.

electron in the semiconductor. For an intrinsic semiconductor, the Fermi level lies exactly in the middle of the band gap (Figure 8B).

### 3.III Doping

Semiconductors are doped in order to induce reasonable electronic conductivity. This is done by incorporating foreign elements into the semiconductor lattice (32) so that it introduces vacant or filled energy levels in the bandgap region, the former near the valence band and the latter near the conduction band. When the donor (filled) levels are located near the conduction band, the electrons are excited into it by thermal energy, creating a population of loosely bound electrons in the conduction band. Semiconductors in which the bulk of the current is carried by the electrons are called n-type (Figure 9A). Similarly, acceptor levels may be introduced near the valence band, so that electrons are thermally excited into these levels creating mobile holes in the valence band. These are called p-type semiconductors (Figure 9B). The electrons in the conduction band and the holes in the valence band will carry the electrical current in the respective semiconductors. Upon doping the semiconductor, the Fermi level moves either towards the conduction band (n-type) or towards the valence band (p-type).

### 3.IV Band Bending in Semiconductors

Now if we consider a semiconductor/electrolyte system (Figure 10A), the following phenomena occur depending on the potential to which the semiconductor electrode is being subjected:

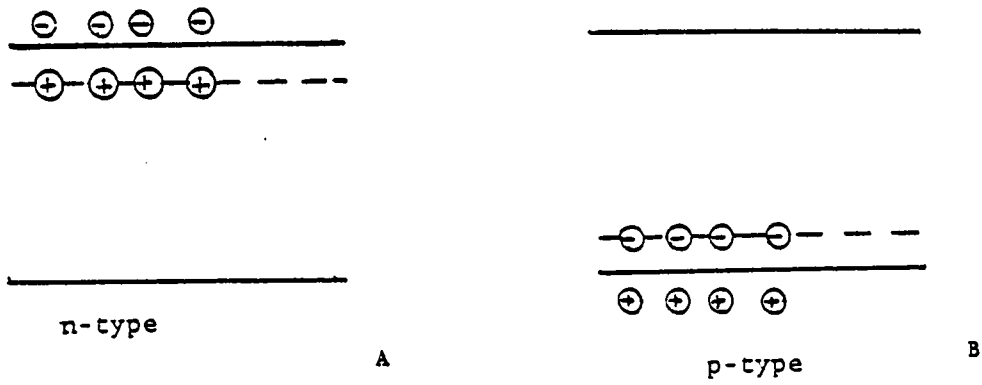


Figure 9: Doped semiconductors (a) n-type (b) p-type

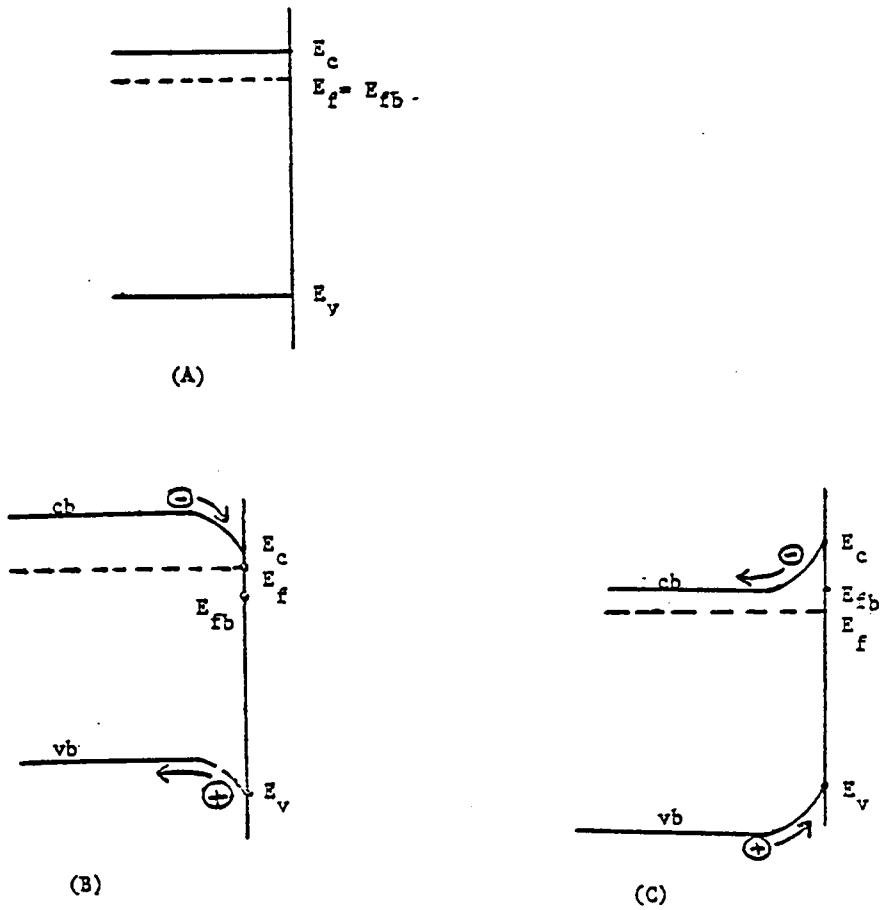


Figure 10: Band bending situation of a semiconductor (A) flat band condition, (B) under negative potential, (C) under positive potential, compared to flat band potential.

(a) For each semiconductor/electrolyte system, there exists a potential at which there is no electric field or space charge region in the semiconductor. At this potential  $E_f = E_{fb}$ .  $E_{fb}$  is known as the flatband potential of the semiconductor for the system concerned. Under this condition there is no band bending occurring in the semiconductor.

(b) If the semiconductor (n-type) is subjected to a potential of negative  $E_{fb}$ , the Fermi level moves above  $E_{fb}$  and both the conduction and valence band bend downwards (Figure 10B). Under this situation the electrons move toward the semiconductor/electrolyte interface and the holes move towards the bulk of the semiconductor.

(c) If the semiconductor (n-type) is subjected to a potential positive of  $E_{fb}$ , the Fermi level of the semiconductor moves below  $E_{fb}$  and positive band bending occurs in both the conduction band and the valence bands (Figure 10). Under this condition the holes flow to the semiconductor/electrolyte interface and the electrons flow to the bulk of the semiconductor.

### 3.V Energy Scales

The band edges ( $E_c$  and  $E_v$ ) can be located on an electrochemical energy scale as shown in Figure 11. The actual positions depend on the nature of the electrolyte, especially the pH (31). The positions of energy bands and the Fermi level may be expressed on an absolute vacuum scale or with respect to any electrochemical reference electrode. There are two different (33,34) energy scales which one uses in photoelectrochemistry.

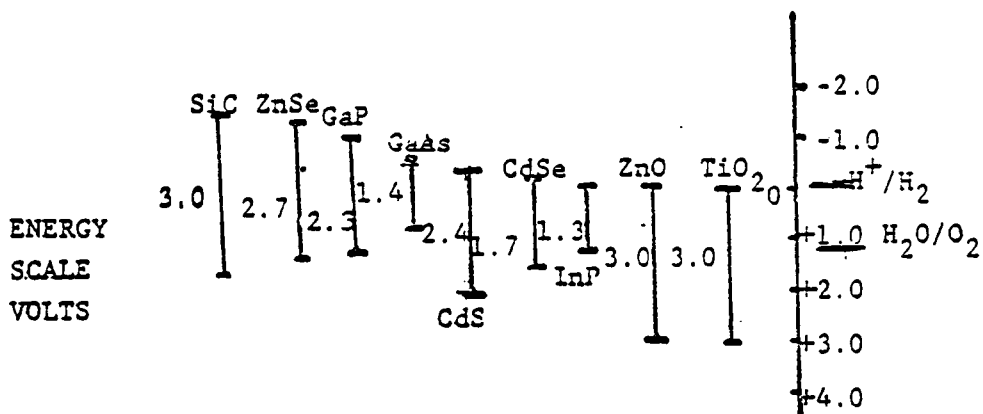


Figure 11: Positions of conduction and valence band edges for several semiconductors at pH=1.0,(31).



(i) The vacuum scale (preferred by solid state physicists), which considers vacuum level as a reference point, and all other possible electronic energy levels are considered as lower than the vacuum level. Therefore in this scale all the electronic energy levels carry negative values.

(ii) The normal hydrogen electrode (NHE) is normally used by chemists as the reference point. The two energy levels differ by about 4.5 eV, ie.

$$E_{\text{nhe}} = -4.5 \text{ eV vs vacuum} \quad (11)$$

The redox potential of a redox couple ( $E_{\text{f.e}}$ ) is considered to be equivalent to a Fermi energy, which can be converted by the following equation:

$$E_{\text{f.e}} = -(4.5 \text{ eV} + e U_{\text{redox}}) \quad (12)$$

### 3.VI Semiconductor/Electrolyte Interface

In 1975, Gerisher (35) proposed a working model for a semiconductor/electrolyte interfacial system. According to this model, on a strictly thermodynamic basis, one can predict the electrochemical processes of photoexcited semiconductor/electrolyte (redox couple)/metal systems.

Compared to p-n junction photovoltaic devices or Schottky junction [semiconductor/metal] cells, setting up a SLJSC is extremely simple.

As shown in Figure 12, it can be formed by immersing a semiconductor electrode and a metal electrode in an electrolyte and externally connecting them together, provided the semiconductor and redox couple energy requirements are satisfied. If the redox potential of the redox couple lies in the band-gap region, then upon shining light on the semiconductor electrode, an electric current begins to flow through the external circuit.

### 3.VI.A Equilibrium in the dark

As the  $E_{\text{redox}}$  for the redox couple lies below the Fermi level ( $E_F$ ) of the semiconductor, electron flow occurs from the SC (n-type) to the electrolyte forcing the reduction process.



Due to this process there are two changes occurring in the semiconductor. (i)  $E_F$  moves in a positive direction in order to reach equilibrium with the redox couple. (ii) Due to the depletion of electrons at the surface region a positive charge develops in this region and this in turn causes band bending in the surface region of the semiconductor electrode. Under the present situation, positive band bending occurs in both the conduction and valence bands, due to the direction of electric field present. The electrons at the surface flow into the bulk of the semiconductor, and any holes present move towards the semiconductor/electrolyte interface. As the semiconductor and the counter electrode are externally connected at the point of

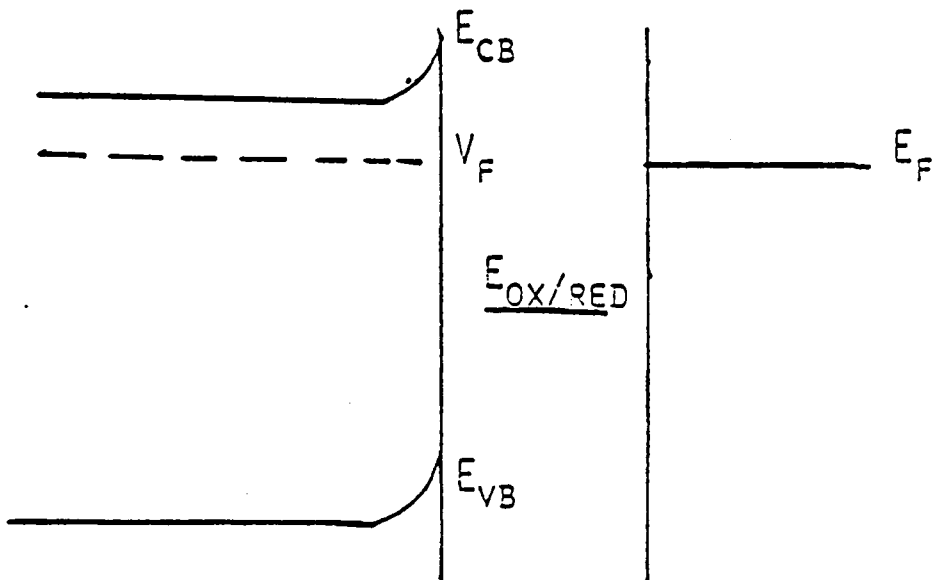


Figure 12: Regenerative SLJSC using n-type semiconductor.

equilibration this Fermi level (counter electrode) also matches with the  $E_{\text{redox}}$  of the redox couple. The space charge layer thickness may vary from 50 - 2000 Å, depending on the doping level of the semiconductor. Dark equilibration is shown in Figure 13B.

### 3.VI.B Illumination

If the semiconductor electrode is illuminated with light  $h\nu > E_{\text{b.g.}}$ , excitation of electrons occur from the valence band to the conduction band. As the electric field exists at the space charge level, as in the previous situation, the photogenerated holes ( $h^+$ ) move towards the semiconductor/electrolyte interface and the electrons into the bulk of the semiconductor. This reduces the recombination efficiency of photogenerated holes and electrons, making more of them available for the photoelectrochemical process. The photogenerated holes possess adequate oxidation power to oxidize the redox couple. Therefore it drives the oxidation reaction at the semiconductor/electrolyte interface:



The photoexcited electrons in the conduction band move towards the bulk of the semiconductor and flow into the counter electrode through the external load resistor. These electrons in turn possess adequate potential to cause the reduction at the counter electrode. This system shows the operative principal of a regenerative semiconductor liquid-junction solar cell, as there is no consumption of the redox species during the photocurrent generation process.

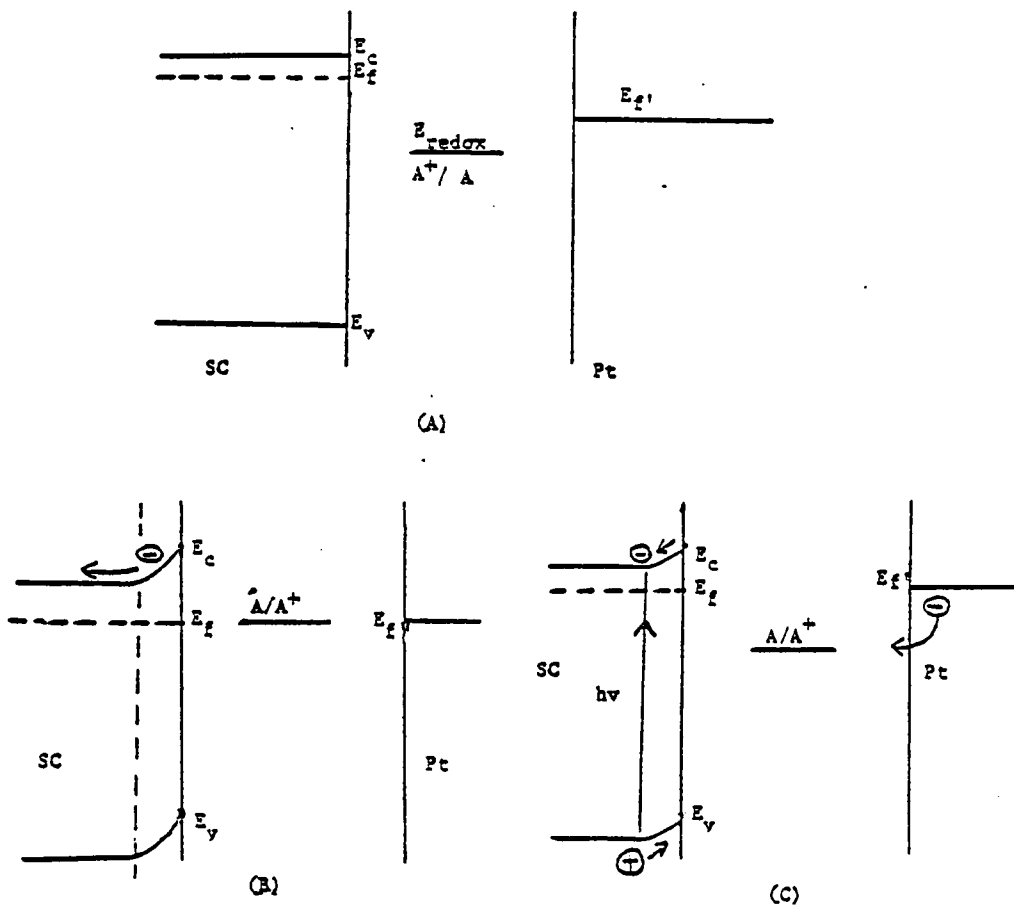


Figure 13: Semiconductor liquid junction solar cell (a) initial conditions, (b) equilibrium under dark (c) photocurrent generation under illumination.

In our studies we have been interested in photoelectrolysis of water using n-TiO<sub>2</sub> semiconductor electrodes. The principles underlying this process are somewhat parallel to that of a regenerative SLJSC. One major difference is the electrode reactions in this type of a cell consumes the electrolyte (water) and leads to the synthesis of new products (O<sub>2</sub> and H<sub>2</sub>) by the oxidation and reduction processes of the anode and cathode, respectively. The valence band edge of n-TiO<sub>2</sub> lies below (more positive) the oxidation potential of water, therefore the oxidation of water by n-TiO<sub>2</sub> is a thermodynamically favored process. But the cathode of this system [n-TiO<sub>2</sub>/electrolyte/Pt] has to be negatively biased in order to carry out the reduction process at a reasonable rate. This negative biasing of cathodes moves its fermi level in a negative direction, so that the reduction of water is thermodynamically favored.

### 3.VII Blocking Behaviour of Semiconductor

For any system of semiconductor/electrolytes, there exists a potential at which there is no band bending. This potential is known as the flatband potential ( $V_{fb}$ ). At potentials positive of  $V_{fb}$  the bands bend upwards; consequently the electrons are driven towards the bulk of the semiconductor and the holes towards the surface of the semiconductor. At potentials negative of  $V_{fb}$ , the reverse process takes place. The separation of electrons and holes under the influence of surface potential is an important factor for an efficient photo-conversion process. In n-type semiconductors the majority of carriers are electrons. In the dark, potentials negative of  $V_{fb}$  cause negative

band bending in both conduction and valence bands. This drives the electrons (majority carrier) to the semiconductor/electrolyte interface. These electrons can be transferred to the oxidized species in the electrolyte inducing a reduction process. Therefore n-type semiconductors can act as dark cathodes. Under the influence of a potential positive of  $V_{fb}$  (in the dark) the holes are driven to the semiconductor/electrolyte interface due to positive band bending. But the concentration of holes in the n-type semiconductor is so low (in the dark), there is essentially no current flow across the interface; the electrode is blocking. Therefore n-type semiconductors act as dark cathodes and in the same token p-type semiconductors act as dark anodes.

### 3.VIII Efficient PEC Systems

There are several parameters which have to be optimized in order to design an efficient photoelectrochemical conversion cell (32).

#### 3.VIII.A Bandgap

The minimum energy requirement for the splitting of water into  $H_2$  and  $O_2$  is 1.23 eV per molecule. Therefore, the  $E_{bg}$  of semiconductors is designed to be in this range. In addition to that, as the  $E_{bg}$  increases, the fraction of solar radiation that is unusable increases. Therefore, the conversion efficiency obtainable from higher bandgap semiconductors is quite low. An  $E_{bg}$  of up to 2 eV may provide an acceptable conversion efficiency (31).

#### 3.VIII.B Bandgap Location

The  $E_c$  and  $E_v$  values represent maximum reduction and oxidation

potentials of photogenerated electrons and holes, respectively. These levels as well as the  $V_{fb}$  depend on the nature of the solvent and specific adsorption on the semiconductor surface. For n-type semiconductors, a more negative  $V_{fb}$  leads to a higher reducing power of photogenerated electrons; and this maximizes the output voltage of the system. For p-type semiconductors, a more positive  $V_{fb}$  leads to a higher output voltage.

### 3.VIII.C Stability

The semiconductor should be stable under the operational conditions of the photoelectrochemical cell in order to design a durable system. This is particularly a problem for semiconductors with smaller bandgaps. The underlying condition for the stability of the semiconductor can be either kinetic or thermodynamic (33). The latter is much easier to predict, and the former depends on the relative rates of redox and the dissociation/decomposition reactions at the electrode surface. Small bandgap materials such as GaAs and InP show increased stability in non-aqueous systems (34). It also appears that a layer of metal, or conducting polymer and electroactive polymer coatings (35,77), or derivatization (36) efficiently remove a photogenerated charge from the electrode surface and improve the stability in aqueous systems.

### 3.VIII.D Doping Level

The thickness of the space charge layer and the bulk resistance of the semiconductor are determined by the doping level. The doping level should be adjusted with respect to the absorption coefficient of



incident light so that most of the light is absorbed in the space charge region. The excitation in the bulk tends to reduce the quantum efficiency as the recombination rate ( $h^+(VB) + e^-(CB) \rightarrow 0$ ) is higher in this region.

### 3.VIII.E Redox Couple

The redox couple should be stable in both forms and should not absorb energy above the  $E_{bg}$ . The redox potentials should be at appropriate levels in order to capture holes and electrons. The heterogeneous electron transfer rates should be rapid. The ability of the redox to successfully compete (kinetically) with the electrode decomposition reaction is essential.

### 3.IX Problems Associated with the PEC Devices

As indicated above, conversion of solar radiation provides an alternative means to meet future energy needs. The solar spectrum consists of radiation from about 300 nm to 1500 nm (36). In solar conversion systems such as semiconductor liquid-junction solar cells (SLJCS), it is best to be able to use most of the solar radiation. The critical energy requirement for the splitting of water into  $H_2$  and  $O_2$  is 1.23 eV per molecule. This will be a little higher in actual electrochemical systems due to  $H_2$  and  $O_2$  overvoltages at the electrodes. Therefore it is best to use semiconductors with bandgaps of 1.3 - 1.5 eV. Most n-type semiconductors which are best for this purpose [e.g. GaAs, Si, CdS] have one major drawback in an aqueous medium. The photogenerated electrons and holes, instead of being injected into the solution and inducing the preferred redox process,

may oxidize or reduce the semiconductor electrode itself, causing decomposition (37). This causes a serious drawback with respect to the durability and efficiency of the conversion devices. The larger bandgap semiconductors do not pose this problem (e.g.  $\text{TiO}_2$ ,  $E_{bg} = 3.0$  eV). But they are transparent to a larger portion of the solar radiation and, consequently, the maximum conversion efficiency attainable is lower.

The thermodynamic stability of the semiconductor is assured if the redox potential of the oxidative decomposition reaction lies below the valence band edge and if the redox potential of the reductive decomposition reaction lies above the conduction band edge (38). In reality, this is not true for all photoelectrodes which are suitable for the conversion devices. Thus for n-type semiconductors the oxidative decomposition potential lies within the bandgap; therefore, oxidation decomposition will kinetically compete with the intended oxidative reactions. The reverse is true for p-type semiconductors i.e. reductive decomposition is present. Even if the redox reaction is thermodynamically favored, the kinetic parameters may alter this situation causing electrode decomposition. It is very hard to predict the kinetic behavior, and one has to rely on experimental data. This is the situation in semiconductors such as GaAs, GaP, and ZnO in aqueous solutions.

There are several research groups who have actively studied the problem in order to develop techniques to circumvent this situation. Derivatization of the semiconductor surface with pseudo-metallic redox polymers and with redox polymers have produced reasonable improvements

in the performance of photoelectrochemical conversion systems. These topics will be dealt with in detail in a later section of this chapter.

As it has been presented in the previous chapter, we have developed a technique to obtain monolayer coverages of simple, non-electroactive silanes on  $\text{TiO}_2$ . Our approach is to modify a single crystal of  $\text{TiO}_2$ , which is a stable photoanode in aqueous systems. We take advantage of the stability of this system to study the survivability of silane layers on  $\text{TiO}_2$  electrodes upon photocurrent generation, before extending this study into more complicated systems (unstable semiconductors) such as GaP, GaAs, and ZnO. The basic idea is to reduce the activity of water at the semiconductor electrode surface by forcing the charge transfer kinetics between the electrode and the redox molecules/ions to take place at the surface of the hydrophobic modified layer. It has been reported that silane layers bonded to  $\text{TiO}_2$  are stable against photocurrent generation in water (39). We have surveyed a range of silane reagents as modification agents and also a range of conditions under which their stability will be tested. The key analytical tool is x-ray photoelectron spectroscopy (XPS).

### 3.X Survey of Chemically Modified Semiconductor Electrodes

Earlier, about ten years ago, the applications of chemically modified surfaces had been strictly in non-electrochemical fields. Chromatographers have used surface modification with silane reagents to deactivate gas chromatographic columns and to synthesize bonded phases for HPLC (40) on both silica and alumina substrates. In trace analysis, glass wool has been derivatized with dithiocarbonate reagents

to scavenge metal ions for ESCA analysis (41). Acid-base dye indicators have been attached to silica surfaces to form "solid indicators" (42).

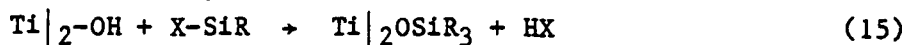
The main objective of surface modification in electrochemistry is transforming heterogeneous unpredictable interfaces into more controlled and predictable ones, of which there could be a wealth of applications (43). For example, in semiconductor electrodes, the surface states which exist in the bandgap region are little understood and there is no way to control or manipulate their properties. By the modification of these surfaces, one could control the surface properties in a more predictable manner. Another example is electrocatalysis (44). The surface-attached molecules can act as fast electron-transfer mediators for substrates dissolved in the solution, which may otherwise react very slowly with the bare electrode.

Murray and co-workers pioneered the covalent attachment of monolayers (45-52). They employed the  $-\text{SiX}_3$  moiety in silane reagents containing amine, pyridyl, and ethylenediamine ligands in order to form covalently bonded monolayers on electrodes such as Pt/PtO,  $\text{SnO}_2$ , carbon, and  $\text{RuO}_2$ . All these syntheses have been carried out in the liquid phase under very carefully controlled conditions in order to avoid the formation of polysiloxane polymers. The presence, stability, and chemical reactivity of these modified electrodes have been studied by XPS. The surface-bound amine molecules exhibit the same chemical properties as if they were free molecules.

Further, Finklea and Murray (50,51) have studied the photoelectrochemical properties of silane-modified (liquid phase)  $\text{TiO}_2$ .

Titanium dioxide has attracted considerable attention due to its stability against photoanodic dissociation in solar conversion devices. The inherent disadvantage of these  $\text{TiO}_2$  systems is a lower efficiency of solar energy conversion due to its large bandgap (3.0 eV), and consequently, only a smaller portion of solar radiation is effectively used in the photoelectrochemical process (31).

Titanium dioxide, like the other oxides (e.g. Pt/PtO,  $\text{SnO}_2$ ,  $\text{RuO}_2$ ), contains surface hydroxyl groups which are capable of reacting with silane reagents (equation 15) (52). ESCA studies reveal a 50% reduction of the Ti ( $2p_{3/2}$ ) signal compared to the naked electrode upon bonding of a monolayer of silane.



An O(1s) peak develops at higher binding energy (532 eV) and the intensity of the original peak (530 eV) decreases. Furthermore, a strong Si(2p) peak appears due to the presence of the silane moiety on the surface. Neither the presence of unreacted surface hydroxyl groups nor the homogeneity of the monolayer can be determined by ESCA. These silane layers have been shown to sustain massive hole generation. This is in contrast to our own observations of similar systems derived from gaseous phase modification (53) as well as other reports (54). The photocurrent voltammograms that have been obtained for both the naked and derivatized electrodes are almost identical. This may either be due to the fact that the modified layer does not impede the hole transfer process or to the presence of a high percentage of unmodified

sites. The  $V_{fb}$  determined for both types of electrodes have been shown to be identical, further indicating the possibility of the latter situation.

Parkinson (55) and Bard (56) have shown in separate reports the ability to improve performance of systems with similar recombination problems by selectively coating the recombination sites with polypyrrole or t-butylpyridine via dark oxidation. The object is to increase the resistance for electron transfer between these sites and the electrolyte.

Yoneyama et al. (54) also have reported using photoelectrodes modified with non-electroactive molecules and have obtained contrasting results to the previous report by Murray et al. (50,51). They have presented results on photocurrent generation of n- and p-type silicon electrodes which were modified by the covalent attachment of trimethylchlorosilane (TMCS) on p-type Si electrodes. Upon modification, a)  $H_2$  evolution at a p-Si electrode stops (this has been attributed to the blocking of  $H^+$  adsorption sites on the electrode prior to the redox process); b) the onset potentials of both derivatized and naked electrodes are the same in  $Fe(CN)_6^{3-/4-}$ -containing solution (Finklea and Murray (50) also have reported similar observations); and c) compared to the naked electrode (p-type Si), the derivatized electrode sustains photocurrent generation over 100 potential scans in 0.01M  $K_3Fe(CN)_6$  solution with very little decay of photocurrent. The slight decay may be due to the oxidation of underivatized sites on the p-Si surface. The n-type Si/TMCS modified layer fails to sustain photocurrent generation.

Haller (51) has reported the modification of Si and GaAs with 3-aminopropyltrimethoxysilane. The reaction has been carried out in the liquid phase under very anhydrous conditions in order to prevent any polymer formation. Electron micrographic studies show the absence of any large (109 nm) size particles on the surface, and the presence of monolayer coverage is demonstrated by adsorption and ellipsometric techniques.

Wrighton et al. have conducted extensive studies of semiconductor electrodes modified with covalently attached silylferrocene. All these modifications have been carried out in the liquid phase. The n-type Si anode is reacted with (1,1-ferrocenyldichlorosilane) in a dry isoctane solution (58a). This electrode exhibits behavior of the surface-bound ferrocene in an acetonitrile electrolyte which is free of any ferrocene derivatives or other electroactive species. The potential scan rate studies show that the peak current is linearly proportional to the sweep rate, further indicating the presence of surface-bound electroactive species. Integrated peak areas in the voltammogram give the concentration of surface-bound ferrocene moiety. Hole capture by the ferrocene kinetically outruns the oxidative surface corrosion reaction of n-Si. This precludes the formation of the SiO<sub>2</sub> layer on the n-Si electrode. In this study, Wrighton et al. have shown the survivability of the surface-bound ferrocene moiety even in a reasonably wet solution. A small decay of photocurrent is observed, and this has been attributed to the oxide growth at the pinholes in the derivatized layer. But this is minimal compared to the naked n-type Si anode. The surface-bound ferrocene exhibits mediated electron-transfer

reactions, and this is the first example of redox reactions mediated by surface-bound species. Ferrocene-modified n-type Ge photoanodes also exhibit enhanced stability towards photodecomposition (58b).

GaAs, also a small bandgap semiconductor ( $E_{bg}$  1.4 eV), has been studied by Wrighton et al. (59). This semiconductor has a bandgap energy which is quite close to that which is required for photo-assisted decomposition of water into  $H_2$  and  $O_2$ , 1.23 eV. Incidentally, GaAs exhibits the highest known efficiency for energy conversion in Schottky barrier solar cells (60) and in liquid junction devices (61). Wrighton and Bolts (59) have investigated both the underivatized and derivatized GaAs with (1,1-ferrocenyl)-dichlorosilane in acetonitrile containing 0.1 M TBAP. The GaAs electrode which was derivatized with (1,1-diferrocenyl)-dichlorosilane shows the expected redox characteristics of the surface-bound ferrocene moiety both under illumination and in the dark. Under illumination and in the presence of a solution of ferrocene, diffusion limited oxidation/reduction currents have been observed, as in the previous reports.

Wrighton et al. (62) have attempted to extend the study of n-type (derivatized)-Si anodes into aqueous media. As it was evident in the previous reports, the potential of oxidation of solution species does not depend on the kinetics of hole transfer from the semiconductor to the solution species but on the nature of the surface bound species. This situation may be exploited in order to enhance the efficiency and durability of solar energy conversion systems. In aqueous solutions, the photoanodic corrosion of n-type semiconductors is very rapid compared to that in non-aqueous systems, and consequently, the decay of



photocurrent is also very rapid. Even in the presence of redox couples such as  $I^-$ ,  $Fe(CN)_6^{4-}$  and  $[Ru(NH_3)_6]^{2+}$ , hardly any improvement of this situation has been observed. This indicates the inability of naked n-type Si photoanodes to sustain the electron transfer reactions. Under routine aqueous experimental conditions, passage of  $10^{-8}$  moles of electrons/cm<sup>2</sup> is sufficient to form a passive SiO<sub>2</sub> layer which significantly attenuates the photocurrent. The general characteristics observed in an aqueous medium of a derivatized n-type Si electrode are comparable to those which have been reported for non-aqueous media (57,58,59). The derivatized electrodes have sustained photocurrent in aqueous media in the presence of  $Ru(NH_3)_6^{2+/3+}$  even after passage of photocurrent to the extent of 1000 charge reversals of the surface-bound species. Oxidation of  $Fe(CN)_6^{4-/3-}$  and  $I^-/I_3^-$  has been achieved in aqueous media and a reasonably durable photocurrent is sustained by the derivatized n-type Si electrode. But the overall efficiency (light-to-current) for all these systems has been low (1%) even for monochromatic light.

In contrast to n-type small bandgap semiconductors, p-type photocathodes do not undergo photochemically-induced electrode decomposition. Therefore, this property offers an incentive to use them as photocathodes in energy conversion devices. But, in the literature (31) it has been pointed out that these p-type semiconductors are poor photocathodes in general and specifically for H<sub>2</sub> generation. Further, these systems typically offer (31) lower conversion efficiencies and photovoltages. The surface modification of p-type semiconductors may provide a way to overcome this problem.

Wrighton et al., have investigated derivatization of p-type Si with N,N-dialkyl-4,4'-bipyridinium (also known as paraquat or  $PQ^{2+}$ ) (63,64). In  $CH_3CN$ , both redox processes [ $PQ^{2+} + e^- \rightarrow PQ^+ + e^- \rightarrow PQ^0$ ] have been observed upon irradiation of the electrode, but in aqueous electrolytes, only the first redox process is reversible. These surface-confined species have shown the capability of mediating electron transfer to ferrocenium in the electrolyte.

In an earlier study it was shown that Pt is an excellent catalyst for  $PQ^{2+}$ -mediated reduction of  $H_2O$  to  $H_2$  (63). Therefore, incorporation of Pt into the ( $PQ^{2+}$ ) polymer matrix should improve the hydrogen generation capability of the modified p-type Si electrode. It has been observed by the same authors that p-type Si, when coated with Pt, is a better hydrogen-evolving electrode than either naked p-Si or p-Si(PQ) systems (65). The  $Br^-$  counter ion of P-Si/ $PQ^{2+}$  system can be exchanged with  $PtCl_6^{2-}$  ions. The photoreduction of [ $P-Si/PQ^{2+}, PtCl_6^{2-}$ ] yields [ $P-Si/PQ^{2+}.Pt$ ] [ $Br$ ] $_2$ . In these systems, hydrogen evolution with significant photocurrent density has been observed at 300-400 mV positive of the water reduction potential whereas the naked p-type Si or p-type Si/ $PQ^{2+}$  systems do not show  $H_2$  evolution even at potentials significantly negative of the water reduction potential  $E_{(H_2O/H_2)}$ . The efficiencies that have been obtained for these systems (5%) are the best solar-to-chemical energy conversion efficiency achieved, at the time of reporting. The long term durability of these systems has not been tested, but in  $10^4$  reversals of the surface-bound catalysts, about 20% decay of efficiency is observed.

A major drawback of the covalently-modified photoelectrodes is the inhomogeneity of the modified layer. Both Murray (50) and Wrighton

(58) have indicated the possibility of the existence of active or reactive sites on the electrode surface even after the modification process. Later Murray and co-workers (66) have shown the superiority of electrochemically-formed polymer films on electrode surfaces over covalently modified surfaces with respect to thickness control and homogeneity (pinhole freeness) of the modified layer.

### 3.XI Experimental

#### 3.XI.A Electrode preparation

Disc electrodes (6.0 mm diameter) were cut from a single crystal boule of rutile (Commercial Crystal Laboratories) exposing (001) face. The discs were polished in 5 $\mu$  alumina for about 10 min each, rotating the crystal position in every minute or so in order to obtain an evenly polished surface. Polished crystals were heated in a quartz tube at 600°C for about 20 min in a H<sub>2</sub> stream to dope the crystals and then etched in conc. H<sub>2</sub>SO<sub>4</sub> at 250°C for about 1 hr. Prior to the silanization these electrodes were steamed for 4-5 hrs to ensure surface re-hydroxylation. The electrodes were repolished, etched, and steamed before subsequent experiment.

#### 3.XI.B Silanization

Derivatized TiO<sub>2</sub> (rutile) discs were prepared by using the silanization conditions developed in the previous section. The discs were heated under vacuum for 2 hrs at 150°C., and were exposed to silane vapour at the same temperature, while controlling the silane flask at 15°C. After 1 hr of reaction, the excess silane was pumped

away for about 20 min and the discs were heated at 150°C for 2 hrs.

### 3.XI.C Electrochemistry

All the electrochemical measurements were carried out in a conventional 3-compartment glass cell, under Ar sparging. Photocurrent generation was performed in four different electrolytes of varying pH: 0.5M H<sub>2</sub>SO<sub>4</sub> (pH 0.5), H<sub>3</sub>PO<sub>4</sub>/KH<sub>2</sub>PO<sub>4</sub> buffer of ionic strength 0.2 M (pH 2.0), KH<sub>2</sub>PO<sub>4</sub>/Na<sub>2</sub>HPO<sub>4</sub> buffer (pH 6.0), and 0.1M NaHCO<sub>3</sub>/Na<sub>2</sub>CO<sub>3</sub> (pH 10.0). The TiO<sub>2</sub> electrode was irradiated with the water-filtered output of a 150-watt Xe arc lamp. The electrode potential was set at 1.0 volts vs. SCE, using a PAR 173 potentiostat, and photocurrent densities in the range 0.7 to 2 mA/cm<sup>2</sup> were obtained. The photocurrent generation was terminated after approximately 1 coul of charge (3.5 coul/cm<sup>2</sup>) had passed. The photoelectrochemical setup is shown in Figure 14.

### 3.XI.D XPS

All XPS spectra were recorded on a DuPont 650B spectrometer with the Mg anode. Titanium, oxygen, carbon and silicon signals were monitored after the silanization and photocurrent generation experiments. On each experiment a clean unreacted blank was run as a control. The peak areas of the Ti(2p<sub>3/2</sub>) and Si(2p) peaks were calculated by triangular approximation. Peak energies are referred to C(1s) at 285.0 eV.

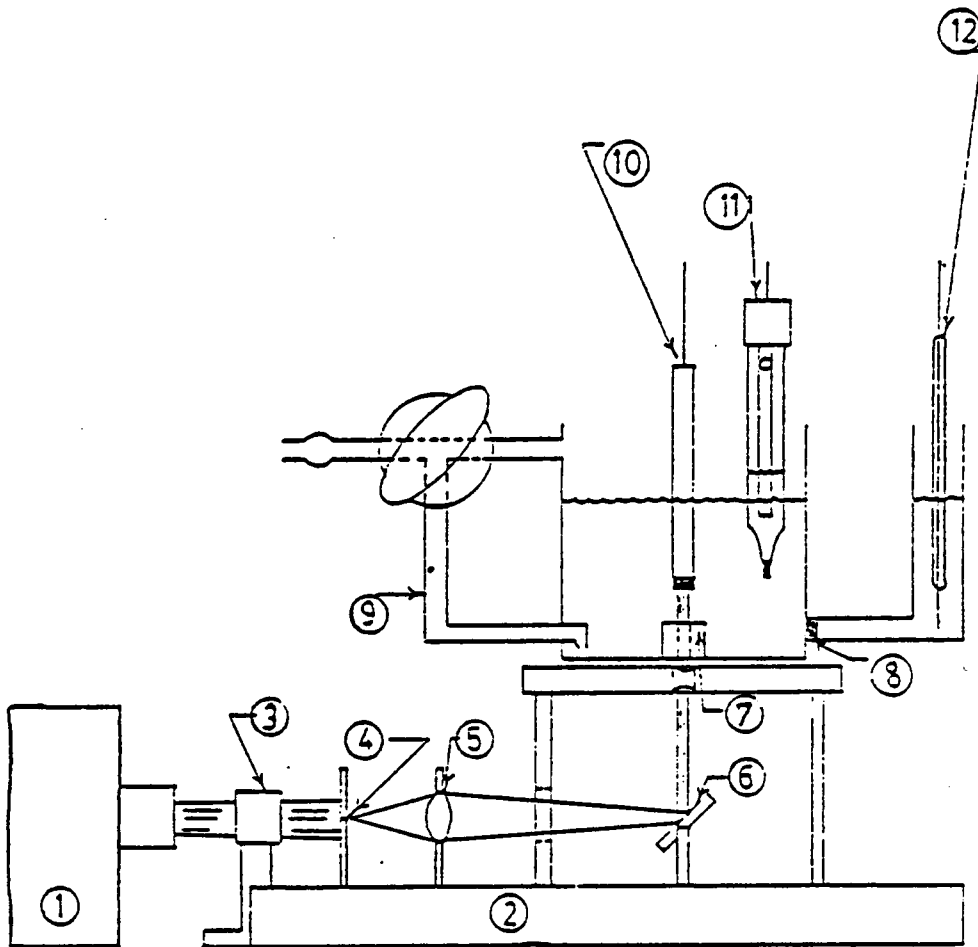


Figure 14:

Photoelectrochemical experimental set-up:

1 light source

2 optical bench

3 water

4 disc aperture

5 lens

6 mirror

7 window

8 glass frit

9 sparging arm

10  $\text{TiO}_2$  working electrode

11 SCE reference electrode

12 Pt counter electrode

### 3.XII Results and Discussion

#### 3.XII.A XPS of Modified Titanium Dioxide

As it has been discussed previously the surface hydroxyl groups of  $\text{TiO}_2$  react with silane reagents to yield a modified surface, as shown in equation 15 (p. 105).

The XPS-spectrum of clean  $\text{TiO}_2$  has the following characteristics with respect to the elements O(1s), Ti(2p), C(1s) and Si(2p) [Figure 15A and 16A].

- (i) O(1s) shows a peak centered around 532 eV.
- (ii) Ti(2p) shows two peaks centered around 459 and 462 eV.
- (iii) C(1s) shows a relatively strong peak around 285 eV.
- (iv) There are no Si(2p) peaks observed in clean  $\text{TiO}_2$  surface.

The surface structure of silane modified  $\text{TiO}_2$  shows several changes in the XPS-spectrum with respect to the elements stated before.

- (i) The O(1s) develops a new peak at the higher energy side. An attenuation of the lower energy (original peak) O(1s) peak is also observed.
- (ii) The intensity of the Ti(2p<sub>3/2</sub>) peaks are attenuated.
- (iii) A new Si(2p) peak appears.

These XPS-spectral changes are shown in Figures 15B and 16B. The second O(1s) peak is believed to be due to the formation of Ti-O-Si linkage during the process of surface modification. The reduction in the intensity of the higher energy O(1s) peak may be due to two reasons. It may be only (i) part of the surface Ti-OH groups undergoing derivatization reaction, or (ii) the reduction of intensity may be due to the loss of scattering O(1s) electrons for the presence

As it has been discussed previously the surface hydroxyl groups of  $TiO_2$  react with silane reagents to yield a modified surface, as shown in equation 15 (p. 105).

The XPS-spectrum of clean  $TiO_2$  has the following characteristics with respect to the elements O(1s), Ti(2p), C(1s) and Si(2p) [Figure 15A and 16A].

- (i) O(1s) shows a peak centered around 532 eV.
- (ii) Ti(2p) shows two peaks centered around 459 and 462 eV.
- (iii) C(1s) shows a relatively strong peak around 285 eV.
- (iv) There are no Si(2p) peaks observed in clean  $TiO_2$  surface.

The surface structure of silane modified  $TiO_2$  shows several changes in the XPS-spectrum with respect to the elements stated before.

- (i) The O(1s) develops a new peak at the higher energy side. An attenuation of the lower energy (original peak) O(1s) peak is also observed.
- (ii) The intensity of the Ti( $2p_{3/2}$ ) peaks are attenuated.
- (iii) A new Si(2p) peak appears.

These XPS-spectral changes are shown in Figures 15B and 16B. The second O(1s) peak is believed to be due to the formation of Ti-O-Si linkage during the process of surface modification. The reduction in the intensity of the higher energy O(1s) peak may be due to two reasons. It may be only (i) part of the surface Ti-OH groups undergoing derivatization reaction, or (ii) the reduction of intensity may be due to the loss of scattering O(1s) electrons for the presence of overlying surface (silane) layer.

Both Ti(2p) peaks show peak attenuation after the

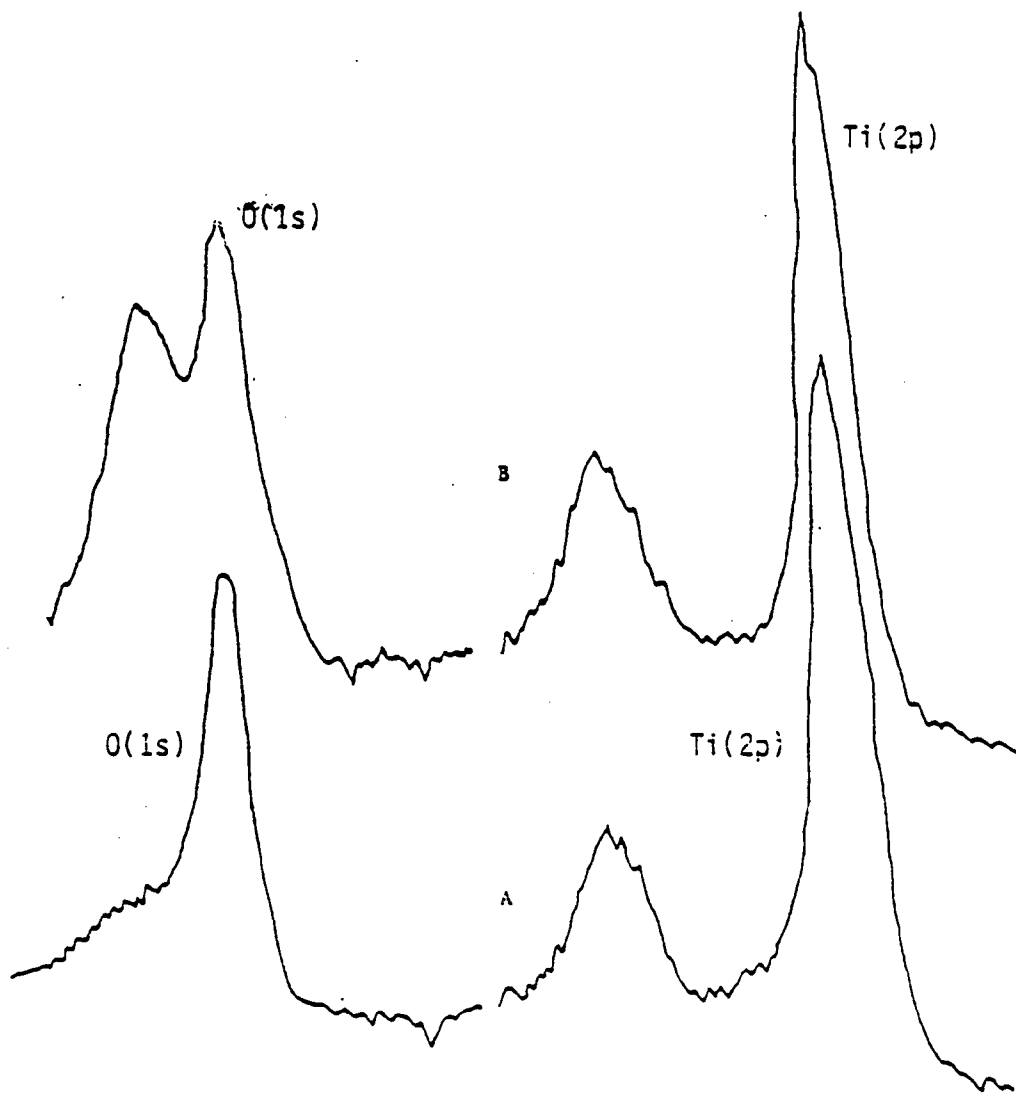


Figure 15: XPS traces:

(a) O(1s) and Ti(2p) before derivatization

(b) O(1s) and Ti(2p) after derivatization

Vertical scale O(1s) - 1024 units

Ti(2p) - 512 units



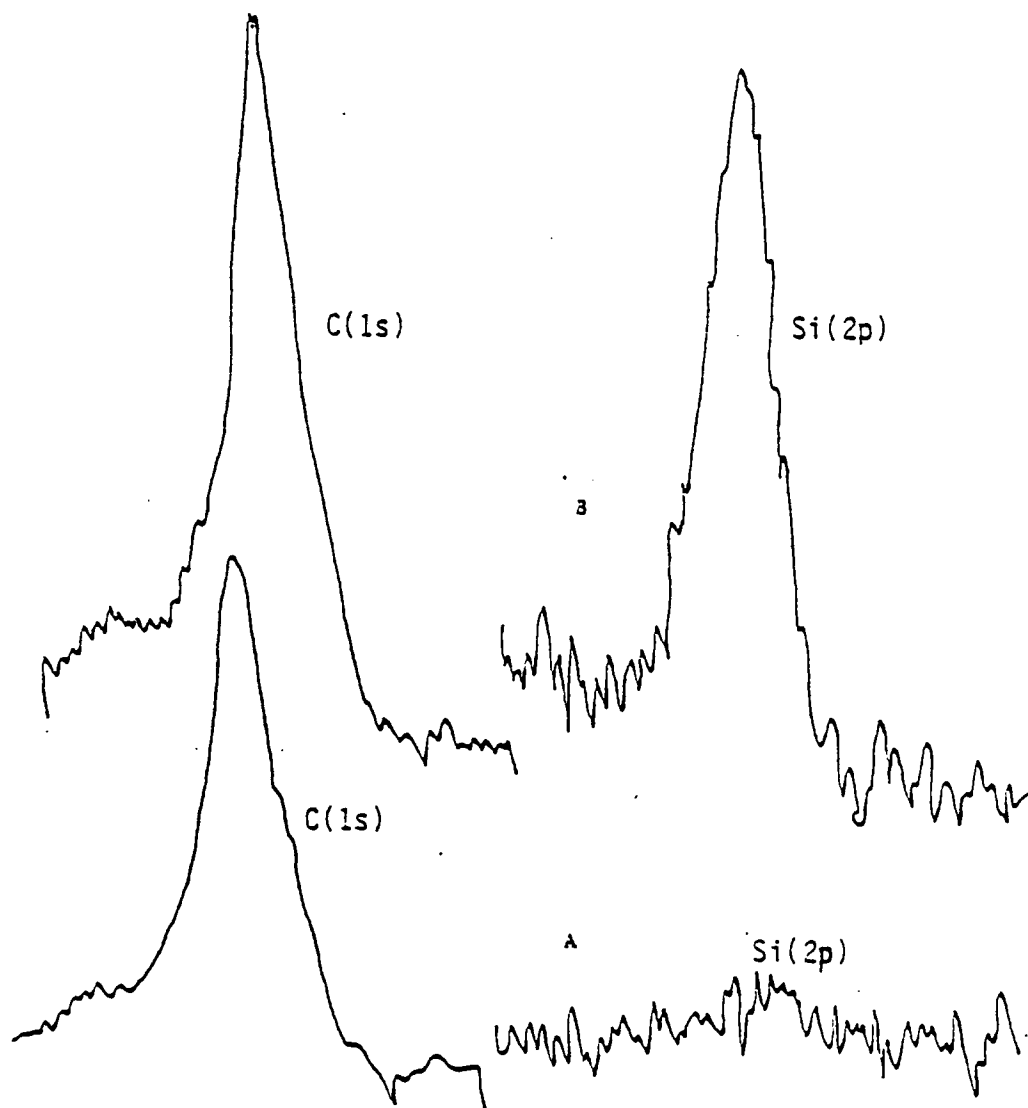


Figure 16: XPS traces:

(a) C(1s) and Si(2p) before derivatization

(b) C(1s) and Si(2p) after derivatization

Vertical scale C(1s) - 512 units

Si(2p) - 128 units

of overlying surface (silane) layer.

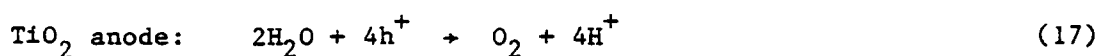
Both Ti(2p) peaks show peak attenuation after the derivatization process. The changes observed in these (Ti(2p)) peaks is also believed to be due to the presence of the overlying silane layer present in the modified layer. These changes in the Ti(2p<sub>3/2</sub>) signal can be used in order to calculate the thickness of the surface layer (modified) using the following equation (67).

$$I_{\text{Ti(coated)}}/I_{\text{Ti(clean)}} = \exp[-d/\lambda_{\text{Ti}}] \quad (16)$$

where  $d$  is the scattering layer thickness,  $\lambda_{\text{Ti}}$  is the characteristic scattering length of Ti photoelectrons. For Ti(2p<sub>3/2</sub>) this is reported to be 1.7 nm (67). The calculation of layer thicknesses based on this equation shows the presence of approximately one to two monolayers of silane on the modified TiO<sub>2</sub> surface (1 - 2 nm).

### 3.XII.B Photocurrent Generation Process

Titanium dioxide, which is a wide bandgap (3.0 eV) n-type semiconductor, has been reported to be a stable photoelectrode (59). The conduction band edge is at +0.05 v (vs SHE) at pH = 1 (28). The  $V_{\text{Fb}}$  at pH = 1 is reported to be -0.04 v (vs SHE), (53b). When illuminated in the presence of a suitable redox couple, photocurrent is generated. At the TiO<sub>2</sub> anode oxidation of water occurs, and at the cathode (Pt), reduction of protons occur. The redox reactions can be written as follows:





The cyclic voltammetric plots of  $\text{TiO}_2$  anode in the dark conditions and under illumination are shown in Figure 17. In  $\text{TiO}_2$  the plateau of photocurrent occurs around +1V (vs SCE) region. Since photocurrent is nearly maximum at +1.0 V, this is the potential at which the stability tests were performed.

### 3.XII.C Criteria for Silane Layer Stability

The objective of the surface modification of  $\text{TiO}_2$  was to force the electron transfer process between the electrode and the electrolyte out to the modified layer/electrolyte interface. Therefore a stable silane layer is expected to remain intact both before and after the photocurrent generation, ie. the XPS-signal due to Si would be expected to be the same before and after the photocurrent generation process, provided the other parameters such as instrument sensitivity remain constant during the process of the experiment. In reality the latter situation was not true. The instrument sensitivity, measured by using a solid sample, was found to vary to a certain extent from one day to another and in certain instances between the beginning and the end of the accumulation of XPS-data. Therefore, even if the same sample was examined on different days, a certain variation of individual signal intensities was observed. But examination of the intensity ratio ( $I_{\text{Si}}/I_{\text{Ti}}$ ) of the same  $\text{TiO}_2$  electrode yields reproducible results, independent of ESCA sensitivity (Table XXXIX). However, different  $I_{\text{Si}}/I_{\text{Ti}}$  ratios were observed for different electrodes, ie. there was no reproducibility of silane coverage from one electrode to another. This

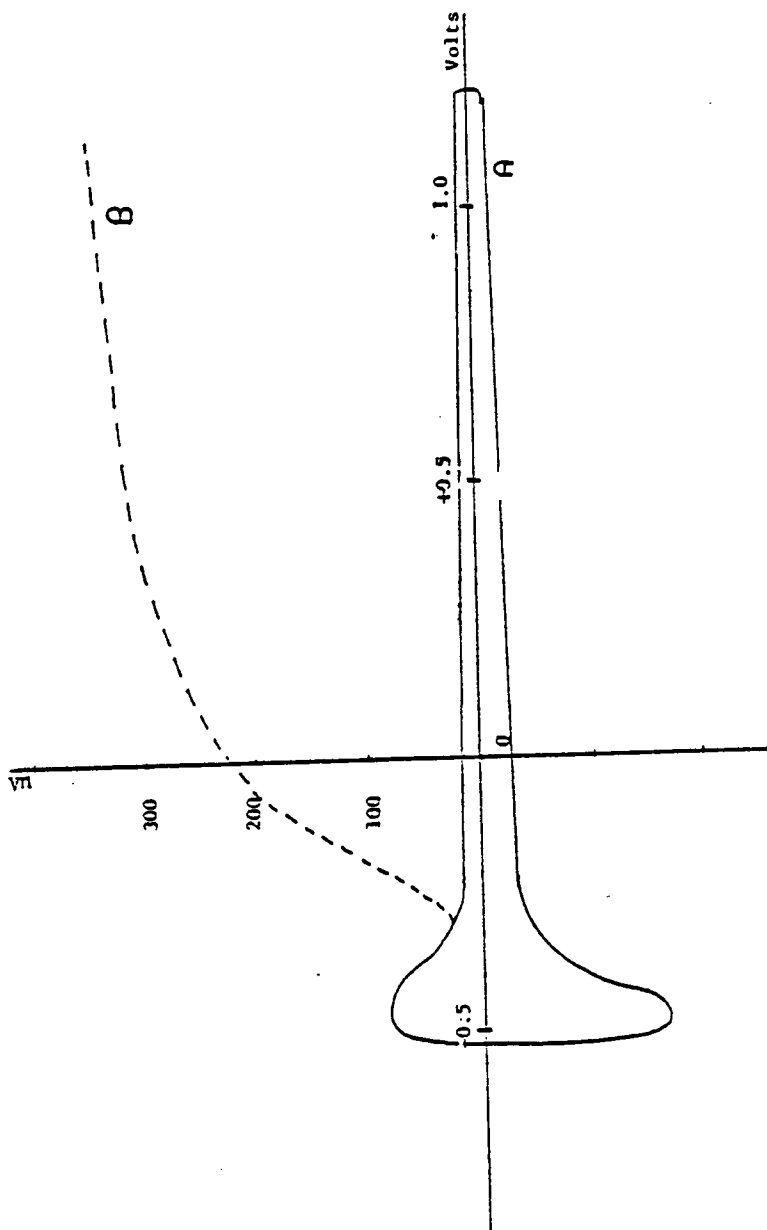


Figure 17: Cyclic voltammetric curves of titanium dioxide photoanode (a) under dark conditions (b) under illumination. (electrolyte: 0.5M sulphuric acid)

Table XXXIX

XPS  $I_{Si}/I_{Ti}$  data of control electrode\*\*

Electrode	$I_{Si}/I_{Ti}$				
T <sub>12</sub>	0.41	0.42	0.40	0.43	0.43

\*\* (1) This data is based on the measurements carried out over a period of two weeks.

(2) This was a derivatized electrode.

may be due to the surface reactivity of a particular electrode being somewhat related to the prior surface treatments it has undergone.

Therefore, the criteria for stability of the individual electrodes is defined as constant  $\frac{I_{Si}}{I_{Ti}}$  before and after the photocurrent generation process. In the case of loss of silane,  $I_{Si}$  would be lower and  $I_{Ti}$  would be higher, once the variation for instrumental sensitivity is corrected. Therefore in the event of an unstable silane layer the observed  $I_{Si}/I_{Ti}$  should be lower than that prior to the photocurrent generation.

### 3.XII.D Direct Silanization

The XPS data on directly silanized  $TiO_2$  is shown in Figures 18-20. The upper bar graphs show the  $I_{Ti}$  after the silanization reaction and after the photocurrent [cross hatched] generation experiments. The photocurrent generation experiments have been carried out in pH 0.5, 2; 6 and 10 buffers respectively. The upper bar graphs (open) further show lack of reproducibility of  $I_{Ti}$  from one electrode to another. The lower bar graphs show  $I_{Si}/I_{Ti}$  ratios before and after silanization and after photocurrent generation processes.

As it is evident in the upper bar graphs, the  $I_{Ti}$  signal in general has been reduced. After a detailed examination of XPS-traces, it was observed that in general, after the photocurrent generation experiment all the XPS-signal intensities of O(1s), Ti(2p) and Si(2p) had been lowered and C(1s) had slightly increased. This is believed to be due to coating of the photoelectrode by a carbonaceous layer during the photocurrent generation. Due to the presence of this layer, signal intensities for O(1s), Ti(2p) and Si(2p) should be generally reduced.

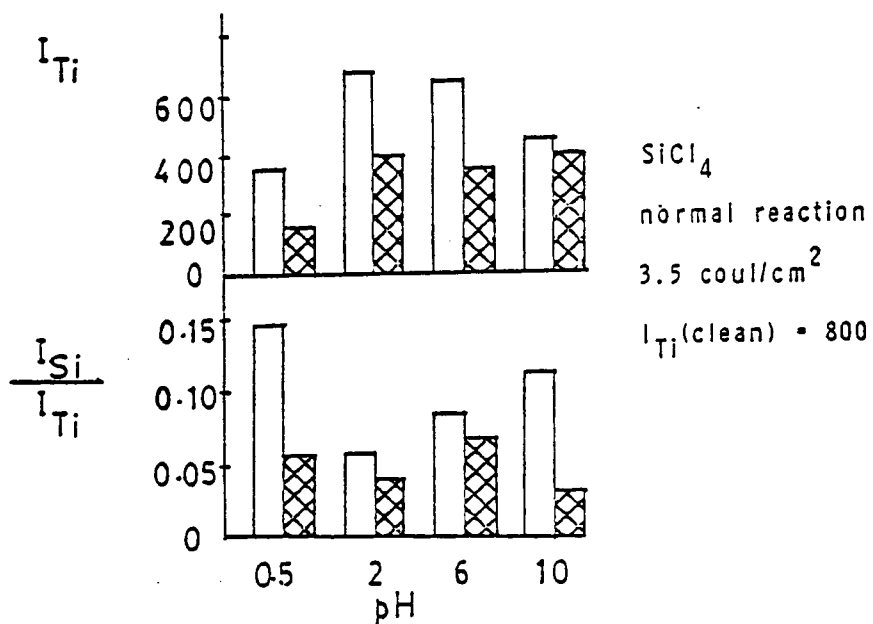




Figure 18 : Bar graphs based on the XPS-data of SiCl<sub>4</sub>- derivatized TiO<sub>2</sub> electrodes , before  and after  photocurrent generation.

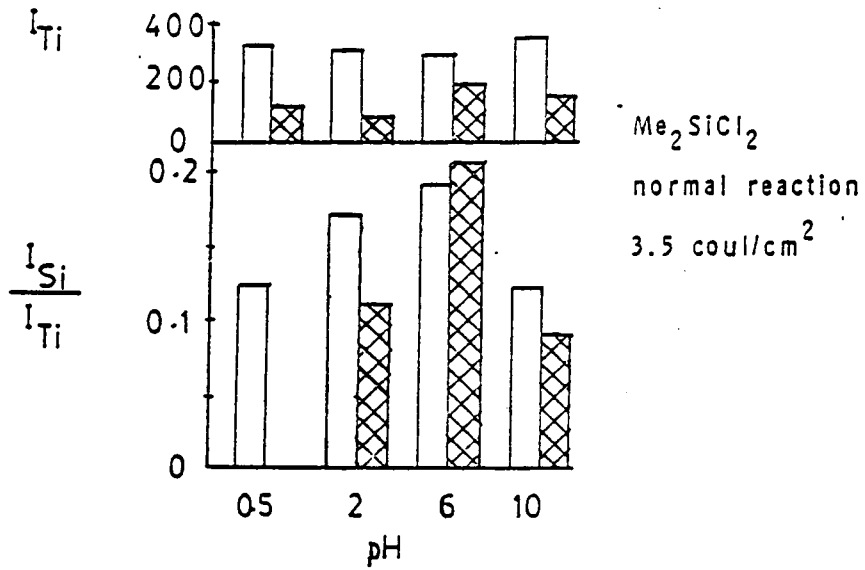




Figure 19: Bar graphs based on the XPS-data of Me<sub>2</sub>SiCl<sub>2</sub>-derivatized TiO<sub>2</sub> electrodes, before  and after  photocurrent generation.



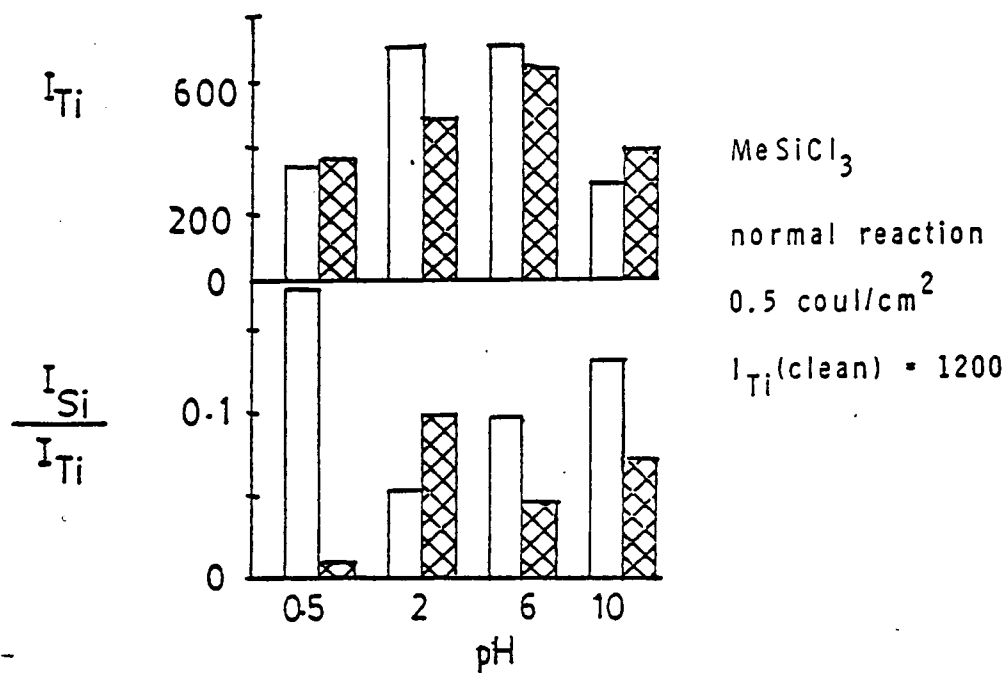




Figure 20: Bar graphs based on the XPS-data of MeSiCl<sub>3</sub> derivatized TiO<sub>2</sub> electrodes, before  and after  photocurrent generation.

For this reason, the previously defined criteria for the silane layer stability has to be further modified.

The XPS signal intensities for Ti(2p) and Si(2p) peaks are given by the following equations.

$$I_{\text{Ti}(\text{coated})}/I_{\text{Ti}(\text{silanized})} = \exp(-d'/\lambda_{\text{Ti}}) \quad (19)$$

$$\lambda_{\text{Ti}} = 1.7 \text{ nm (67)}$$

$$I_{\text{Si}(\text{coated})}/I_{\text{Si}(\text{silanized})} = \exp(-d'/\lambda_{\text{Si}}) \quad (20)$$

$$\lambda_{\text{Si}} = 2.2 \text{ nm (67)}$$

$d'$  = thickness of the carbonaceous overlayer.

By closer examination of these two equations it is evident that in the event of an overlayer [of constant thickness] the  $I_{\text{Ti}}$  signal will be more attenuated than  $I_{\text{Si}}$ . Therefore,

$$\frac{I_{\text{Si}(\text{coated})}}{I_{\text{Ti}(\text{coated})}} \frac{I_{\text{Si}(\text{silanized})}}{I_{\text{Ti}(\text{silanized})}} > 1 \quad (21)$$

This condition is reached with the assumption that the silane layer was unchanged during the photocurrent generation process.

Therefore, the modified criteria for silane layer stability is

- (i) If  $I_{\text{Si}}/I_{\text{Ti}}$  increases after the photocurrent generation, it indicates that the silane layer has survived the photocurrent generation.

(ii) If  $I_{Si}/I_{Ti}$  decreases or is the same as before photocurrent generation, the silane layer appears to have been removed.

On the basis of equation 19 it is difficult to give an exact numerical figure or a range as a criterion for the silane layer stability. This is determined by the thickness of the carbonaceous layer formed on individual electrodes and hence it is reasonable to expect different ratios for  $I_{Si}/I_{Ti}$  on different electrodes.

On the basis of XPS data obtained for chlorosilane-modified electrodes (Figure 18-20) it appears that the silane layers did not survive the photocurrent generation at all the pH's. But the loss appears to be lower at pH 2 and 6 buffers. In the case of dimethyldichlorosilane (Figure 19), the silane layer seems to have survived in the pH 6 buffer. In these directly modified electrodes some silane loss is observed at one pH or another. But in 0.5M  $H_2SO_4$  the loss of silane seems to be drastic. This further indicates that the carbonaceous layer formed on the electrode surface during the photocurrent generation step does not preclude the surface bound silane decomposition or hydrolysis mechanisms. A general discussion on modified layer decomposition mechanisms will be presented in a later section.

In the prior soaking experiments which were carried out to investigate the stability of modified layers in different pH buffers, neither the carbonaceous layer formation, nor the silane decomposition [except at extreme pH buffers] was observed. Therefore, it seems that the loss of silane and as well as the formation of carbonaceous layer occurs during the photocurrent generation process. Somerjai et al.

(68) have reported the presence of carbon contaminants on freshly sputtered surfaces after exposure to triply distilled water. But this did not seem to be a problem in our soaking experiments of derivatized electrodes.

### 3.XII.E Crosslinking Scheme

In the XPS studies of directly silane modified electrodes it was evident that the silane layers did not show adequate stability during the photocurrent generation, especially because the objective of the derivation of these modified surfaces was to be used in systems containing less stable photoanodes, such as GaP, GaAs, InP.

Therefore we have devised a two dimensional crosslinking scheme in order to enhance the survivability of the modified layer during the photocurrent generation process. In the kinetic studies of Hair and Hertl (20-23), as well as the derivatization model discussed on p. 36 (Chapter 2), it was evident that the reactive groups present in di-, tri-, and tetrafunctional silanes did not react completely with the surface hydroxide groups. Therefore, it is apparent that after the first reaction the surface bound silanes still carried unreacted hydrolytically unstable groups such as Cl, OMe etc. In fact this was evident in our infrared studies of methoxysilane-modified  $TiO_2$  surfaces (p. 58).

Therefore, after the first derivatization reaction, the reacted surface was exposed to water vapour (~20 torr) at room temperature. This causes hydrolysis of unreacted Si-X (X = OMe, Cl) bonds (Figure 21). Upon heating, this  $H_2O$  vapour-treated surface forms intersilane Si-O-Si linkages. This newly formed crosslinked surface has an added

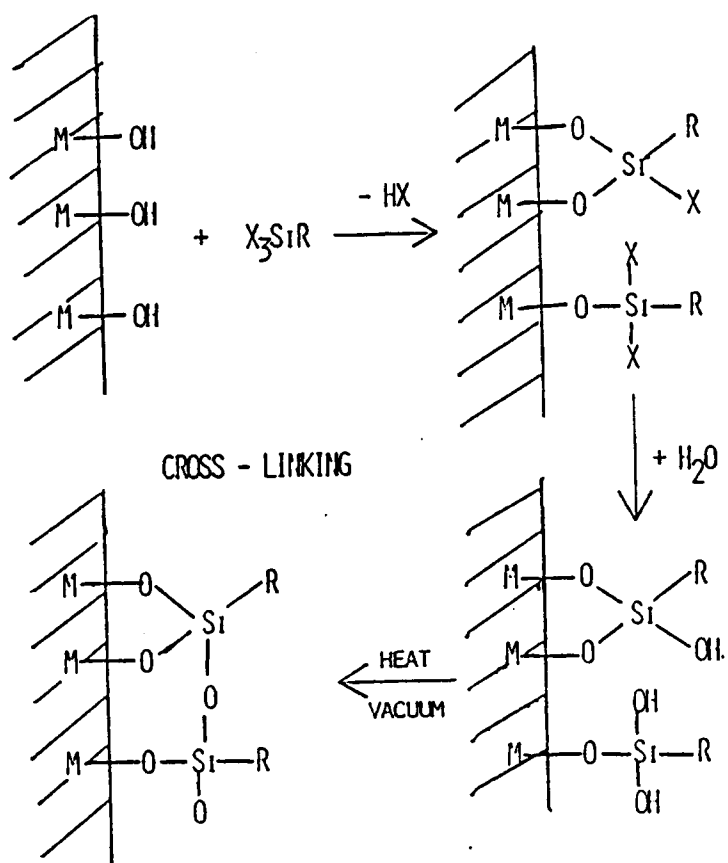


Figure 21: Cross-linking scheme for titanium dioxide modification.

advantage compared to the directly modified surfaces. In the latter case the silane moiety is not only attached to the  $\text{TiO}_2$  surface, but linked to the neighbouring silane moieties via one or two Si-O-Si links as well. Therefore in the event that the silane moiety is detached from the surface, still it has a reasonable lifetime in the neighbourhood of its former site of attachment, as it is held by the linkages to the neighbouring silane moieties. This provides a second chance for the detached silane moiety to recombine with the surface, and this in turn enhances the overall stability of the modified silane layer.

Therefore in the second phase, the derivatization procedure which is shown in Figure 21 was followed. In some instances the reaction procedure was repeated in order to obtain a more homogeneous modified layer. In the discussion this is referred to as a double crosslinking process.

### 3.XII.F The Stability of Crosslinked Modified Layers

Compared to the modified surfaces derived from direct surface modification, the latter modified surfaces derived from the crosslinking method (Figure 21) show overall enhancement of the stability. This observed improvement of the stability of modified layers is attributed to the mechanism which was discussed in the previous section.

The best modified layer has been derived from  $\text{SiCl}_4$  followed by  $\text{SiCl}_2\text{Me}_2$  (Figure 22) derivatization. This surface shows a very good stability in the three higher pH buffers (2, 6, 10). This may be due to the hydrophobicity of the outer surface derived from  $\text{Me}_2\text{SiCl}_2$ , in

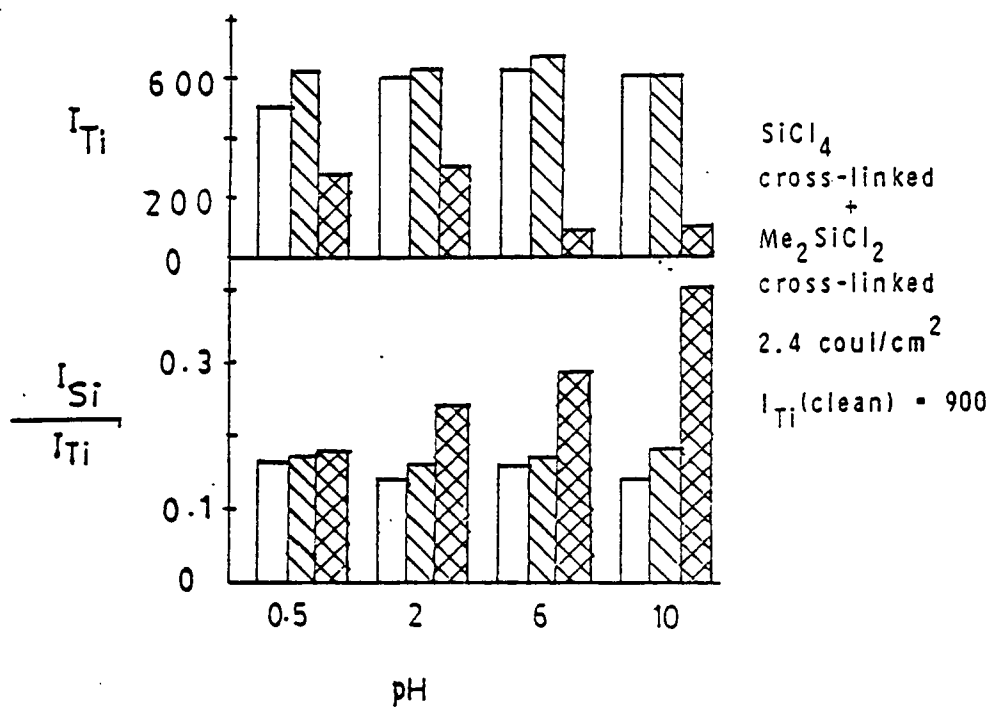





Figure 22: Bar graphs based on the XPS-data of TiO<sub>2</sub> electrodes modified with SiCl<sub>4</sub>/Me<sub>2</sub>SiCl<sub>2</sub>; (i)  after SiCl<sub>4</sub> modification (ii)  after SiCl<sub>4</sub>/Me<sub>2</sub>SiCl<sub>2</sub> modification (iii)  after photocurrent generation.

which the  $-\text{Si}(\text{Me})_2$  group induces the hydrophobicity and the  $-\text{SiCl}_2$  moiety provides an opportunity to crosslink to more than one silane moiety in the surrounding. This situation seems to have produced the best condition for the survivability of the modified layer during the photocurrent generation process.

All the other crosslinked modified layers have been derived from both tri- and tetrafunctional silanes. The hydrophobic nature of the modified layers derived from these silanes is much less than that of  $\text{Me}_2\text{SiCl}_2$ , due to the lower number of hydrocarbon functionalities available in these silanes. The lesser degree of stability observed in these surfaces most likely is due to this reason, in addition to the enhancement of the stability due to the presence of the crosslinking (Figure 23-26).

With some exceptions the following observations can be made on these crosslinked surfaces.

- (a) The most silane loss is observed in 0.5M  $\text{H}_2\text{SO}_4$ .
- (b) The greatest stability is observed in the pH - 6.0 buffer.
- (c) Moderate stability of the modified surfaces are observed in pH 2 and 10 buffers.

### 3.XII.G Silane Decomposition Mechanisms

With all the efforts to make a homogeneous modified layer by covalent attachment, it is doubtful whether this situation can be achieved in reality. In our infrared experiments we have observed the ability of silane reaction byproducts ( $\text{HCl}$ ,  $\text{NH}_3$  and  $\text{MeOH}$ ) to react with surface hydroxyl groups of  $\text{TiO}_2$ . This in turn removes some of the surface OH species which are expected to react with silane, causing



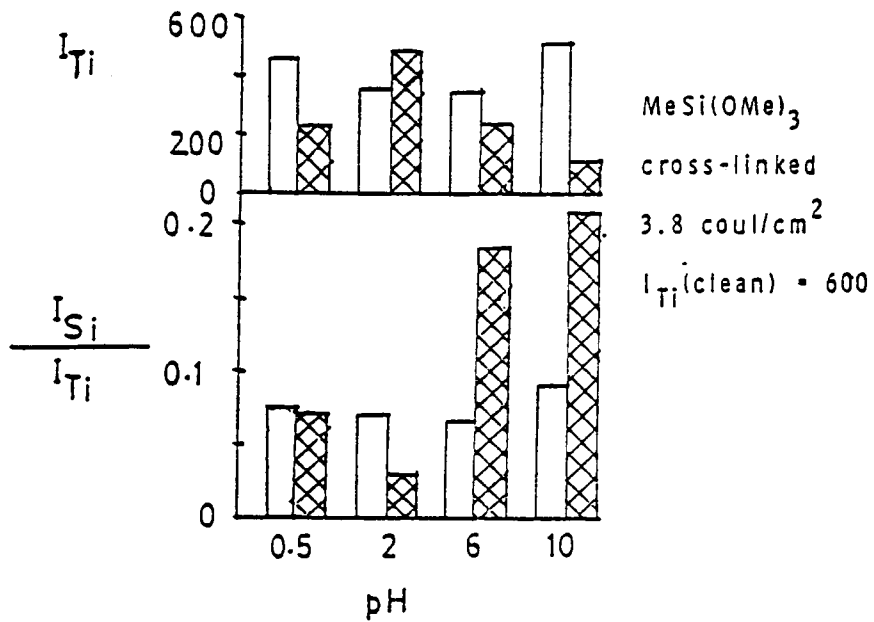


Figure 23: Bar graphs based on the XPS-data of modified  $TiO_2$  electrodes,

before and after 
  photocurrent generation.

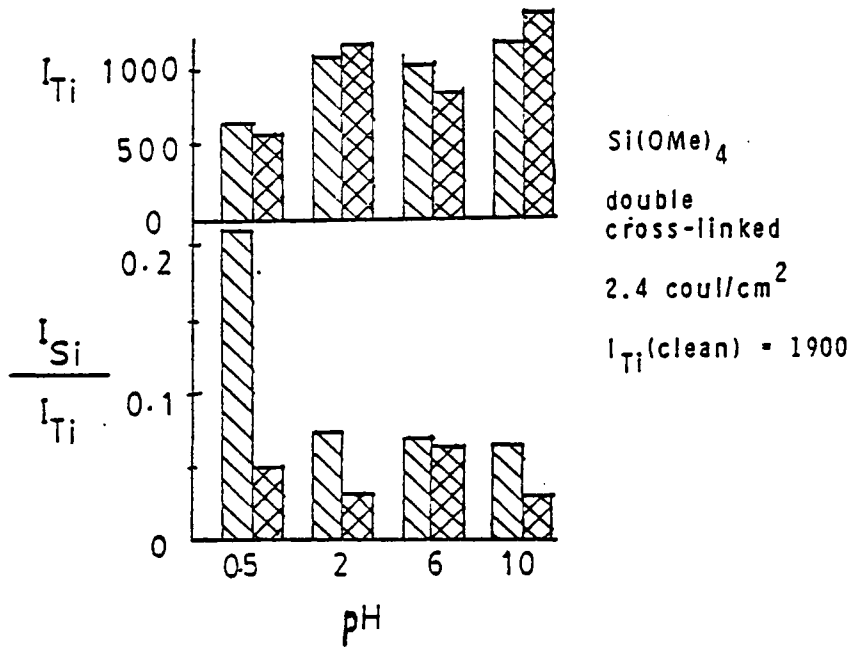




Figure 24: Bar graphs based on XPS-data of modified TiO<sub>2</sub> electrodes, before  and after  photocurrent generation.

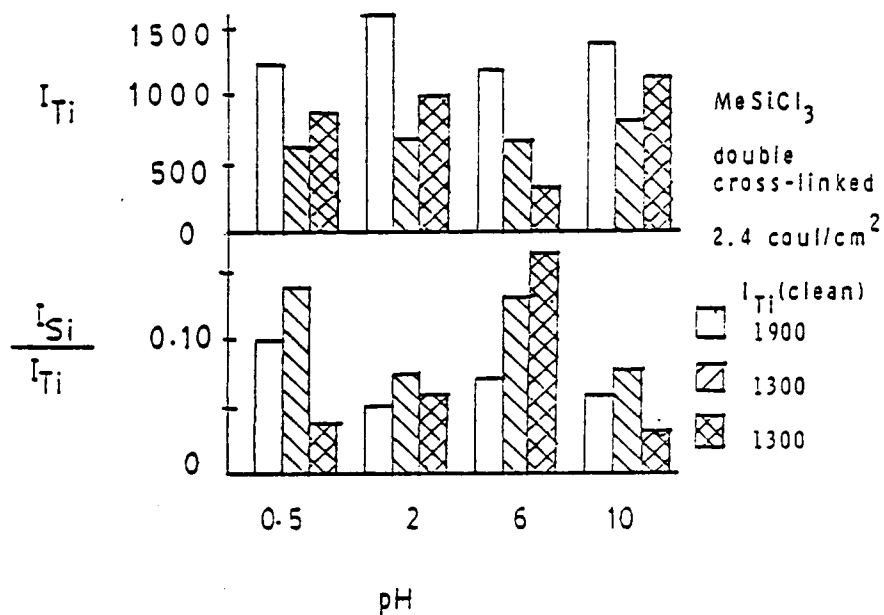
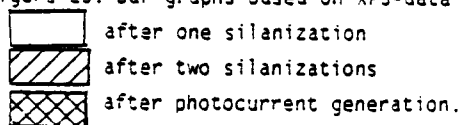


Figure 25: Bar graphs based on XPS-data of modified  $TiO_2$  electrodes.



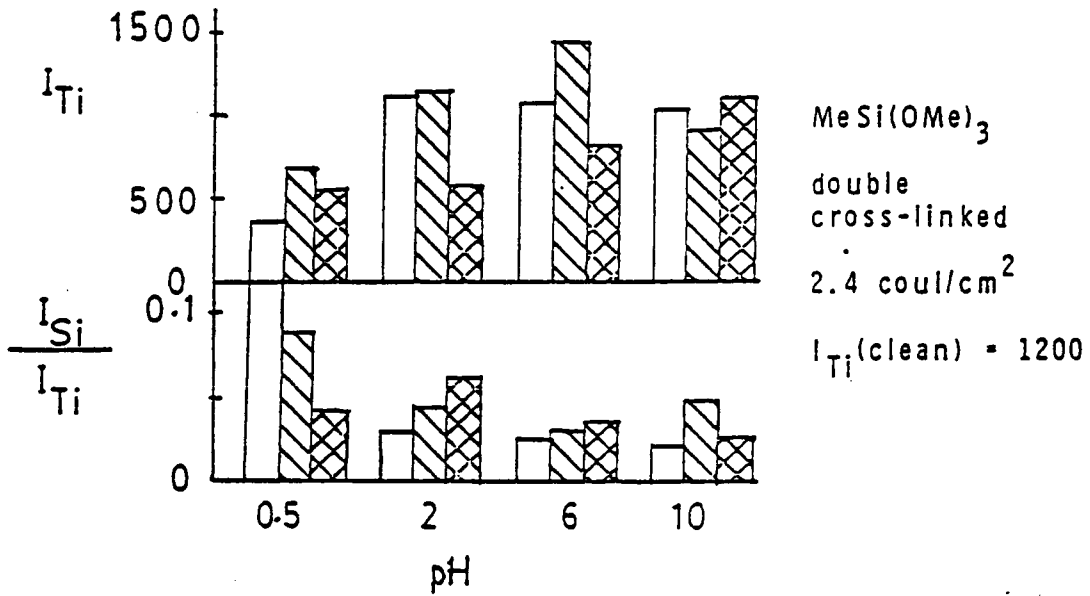
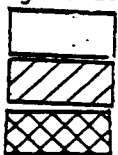


Figure 26: Bar graphs based on XPS-data of modified  $TiO_2$  electrodes



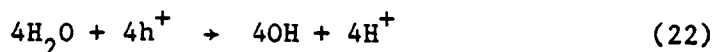
after one silanization

after two silanizations

after photocurrent generation

inhomogeneity in the modified layer. Both Wrighton (57) and Tamura (54) have observed decay of photocurrents of n-Si photoanodes which were derivatized with silylferrocene and TMCS respectively. They have attributed this decay to the formation of an oxide layer on the n-Si electrode at the sites which were left underivatized. There may be additional underivatized sites on the  $\text{TiO}_2$  surface due to thermal decomposition of surface  $-\text{OH}$  species. All these facts lead to the formation of an inhomogeneous modified layer.

During photocurrent generation, active hydroxyl radicals are formed due to the following  $\text{H}_2\text{O}$  oxidation reaction at the photoanode:



The intermediate  $\text{OH}$  is a very reactive entity. At the sites of surface inhomogeneity these species can reach underneath the modified layer and attack  $\text{Si-O-Ti}$  linkages. This in turn could cause loss of silane from the modified  $\text{TiO}_2$  surface.

In  $\text{SiCl}_4$ -derivatized electrodes (Figure 18) the silane loss is more severe than the other two silanes. This may be due to the lack of hydrophobic groups on this molecule and hence greater accessibility of  $\text{H}_2\text{O}$  molecules to the electrode surface.

Wilson and Harris (69a) have studied ageing effects of single crystal rutile anodes in  $0.5\text{M H}_2\text{SO}_4$ . Scanning electron micrographic studies of the (001) plane, before and after the photocurrent generation have shown striking alterations of the  $\text{TiO}_2$  surface

morphology. Due to this reason they have raised doubts about the ability to use wide bandgap  $\text{TiO}_2$  as a photochemical solar energy collector. In a later publication (69b), Wilson et al. have reported investigation of photocurrent generation in a series of electrolytes using  $\text{TiO}_2$  photoanodes. In this study they have observed that the photocorrosion of  $\text{TiO}_2$  did not occur in basic solutions and the observed photocorrosion in  $0.5\text{M H}_2\text{SO}_4$  could be suppressed by the addition of  $1\text{M}$  cobaltous ions.

In our studies of photocurrent generation in  $0.5\text{M H}_2\text{SO}_4$ , modified  $\text{TiO}_2$  has shown the most drastic loss of silane in almost all cases that have been studied. Murray et al. (70) have shown the stability of Sn-O-Si linkages under extremely acidic conditions. By analogy, it is reasonable to expect that Ti-O-Si is also stable in an acidic medium. Therefore, it seems that the strong silane losses observed in acidic medium are due to the morphological changes of the  $\text{TiO}_2$  surface during the photocurrent generation process.

Murray et al. (70) have demonstrated the rapid dissociation of silanes from modified tin oxide electrodes in the basic media. Similar behaviour can be expected from Ti-O-Si linkages as well. In our soaking experiments also we have observed a severe loss of the modified silane layer.

On the basis of the above discussion, it can be explained why we observe the best stability of the modified layers in the medium pH buffer solutions. There are three different mechanisms operative against the stability of the silane modified layer. The first mechanism, i.e. the decomposition of modified layer due to the

photogenerated OH is common at all the pH buffers. The surface etching or morphological changes of  $TiO_2$  have been observed only in lower pH buffer solutions (during photocurrent generation). The silane linkage decomposition is most drastic at basic pH conditions. Therefore, it is evident that at both lower and higher pH buffers, there are two mechanisms operative against the stability of the modified layer, whereas in the medium pH buffer only one mechanism effectively operates against it. This seems to be the reason why the best stability of the modified layer is evident in the medium pH buffer solutions.

### 3.XIII Conclusion

(1) Normal surface modification with simple silanes does not preclude photocorrosion due to inhomogeneity of the modified layer.

(2) Crosslinking and capping of the modified layer with a hydrophobic layer both enhance the stability of the modified layer.

(3) The modified layer seems to be most stable at moderate pH values due to the absence of corrosion and bond disruption mechanisms that are operative more extensively at extreme pH's.

## Chapter 4

### ELECTROCHEMICAL POLYMERIZATION

#### 4.1 Introduction

Organic synthesis is a discipline which has been very extensively developed during the last few decades and presently entertains a very rapid growth. It involves the use of very specific reaction conditions, such as catalysts, reagents, temperature, concentration, and other experimental parameters in a very precisely controlled manner. The much simpler and more selective synthetic potential of electrochemical systems is not extensively used by the organic chemists. This is most probably due to the lack of published treatments of electrochemical fundamentals as they specifically relate to organic principles. Electrochemical systems present several advantages; they are simple to operate, and control of the reaction conditions ie. rates, reaction extent, etc., is much easier. In addition to that there are a large number of electrode-specific synthetic reactions which are not obtainable by other means (71). Further, recent advances in electrochemical methods, especially in polarography and cyclic voltammetry of organic compounds, have provided more insight into the electrochemical applications in organic synthesis (72).

During the electrochemical process, a corresponding chemical process must take place at the electrode for each electron transferred



through the solution. There can be a number of competing oxidation or reduction processes that take place simultaneously, provided that the existing thermodynamic and kinetic conditions satisfy the requirements for those processes. The control of the electrode potential may be very useful under these circumstances. By proper selection of the electrode potential certain possible reactions may be eliminated, thereby enhancing the selectivity elements. The newer polarographic and potentiostatic equipment which has higher performance with respect to controlability and response can only enhance these possibilities. The tremendous potential of the electro-organic chemistry has been amply demonstrated in the published literature. Very difficult syntheses have been achieved with remarkable simplicity, selectivity, and high yields (71).

The applications of electrochemical reactions in polymerization have received much less attention even though there is a considerable range of possibilities existing for the electrochemical synthesis of polymers. The polymerization process may be induced by the passage of current through the electrolytic cell in the presence of the monomer. It may take place to a varying degree depending on current density, monomer concentration, applied potential, etc. (71). Further, the polymerization may be induced by electrochemistry of the monomer, or by electrochemistry of species other than the monomer. The initiation occurs by the generation of radical ions by electrochemical means. Alternatively, electrolysis may be employed to scavenge or remove an inhibitor present in the system, resulting in normal uninhibited polymerization. The reactions taking place at the opposite electrode

to that at which the initiation takes place may act as a source of termination or inhibition of electrochemical polymerization. The prevention of diffusion between the anodic and cathodic compartments may improve the polymerization process. The polymerization by electrochemical techniques may be controlled by several different means (71):

a) The rate of the reaction may be controlled by the current-time profile.

b) The molecular weight distribution can be controlled through the variation of imposed current, concentration of monomer, etc.

c) New synthesis of polymeric materials may be possible through the coupling reactions generated by electrochemical means.

d) Polymerization of a particular monomer may be initiated by selective voltage control.

It should be noted that, except for the initiating step, the electrochemical polymerization will proceed by the same mechanism as the thermal polymerization for the same monomer system in a similar environment. Once the initiating radical or anion is formed electrochemically, whether by direct electron transfer at the electrode or by interaction with a transient species, the further course of the reaction is unaffected by the passage of electric current. Another advantage of electrochemical systems is that it is possible to reverse the current, or employ an alternating current, so that the chemical environment is changed as a function of time, and the course of the reaction is changed accordingly. On the other hand, some limitations are imposed by electrochemical systems. The systems must have

reasonable conductivities, chemical compatibility, and adequate solubility characteristics. The choice of solvents and supporting electrolytes also impose further limitations on electrochemical systems.

The earlier studies of electrochemical polymerization have been focused on a means to synthesize polymers in the solution medium (72). The coating of the electrode during this process is unexpected and is considered undesirable. This situation has been described by such terms as 'electrode poisoning'. Subramaniam et al. (73) were first to attempt polymerization by electrolysis with the objective of depositing these polymers (73,74) onto different materials to form protective coatings. In electrochemical polymerization, since the coating is directly formed from the monomer, deposition is a more economical process and proceeds more uniformly than electrodeposition of polymers on metal surfaces.

The rapid growth of enthusiasm for electrochemically-induced polymerization as a means to synthesize modified surfaces is for several reasons;

a) Electrochemists are widely interested in tailor-made surfaces with predictive and externally controllable properties (75), specifically in the applications of (i) photoelectrochemistry and (ii) electrocatalysis.

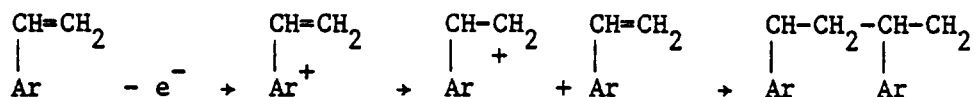
b) The surface modification using silanes containing hydrolytically unstable bonds is perceived not to be very successful. After extensive work conducted in this respect by the Murray (45-49) and Wrighton (57-59) research groups, they were doubtful if homogeneous

modified surfaces can be formed by silanization.

Our work on silane-modified surfaces also raises similar doubts (19,53a). We hypothesize that the loss of silane observed during the photocurrent generation was due to the inhomogeneity of the silane layer, enabling water molecules to move to the electrode surface at unreacted sites. Water oxidation generates highly reactive OH• radicals which in turn attack the silane linkages to the surface.

We were aware of the work done by Murray and co-workers (76) on electrochemical polymerization of metal complexes containing vinyl substituted ligands. They obtained homogeneous, pinhole-free, mechanically robust polymer-modified surfaces. The proposed radical polymerization of these complexes is that reduction is ligand-centered rather than metal ion-centered. Sufficient radical character migrates to the vinyl group by the resonance stabilization of complex so that the vinyl substituents undergo polymerization (76). Substantiation of this point has resulted from elemental ratio analysis of the polymeric complex. This has yielded the expected atomic ratio based on the monomer, indicating that the octahedral ligand structure of the metal ion remains intact during the polymerization process.

With this information in mind, we have attempted the synthesis of non-electroactive polymer coatings by electrochemical means, using the monomers styrene, divinylbenzene, 4-vinylpyridine, N-methyl-4-vinylpyridinium salts, phenol, and m- and p-nitrostyrene. The polymerization process (via oxidation) may be envisaged as follows (in this sketch Ar refers to aromatic moiety):



The polymer formed in the electrolyte adheres onto the electrode surface due to adhesion or precipitation or both of these effects.

#### 4.II Review of Previous Work

The discovery of organic polymers with electrical conductivity e.g.  $[\text{CH}]_n$ ,  $[\text{SN}]_x$ , has encouraged the development of newer polymers for various applications. The electrochemical polymerization (which is a much newer aspect) has also received considerable attention in the recent years due to the enhanced interest in surface modification for the purposes such as stabilization of n-type photoelectrodes, surface catalysis, etc. Diaz and co-workers have published a series of very interesting papers on electrochemical polymerization (77). Conducting polymer films of polypyrrole have been synthesized on Pt electrodes by electrochemical oxidation of pyrrole (77). The monomers are linked via the  $\alpha$ -carbon atoms in the polymer. The electrical conductivities of these films range from 10 - 100  $\Omega^{-1} \text{ cm}^{-1}$ .

In the second paper in this series (77b), Diaz et al. reported the feasibility of varying the conductivity of these films by controlling the composition of the initial monomer mixture of pyrrole and n-methylpyrrole. This provides a means to synthesize copolymer films, (pyrrole/n-methylpyrrole), with a range of conductivities. Further, these films demonstrate the property that the poly-pyrrole films can be switched between conducting and insulating behavior by mere potential

control.

Further, Diaz et al. (78) have reported the formation of polyaniline films by electrochemical polymerization. They indicate that these films are neutral and conductive in both the positive and negative potential regions, in contrast to polypyrrole films.

In a very recent report, Diaz et al. (79) present the synthesis (via electrochemical polymerization) and characterization of conducting polythiophene films. Thiophene and most of its  $\beta$ -substituted monomers yield polymer films upon electrochemical oxidation. These polymers, like the polypyrroles, show alternation between conducting and insulating behavior with respect to potential scanning.

Following the work done by Diaz and co-workers (77-79), Tourillon and Garnier (80) have surveyed a series of pyrrole type compounds, e.g. pyrrole, thiophene, furan, indole, and azulene. All of these monomers yield conducting polymers upon electrochemical oxidative polymerization. The presence of the counter ion in all of the cases has been confirmed by XPS studies.

Earlier, Murray et al. (45-49) have published a series of reports on surface modification of electrodes with silane reagents containing hydrolytically unstable bonds. They showed that the reactive groups of this surface-bound species undergo chemical reactions in a somewhat similar manner to free solution species. Pham et al. have published a series of reports which are somewhat parallel to the above mentioned work, but the surface modification has been achieved by electrochemical polymerization of 2,6-xyleneol and other alkyl-substituted phenols (81), substituted phenols containing reactive aldehyde and carbonyl groups

(81b), alcohol groups ( $\text{CH}_2\text{OH}$ ) (81c), amino groups (81d), aromatic amines (82) and (d) quinols (83). In these investigations they employ a technique called polaromicrotribometry (PMT), which is essentially a measurement of the frictional coefficient between the electrode being coated and a moving quartz slide. The variation of the frictional coefficient has been correlated to the extent of electrode coating by the electrochemical polymerization process.

Strojeck et al. (84) also have reported on the electrochemical polymerization of phenolic compounds. 4-(2-pyridylazo)-resorcinol (PAR) has an oxidation potential of +1.35 V (vs. Ag/AgCl) and continued scanning across this potential causes passivation of the working electrode (Pt) (gradual decrease of oxidation peak intensity). The structure of the film formed has not been determined, but the authors believe that the resorcinol unit of the PAR molecule undergoes polymerization forming polyoxyphenylene type chains similar to those reported by Pham and Dubois (81b). PAR has been reported as being a strong complexing agent (85) and the  $\text{Cu}(\text{PAR})_2^{2+}$  is considered to be the most stable metal ion complex ( $\log \beta = 38.2$ ), and this complex demonstrates that it also undergoes polymerization upon scanning across +1.35 V. The polymer-coated electrodes show (a) total blocking of o-dianisidine redox chemistry and (b) inhibition and decay of ferrocene redox chemistry.

All of the electrochemical polymerization processes that have been discussed so far besides pyrroles and thiophenes, involved aromatic compounds containing phenolic or amino groups. It seems that the presence of an aromatic moiety provides the right kind of stability to

the electrochemically-formed radical for polymerization. This may be due to the resonance conjugation of free radical character around the aromatic ring. Crown ethers also, in spite of some structural dissimilarities, undergo electrochemical polymerization of aromatic moieties (86). Le Berre et al. report the polymerization of benzo-15-crown-5, dibenzo-18-crown-6, and dibenzo-24-crown-8 ethers. Under micro-electrolysis conditions the redox properties of the film obtained are similar to that of veratrol, a trimeric product. The polymerization is carried out under very anhydrous conditions in order to prevent inhibition of the polymerization process by nucleophiles (i.e.  $H_2O$ ).

The other class of compounds that has been extensively investigated is the pyridyl derivatives. They include derivatives such as bipyridine and vinyl-substituted pyridyl and bipyridylmetallic complexes. The foundation for all of these studies is the accidental discovery of electrochemically-induced polymerization of methyl viologen (1,1'-dimethyl-4,4'-bipyridine) by Landrum et al. (87), even though there are earlier reports of the synthesis of polyviologen by chemical means (88). This report is one of the earlier ones that addresses the question of heterogeneous electron transfer by surface-confined species. The methyl viologen dication ( $MV^{2+}$ ) undergoes two single-step reductions to form a neutral species. Once the potential is scanned beyond  $-0.9$  V (vs Ag/AgCl) where the neutral species is formed, the  $MV^{2+}$  and  $MV^+$  cannot be regenerated. By a series of experiments, Landrum et al. concluded that the failure to regenerate the spectra of  $MV^{2+}$  and  $MV^+$  is due to the polymerization of  $MV^0$ .



In a somewhat similar study, Elliott and Martin (89) report the catalytic reduction of horse heart ferricytochrome-c by a polyvinylviologen-modified electrode. N-vinyl-4,4'-bipyridine ( $\text{VMQ}^+$ ) has been used as the monomer, and it yields an electroactive polymer upon reduction. The surface-bound species exhibits a reversible wave at -0.90 V. The alkylation of the free N-atom results in another redox wave centered at -0.45 V. Both the poly $\text{VMQ}^+$  modified electrode and the methylviologen polymer-modified electrode are capable of catalytically reducing cytochrome-c.

The use of various kinds of initiators in order to induce polymerization is very common in polymer chemistry. Following a similar approach, Faulkner et al. (90) have synthesized coatings on electrodes by inducing polymerization via electrochemically generated initiators different from the monomeric precursors. The reduction of 1 mM benzophenone at -2.5V in dimethylformamide/tetrabutylammonium perchlorate solution containing vinyl monomers (styrene and divinylbenzene) results in formation of copolymer films. The films can be sulphonated to yield anionic sites. The surface-bound film, upon soaking in  $\text{Ru}(\text{NH}_3)_6^{2+}$  solution (aqueous), exhibits surface electrochemical waves of  $\text{Ru}(\text{NH}_3)_6^{2+}$ . The Ru species is held by the anionic sulfonate sites in the polymer.

Polyvinylferrocene films also have been obtained by self-initiation via reduction as well as by benzophenone-induced initiation (90). These coated electrodes exhibit the characteristic behavior of a surface-bound redox polymer.

In polymer chemistry there are scores of polymers which are derived

from compounds containing vinyl groups, e.g. polystyrene and poly-DVB. It is only natural that electrochemists also have developed curiosity in electrochemical polymerization of vinyl-substituted compounds. Ghosh and Spiro (91) have moved in this direction, first by synthesizing (91) 4-vinyl derivatives of 4-methyl-2,2' bipyridyl and 1,10-phenanthroline. The Ru(II) complexes of these vinyl-substituted ligands have been employed in the synthesis of modified surfaces by both hydrosilylation (of silyl derivatives) and electrochemically induced polymerization. Both forms of these films show Ru(II/III) electrochemistry, which degrades when the electrodes are subjected to sufficiently negative potentials. A  $\text{TiO}_2$  electrode coated with poly-Ru(phen) $_3^{2+}$  exhibits dye-sensitized photocurrents due to the bound Ru complexes.

Even though Ghosh and Spiro (91) established the synthetic procedures for vinyl substitution of heterocyclic ligands, they did not conduct a detailed study of electrochemical polymerization of these vinyl-substituted ligands or their metal complexes. But the synthetic procedures they developed have set the basis for a series of very interesting papers by Murray and co-workers (92-97) on redox-active polymers formed by transition metal complexes of vinylbipyridine (vbpy) and vinylidiquat. The first paper of this series (92) introduced the synthesis of (electrochemically) redox active polymers,  $[\text{Ru}(\text{bpy})_2-(\text{vpy})_2]^{2+}$ ,  $[\text{Ru}(\text{vbpy})_3]^{2+}$ ,  $[\text{Fe}(\text{vbpy})_3]^{2+}$ , and  $[\text{Ru}(\text{bpy})_2-(\text{vpy})\text{Cl}]$ . Standard procedures for synthesis of these complexes have been previously reported by Meyer et al. (95,96). The backbonding interaction of  $\Pi$ -electrons enhances the electron density on the ligand

$\pi$ -orbitals and the electrochemical reduction of the complex is ligand- rather than the metal-localized (92). The polymerization of these complexes is induced by electrochemical reduction which results in a stable, adhering, pinhole-free polymeric film on the working electrode. The complexes with di- and tri-vinyl substituents appear to be more easily polymerizable than those complexes with mono-vinyl substituents (94). These monomers have been employed in the synthesis of three different types of polymers: a) homopolymers, b) co-polymers from mixed electrolytes of complexes, and c) bilayer films which have been synthesized by forming a polymeric film from one complex and subsequently forming a second polymer film over the first. These studies have demonstrated semiconductor-like unidirectional current flow properties for the bilayer films (92,93,97).

The advantages of redox conductive polymers compared to non-conductive polymers are: (1) the accumulation of polymer can be observed by the gradual increase of redox waves due to the bound species; (2) the extent of coating can be controlled readily; and (3) the amount of the redox-active material and hence the film thickness can be measured easily. These polymers have been synthesized on metal (Pt, Au) and semiconductor ( $\text{TiO}_2$ ,  $\text{SnO}_2$ ) electrodes. The elemental analysis of the homo-polymers shows that the coordination sphere of Ru indeed remains intact during and after the polymerization process. The chain propagation mechanism associated with electrochemical polymerization has been demonstrated by formation of copolymers in mixed electrolytes (with respect to the various complexes); the polymerization is initiated at a potential at which only one complex

has any redox activity. The presence of the second polymer in the film that is formed presents evidence for the chain propagation mechanism. Bilayer films have been synthesized by the deposition of a second film on an electrode which is already coated with a first film.

In a study aimed at a better understanding of the electrochemical polymerization of ruthenium vinylpyridines and vinylbipyridines, Murray et al. (94) have investigated a) the relative ease of polymerization of monomers with different number of vinyl groups, b) the composition of polymer films, and c) charge diffusion rates through the polymeric films. A range of metal complexes have been used in this study, i.e.  $[\text{Ru}(\text{vbpy})_3]^{2+}$ ,  $[\text{Fe}(\text{vbpy})_3]^{2+}$ ,  $[\text{Ru}(\text{vbpy})_2\text{Cl}_2]$ ,  $[\text{Ru}(\text{bpy})_2(\text{bpy})_2]^{2+}$ ,  $[\text{Ru}(\text{bpy})_2(\text{vbpy})_2]^{2+}$ ,  $[\text{Ru}(\text{bpy})_2(\text{vpy})\text{Cl}]^{2+}$ , and  $[\text{Ru}(\text{bpy})(\text{vpy})\text{NO}_2]^+$ . The substrates that have been used are Pt, Au,  $\text{TiO}_2$ , and  $\text{SnO}_2$ . No film accumulation is observed by reduction of  $[\text{Ru}(\text{bpy})_3]^{2+}$ , indicating the importance of the presence of the vinyl group on the ligand. The complexes with more than one vinyl substituent undergo polymerization with considerable ease. The redox waves of deposited films in a clean electrolyte are very similar to those of the respective dissolved complexes. Further, resonance Raman spectra of the films show the expected pattern for ligand vibrations for the metal complexes. A visible spectrum of  $\text{poly}[\text{Ru}(\text{bpy})_2(\text{vpy})_2]^{2+}$  matches the monomer spectrum with only a slight red shift of the main absorption peak. All of this evidence leads to the fact that the integrity of monomer coordination is preserved following the polymerization process.

As these polymer films consist of cationic species, they behave as solid state polyelectrolytes and show ion-exchange properties.

Pt/poly[Ru(vbpy)<sub>3</sub>]<sup>2+</sup> completely suppresses the redox chemistry of methylviologen dication (MV<sup>2+</sup>). Pt/poly[Ru(bpy)<sub>2</sub>(vpy)<sub>2</sub>]<sup>2+</sup>, when soaked in aqueous ferrocyanide solution, shows persistent electrochemical response of electrostatically bound ferrocyanide, when it is transferred to a clean electrolyte. Similar observations have been reported for poly-4-vinylpyridine (protonated) (98) and poly[N-methyl-4-vinylpyridinium] (99) coated electrodes. In addition to that, these highly cross-linked films exhibit size-exclusion. For example, poly[Ru(vbpy)<sub>3</sub>]<sup>2+</sup> excludes both the cationic [Fe(bpy)<sub>3</sub>]<sup>2+</sup> and the neutral [Fe(CN)<sub>2</sub>(bpy)<sub>2</sub>], whereas the smaller ferrocene (neutral) diffuses into the polymer film at a measurable diffusion rate. The oxidation of [Fe(CN)<sub>2</sub>(bpy)<sub>2</sub>] does not occur until the [Ru(vbpy)<sub>3</sub>]<sup>2+</sup> film reaches its own redox potential, at which point the Fe complex is oxidized by mediated electron transfer. Further, this exclusion of cations and large neutral species indicates that the modified surface is free of pinhole defects.

The chain propagation step involved in the polymerization process has already been discussed (92). But this does not seem to be a completely general effect because the reduction of vinyl diaquat dication at -1.0 V in the presence of [Ru(vbpy)<sub>3</sub>]<sup>2+</sup> monomer does not produce a copolymer. Also, the polymerization efficiencies that have been observed for most of these systems are much lower than expected. In the event of an efficient chain mechanism the film coverage should very much exceed the amount of charge passed during the initiation step. But the rate of the polymerization reaction is coupled to several factors:

- a) the rates of mass transfer to the electrode and reduced monomer away from the electrode;
  - b) reaction of the reduced monomer with fresh monomer in the diffuse layer;
  - c) eventual oxidation of radicals and film by trace impurities such as  $O_2$  in the electrolyte, which essentially terminates the polymerization process;
  - d) the soluble oligomer which remains in the solution;
  - e) particulate polymer which does not adhere to the electrode.
- These factors may well account for the lower efficiencies of the polymerization process.

Another potential application of the coated electrode is pH sensing. Heineman et al. (100) have reported pH response of coated electrodes derived from 1,2-diaminobenzene. The oxidation of the diamine in pH-7 buffer is irreversible, with gradually decreasing peak currents on successive potential scans. In the range pH 4 - 10, these coated electrodes yield a linear response with a slope of 53 mV and a linear correlation coefficient of 0.991. However, Cheek et al. (101) showed that phenol-coated electrodes and even bare Pt electrodes exhibit a potentiometric response to pH.

#### 4.II.A Characteristics of Surface Bound Redox Species

As it has been already shown, the chemical modification of electrodes could be brought about by (i) covalent attachment of molecules to the surface functional groups (ii) electrochemically induced polymer deposition. Regardless of the way the surface

modification is carried out, the surface bound species essentially carry the same electrochemical characteristics (102).

(i) The amount of electroactive species bound to the electrode surface can be measured by the area [number of Coulombs,  $Q$ ] under the particular redox wave. The number of molecules bound to the surface can be determined from this with the knowledge of  $n$ , [number of electrons] associated with the particular redox process. Further, surface density of redox active material ( $\Gamma$ ) is given by

$$\Gamma = \frac{Q}{nFA} \quad (24)$$

ii) In a mass transfer controlled redox system, the peak separation,  $\Delta E_p = [E_{ox} - E_{red}] > \frac{60}{n}$ , the equality being for reversible systems. For an ideal cyclic voltammetric behavior of an electrode surface-confined species (reversible redox),  $\Delta E_p$  should be zero. Deviations from ideal behavior may occur due to the resistance to electron transfer between the electrode and the surface bound redox species due to the (a) thickness of the layer, (b) resistance to counter ion flow, etc.

(iii) The surface bound redox species ideally should yield linear  $i_p$  dependence to scan rate.  $I_p$  is the redox peak height of the surface bound species; unlike the mass transfer controlled system, the peak current ( $i_p$ ) is directly proportional to the scan rate (102).

$$i_p = \frac{n^2 F^2 v C^*}{4RT} \quad (25)$$

$v$  - scan rate.

#### 4.III Experimental

Commercially available reagents [Aldrich] were used without further purification. Divinylbenzene (DVB), analyzed by both GC and HPLC, showed the presence of all three isomers.

##### 4.III.A Synthesis: [N-methyl-4-vinylpyridinium salts]

4 ml of 4-vinylpyridine (Aldrich) in 50 ml of dry ether (Fisher) was cooled to  $-10^{\circ}\text{C}$ . 10 ml of methyl iodide (Fisher) was added gradually, with stirring. The mixture was kept at  $-10^{\circ}\text{C}$  overnight, filtered and was washed with dry ether. On some experiments the counter ion ( $\text{I}^{-}$ ) was replaced with  $\text{BF}_4^{-}$  by metathesis. N-methyl-4-vinylpyridinium iodide was dissolved in a minimal amount of water and this was mixed with saturated solution of  $\text{NaBF}_4$  (0.5 ml). The mixture was centrifuged and the supernatant liquid was discarded. The centrifugate was dried in the vacuum line. A solution of this solute in acetonitrile was used for the electrochemical polymerization reaction.

##### 4.III.B Electrochemistry

The three compartment cell used in the electrochemical experiments was first cleaned with soap, secondly with methanol. The frits of the cell were cleaned by forcing through them both water and methanol under suction. Thirdly the cell was heated for 3-4 hrs in hot concentrated  $\text{H}_2\text{SO}_4$ . Both the cell and frits were finally rinsed with deionized water and stored in the oven at  $110^{\circ}\text{C}$ .

At the beginning of each experiment the hot cell was stoppered with



serum septa while Ar was flowing through the cell. Acetonitrile (Burdick and Jackson) was stored over activated molecular sieves (Fisher) to ensure dryness. In the electrochemical experiments the electrolyte was 0.1M tetraethylammonium perchlorate (TEAP) (Eastman) in dry acetonitrile. The TEAP was also dried at 100°C prior to the electrolyte preparation. The electrolyte was transferred into the argon-purged electrochemical cell through a chilled (-20°C) alumina (Fisher) column to ensure the dryness. The working electrode compartment was quickly stoppered with a serum septa. The electrolyte was forced into the other two stoppered compartments by sucking air in those compartments with a syringe.

The working electrodes and the counter electrode were platinum beads sealed in soft glass, platinum rotating disc electrodes (Pine Instruments), or gold flags attached to gold wire. The working and counter electrodes were cleaned by (a) heating in hot concentrated H<sub>2</sub>SO<sub>4</sub> for several hours, and (b) subjecting them to O<sub>2</sub> and H<sub>2</sub> evolution in 0.5M H<sub>2</sub>SO<sub>4</sub> acid until the characteristic clean cyclic voltammograms of the metal electrodes were obtained. All the potentials were measured against a NaCl-saturated calomel electrode (SSCE).

Deposition of the polymer was carried out by multiple potential sweeps through the appropriate oxidation or reduction wave. During the first scan a large oxidation or reduction wave was evident due to the redox process. Rapid passivation of electrode was evident after the first scan indicating the coating of the electrode surface. After 10-20 scans the electrode was removed, rinsed with methanol and stored at 60°C in the oven.

X-ray photoelectron data of the polymer layers were obtained on a Kratos XSAM80 instrument using a Mg anode.

A Pine Instrument (Philadelphia, PA) rotating disk set up was used in the rotating disk voltammetric studies. Teflon shrouded Pt disk electrodes of 7.0 mm diameter and rotation speeds up to 4900 rpm were used in these studies. All the electrochemical reagents are the same as in the previous experiments.

#### 4.IV Results and Discussion

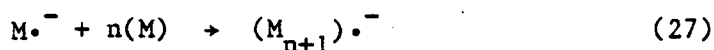
##### 4.IV.A Vinyl-Polymerization

The polymerization of inorganic complexes containing vinyl groups has been reported by several research groups (91,94,95). In these studies the ligands are aromatic components which are reducible by electrochemical means. Once the radical is formed within the aromatic component, conjugation transfers the free electron to the vinyl component which in turn induces the polymerization. This process may be visualized as follows:

- a) Formation of monomer by electrochemical reduction



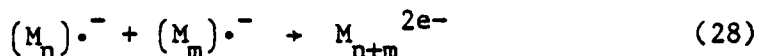
Propagation step



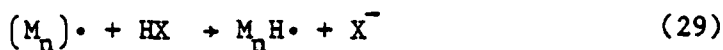
As discussed earlier, Murray et al. have demonstrated that there is a chain propagation step involved in the polymerization process (94). The proof lies in the co-polymerization of two vinyl-substituted metal complexes at a potential where only one of the complexes is reduced.

The chain termination step is much less clear. There are several possible mechanisms (72b),

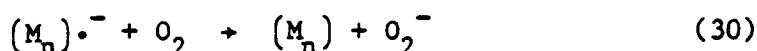
c) combination of two radical chains



d) abstraction of a proton from a solution species



e) electron transfer with oxygen present in the solution



We have attempted polymerization of series of organic compounds: divinylbenzene, 4-vinylpyridine, styrene, p- and m-nitrobenzene, N-methyl-4-vinylpyridinium salts and phenol. Table XXXX shows the oxidation and reduction potentials of these compounds of interest. From these divinylbenzene, 4-vinylpyridine and phenol yielded polymer films upon oxidation. N-methyl-4-vinylpyridinium salts yielded a polymer film upon reduction.

The polymerization scheme for 4-vinylpyridine may be visualized as follows. In 4-vinylpyridine, the highest electron density is located at the nitrogen atom so the abstraction of an electron from the lone pair on the N-atom is most favorable.

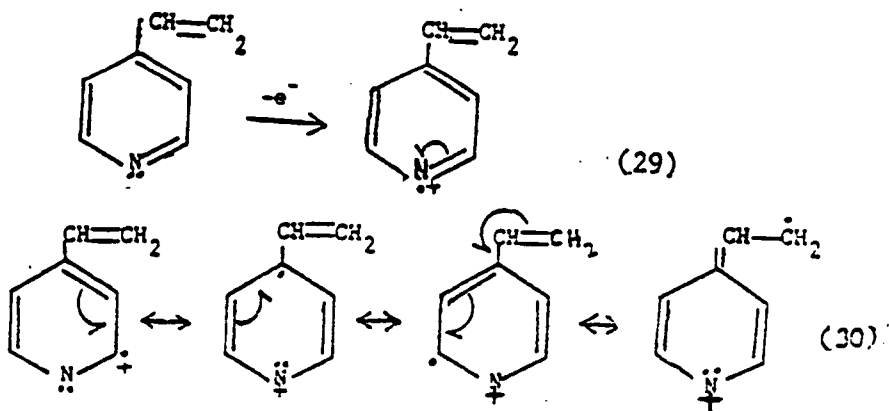
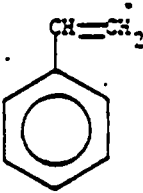
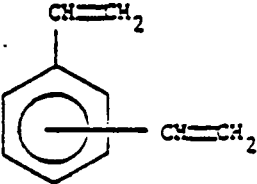
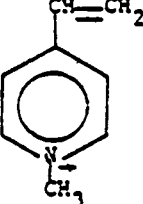
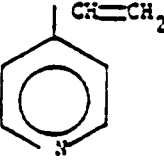
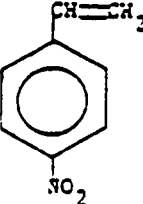
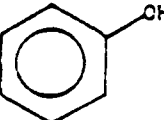
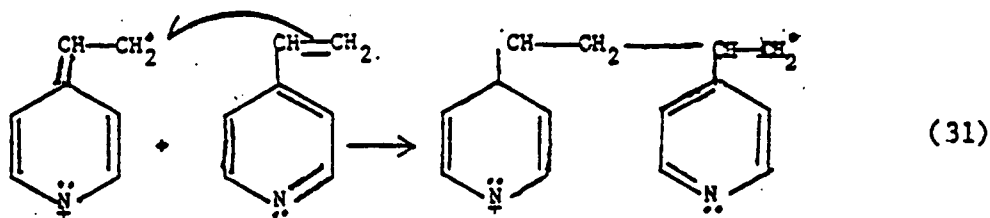


Table XXXX

	first reduction(volts)	first oxidation(volts)
	-2.45	+1.90
	-2.30	+1.75
	-1.30	+2.12
	-2.5	+1.7
	-1.15	+2.3
	-	+1.6

#(ref.SSCE)

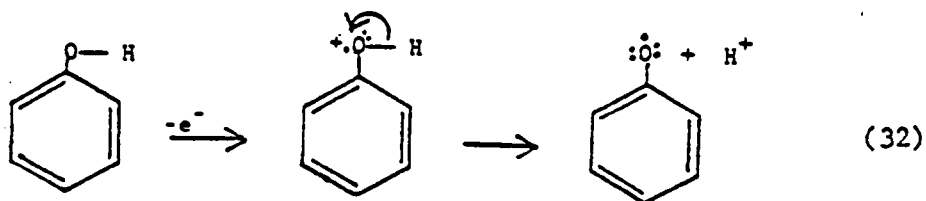
The formation of polymer chains may be visualized as follows;



The oxidative polymerization of divinylbenzene and the reductive polymer formation of N-methyl-4-vinylpyridium salts should follow a similar sequence in the polymerization process as the initial step is very much similar to that of 4-vinylpyridine.

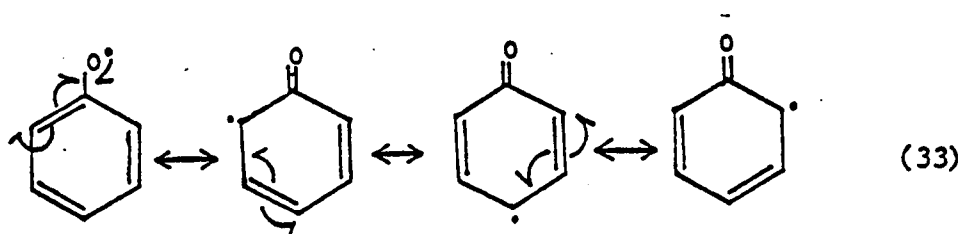
#### 4.IV.B Polymerization of Phenol

In a series of papers published on electrochemical polymerization of phenolic compounds, Pham and Dubois (81) have proposed the initial step to be the formation of the phenolate radical by electrochemical oxidation. These studies have been carried out in alkaline methanolic media whereas our studies have been done in non-aqueous media. In spite of these differences, formation of phenolate radical seems to be a reasonable initiation step even though through a different mechanism.

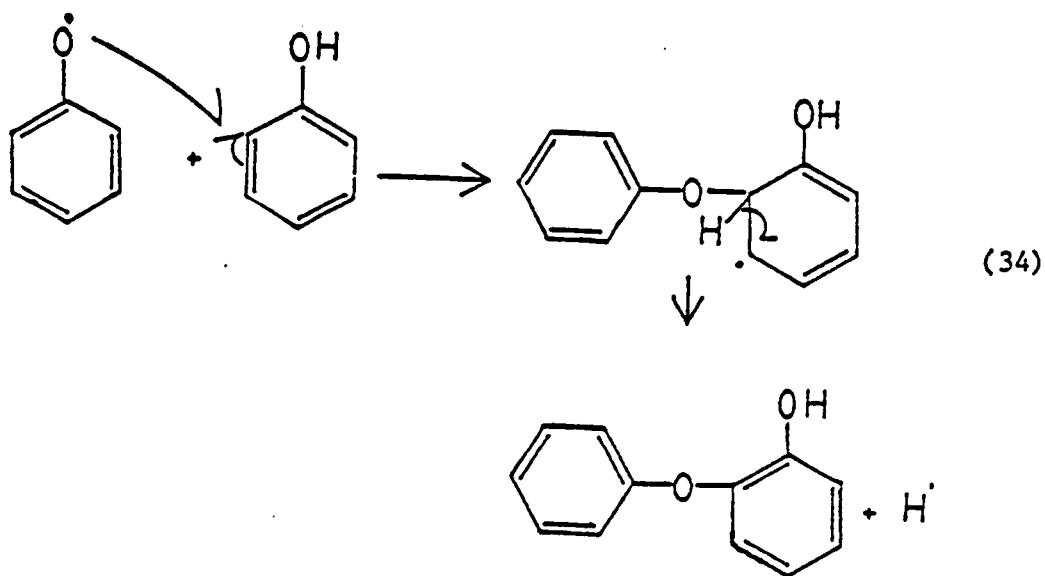


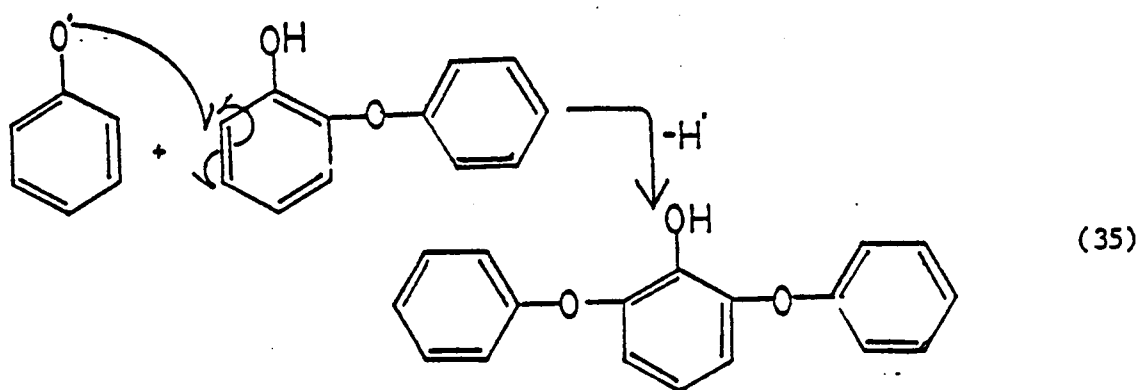
After the polymer deposition using phenolic solutions, there is always a reduction peak around  $-0.7$  V (vs SSCE) when the cyclic voltammetric scanning is carried out using a clean electrode. This

reduction peak does not appear before the deposition step and is believed to be reduction of  $H^+$  ions generated during the deposition step. The phenolate radical ion can undergo resonance conjugation as follows:



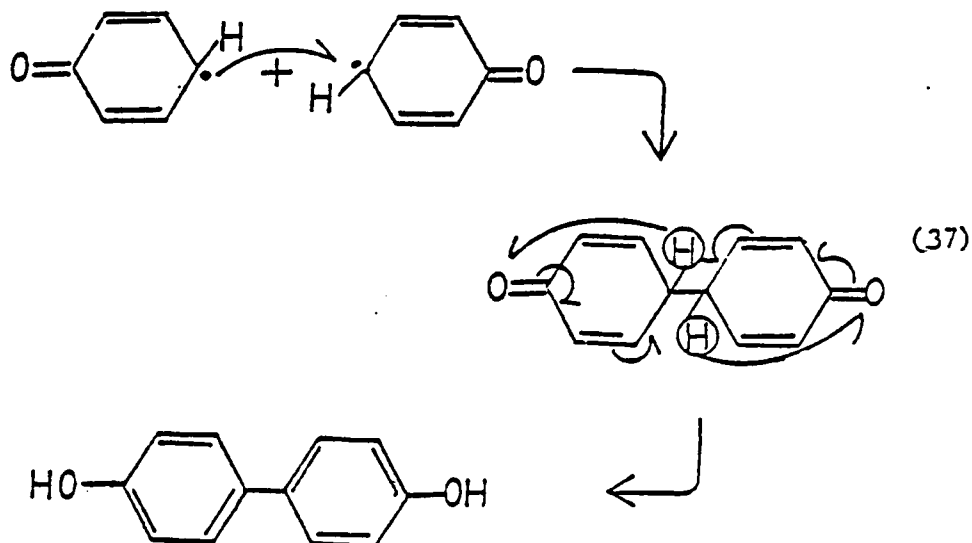
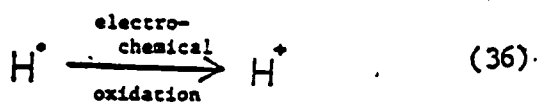
The proposed propagation mechanism is as follows:





The propagation can take place at ortho and para positions of the aromatic moiety.

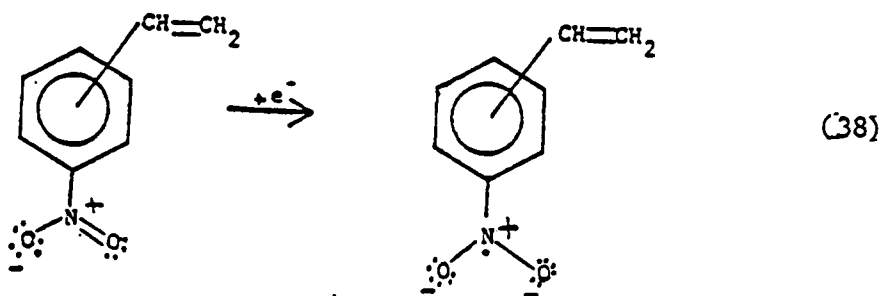
The proposed termination mechanism is as follows:



Similar termination may take place at ortho/ortho, ortho/para positions as well. In these phenol derived polymers, the presence of the C-O-C (polyoxide) linkage has been demonstrated by both infrared spectroscopy (absorption bands around  $1200\text{ cm}^{-1}$  (81b)) and by XPS C(1s) peak at 286.60 eV (81b).

#### 4.IV.C Stability of Electrochemically Formed Radicals

It appears that for successful polymerization the electrochemically-derived radical should be neither too stable nor too unstable. In the former case the polymerization would not be thermodynamically favored. In the latter case polymerization would likely be inhibited by radical quenching mechanisms. We have attempted polymer-coating synthesis by using meta- and para-nitrostyrene as the electroactive monomer. But in both of these cases polymerization did not occur. This may be explained by the radical stability.



It may be that the reductively-formed radical is strongly localized in the  $\text{NO}_2^-$  structure, thereby enhancing the stability and preventing the transfer of radical nature to the vinyl component. Both these factors are unfavorable for effective polymerization (72b).

If the radical species formed is too unstable, the chance that it will be quenched by other species present in the electrolyte is high.



On this basis, it appears that the moderately stable radical species offers the best chance for the effective polymerization. There are several instances where even though the radical formation is observed electrochemically, the effective polymerization does not occur. First, reduction of styrene, DVB, and 4-vinylpyridine occurs beyond  $-2.0$  V (vs SSCE) where the reduction of residual water also takes place to a considerable extent. The quenching of radical monomers may be occurring by the reactive intermediates formed by water reduction. Second, a similar phenomenon is observed for the oxidative polymerization of styrene as well. The oxidation of both the styrene and residual water occurs at about the same potential region (just beyond  $+2.0$  V) [vs SSCE]. A partial passivation of styrene oxidation is observed, but total and permanent passivation of the working electrode is never achieved.

#### 4.IV.D Polymerization of DVB

Upon scanning the working electrode (Pt) potential in the presence of DVB, an oxidation peak is observed about  $1.6$  V (vs SSCE). In the subsequent scans this peak is drastically attenuated indicating the passivation of the working electrode. If this process is carried out in the presence of ferrocene, (Figure 27), during the first scan a redox wave of ferrocene is observed around  $+0.4$  V (vs SSCE). But when the scanning is continued, the ferrocene wave disappears gradually. For the DVB oxidation peak, there is no corresponding reduction wave except for a relatively weak reduction peak around  $0.0$  V (vs SSCE). As the passivation of the working electrode continues, this reduction peak

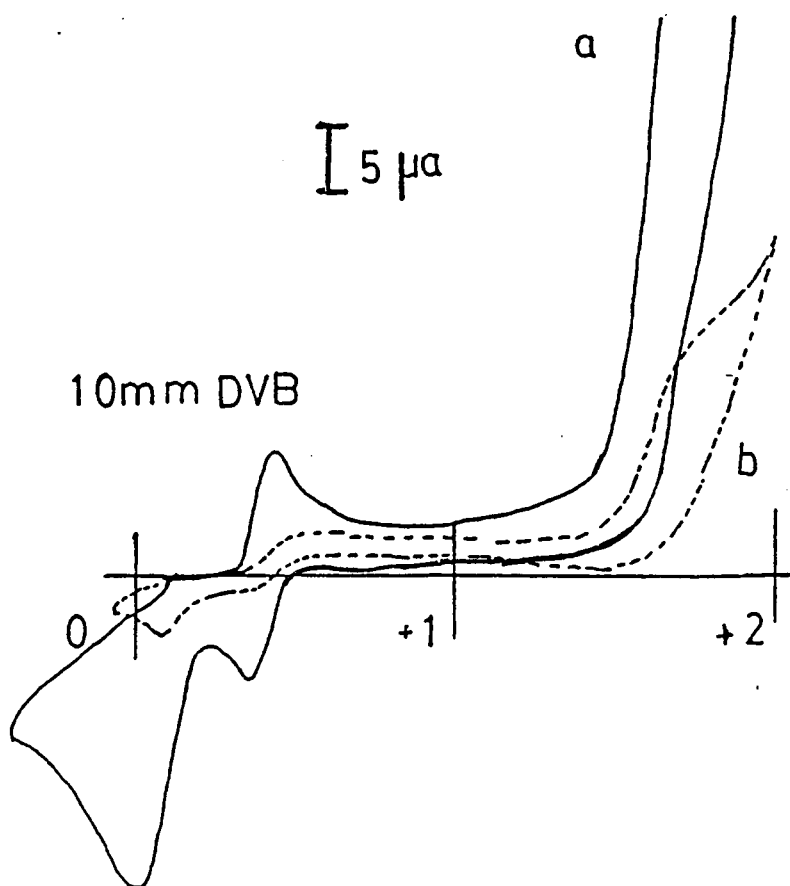


Figure 27: Electrochemical deposition of DVB(10mm) in the presence of 0.5mm ferrocene (a) scan 1 (b) scan 10, in 0.1M TEAP.

disappears, indicating that it is due to species that are in the electrolyte, rather than on the electrode (Figure 28). Also, scanning of the coated electrode in a clean electrolyte does not show this reduction peak. So this peak (0.0 V) may be attributed to lower molecular weight soluble dimeric or oligomeric species generated during the electrochemical polymerization process. These results indicate a change in the chemical nature of the DVB molecule during or after the oxidation. Depositions were carried out both at 10 mM and 100 mM concentrations of DVB. Strangely, the oxidation current observed at the higher concentration is about 10% of that observed for the lower concentration (Figures 28, 29). Therefore, the amount of monomer radicals generated appears to be about 80-90% less than that in the former situation. But, the coated electrodes derived from higher concentration solutions show a greater blocking of solution redox couples compared to that of lower concentrations. This indicates that there is a much larger amount of polymer coating on the electrodes prepared from higher concentration solutions. This observation can be attributed to the more rapid chain propagation step associated with the higher concentration of DVB solutions, causing the deposition of larger amounts of polymer on the electrode. A more rapid deposition and passivation of the electrode at higher monomer concentrations would account for the smaller peak current.

The thinner polymer coatings derived from DVB cause asymmetric redox peaks for both ferrocene and nitrobenzene (Figure 30). In the case of ferrocene  $i_p^{ox} : i_p^{red} = 32:24$ . For nitrobenzene  $i_p^{ox} : i_p^{red} = 30:45$ . In cyclic voltammetry the peak current ( $i_p$ ) can

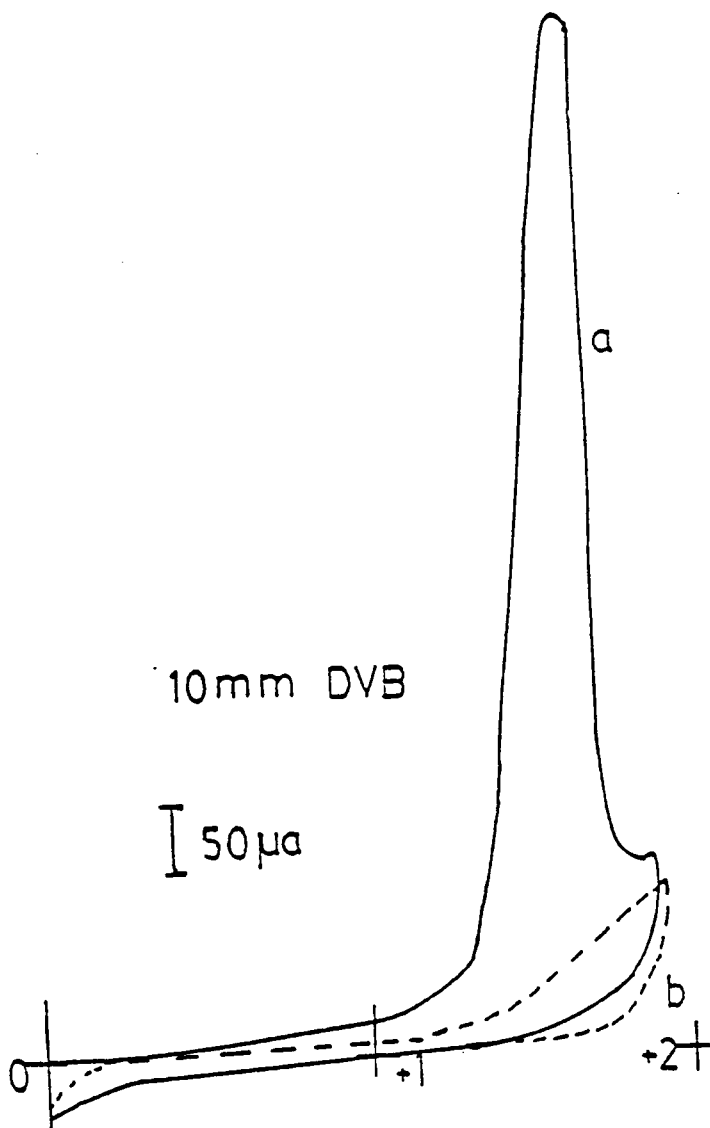


Figure 28: Electrochemical deposition of DVB(10mm), (a) scan 1  
(b) scan 2, in 0.1M TEAP.

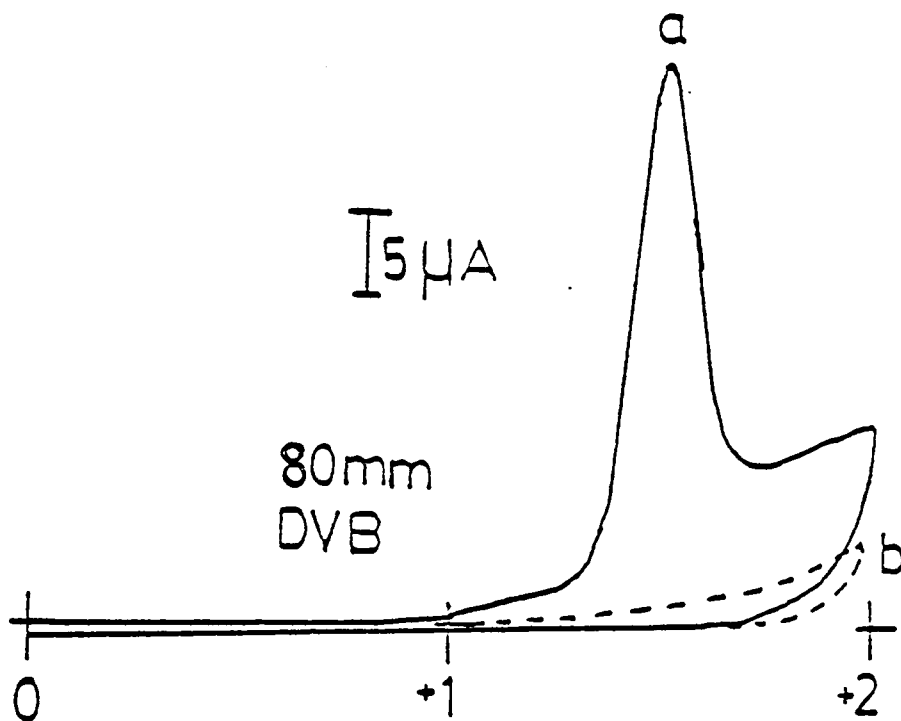


Figure 29: Electrochemical deposition of DVB(80mm), (a) scan 1  
(b) scan 2, in 0.1M TEAP.

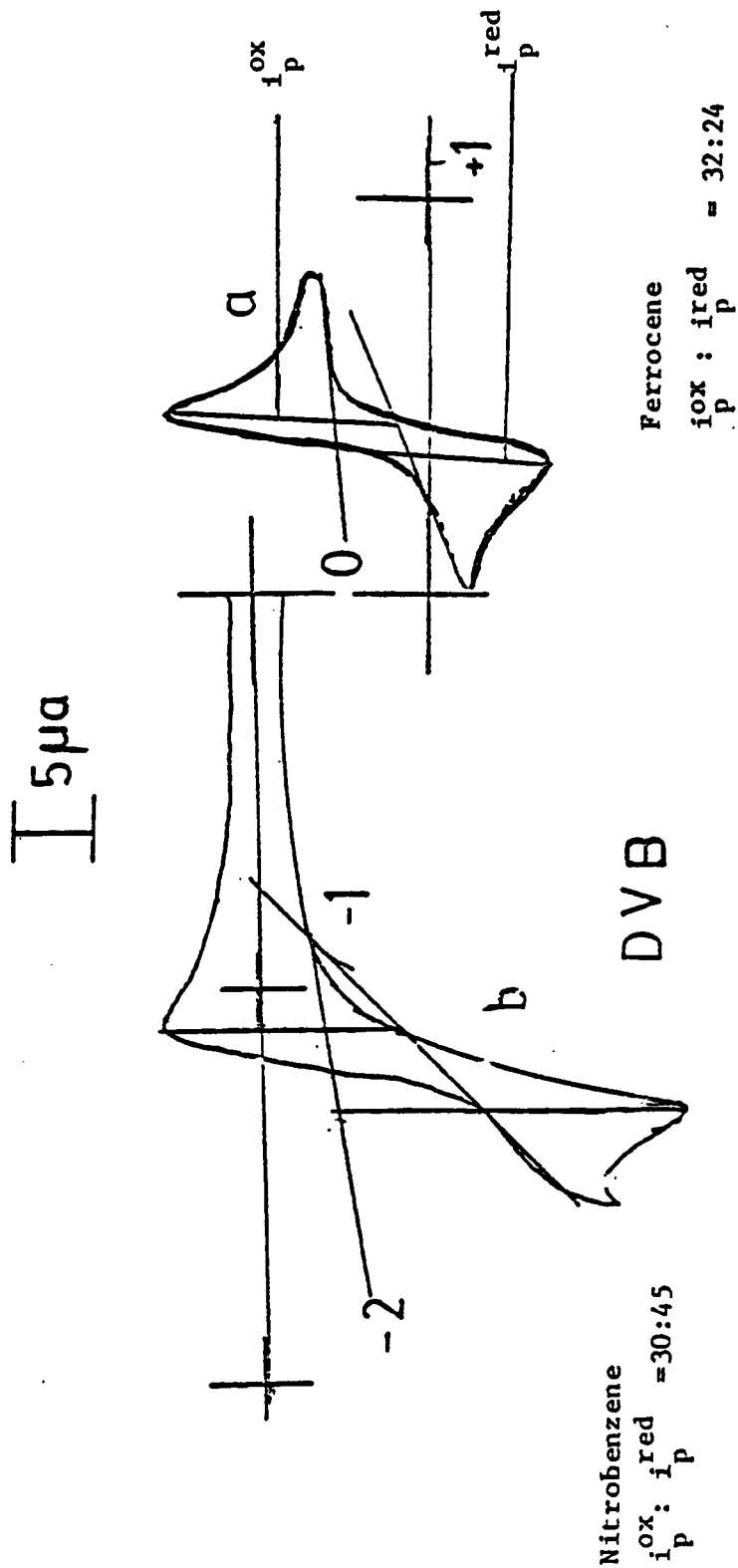


Figure 30: Cyclic voltammetry of poly-DVB coated electrode a) in 1 mm ferrocene b) in 1 mm nitrobenzene, electrolyte 0.1M TEAP.

be expressed as follows, where  $k$  is a constant and

$$i_p = k \cdot n^{3/2} A D^{1/2} C^* v^{1/2} \quad (39)$$

Other symbols have their usual electrochemical meanings except  $D$ . All the other parameters in this equation are the same for both the oxidized and reduced species.  $D$  the diffusion coefficient, determines the mass transfer rate of electroactive species to the electrode. For ferrocene, it appears the mass transfer rate through the polymer film is more favourable for neutral species (reduced) than the positively charged species (oxidized). [ $i_p^{ox} : i_p^{red} = 32:28$ ] Therefore, it appears that the polymer film is either negatively charged or neutral. For nitrobenzene, it appears that the mass transfer rate for neutral species (oxidized) is more favourable than that for negatively charged species (reduced). [ $i_p^{ox} : i_p^{red} = 30:45$ ]

In the above two examples mass transfer rate for neutral species through the polymer film was more favourable over both positively charged and negatively charged species. Therefore on the basis of relative mass transfer rates of species through the polymer film, it appears that the polymer film is neutral.

The XPS studies conducted for film thickness measurements have yielded further supporting evidence for this proposition. The supporting electrolyte used during the film deposition was tetraethylammonium perchlorate (TEAP). If the derived polymeric film was charged, it would have trapped corresponding counter ions in order to maintain the charge neutrality of the film. In the XPS studies there was no evidence observed to indicate the presence of either the

cation  $((\text{Me})_4\text{N}^+)$  or the anion  $(\text{ClO}_4^-)$  in the film. A weak  $\text{O}(1s)$  peak was observed initially, but this peak disappeared with minimal surface etching. Therefore, both of these pieces of evidence support the proposition that the films derived from DVB are neutral.

Similar cyclic voltammetric behavior has been observed for both films derived from 4-vinylpyridine and phenol, therefore, these films are also believed to be electrically neutral in nature.

#### 4.IV.E Coated [thicker] Electrodes in Ferrocene Electrolytes

Figure 31 shows the behavior of a coated electrode [in 100 mM DVB] in the presence of 1 mM ferrocene. Curve a is observed when the coated electrode is scanned in positive direction, beginning from zero potential. Similar behavior is maintained if the potential is reversed at zero after each negative scanning. Coated electrodes, especially those derived from 100 mM DVB solutions, show severe attenuation of ferrocene redox (Figure 31) behavior. Similar peak attenuation has been reported by other workers as well (81,84). This occurs to a much lesser extent with the 10 mM DVB-derived electrodes. In the latter case, a slightly larger peak separation is noted as well. As it has been discussed above the films derived from DVB are neutral and do not have any redox or variable valency sites that would induce redox conductivity in the film (103). Therefore, the film behaves as insulation between the electrode surface and the electrolyte, hindering mass-transfer to the electrode. The dramatic attenuation of redox activity of ferrocene for the thicker coatings as well as the increased peak separation for the thinner coatings are mass-transfer effects.



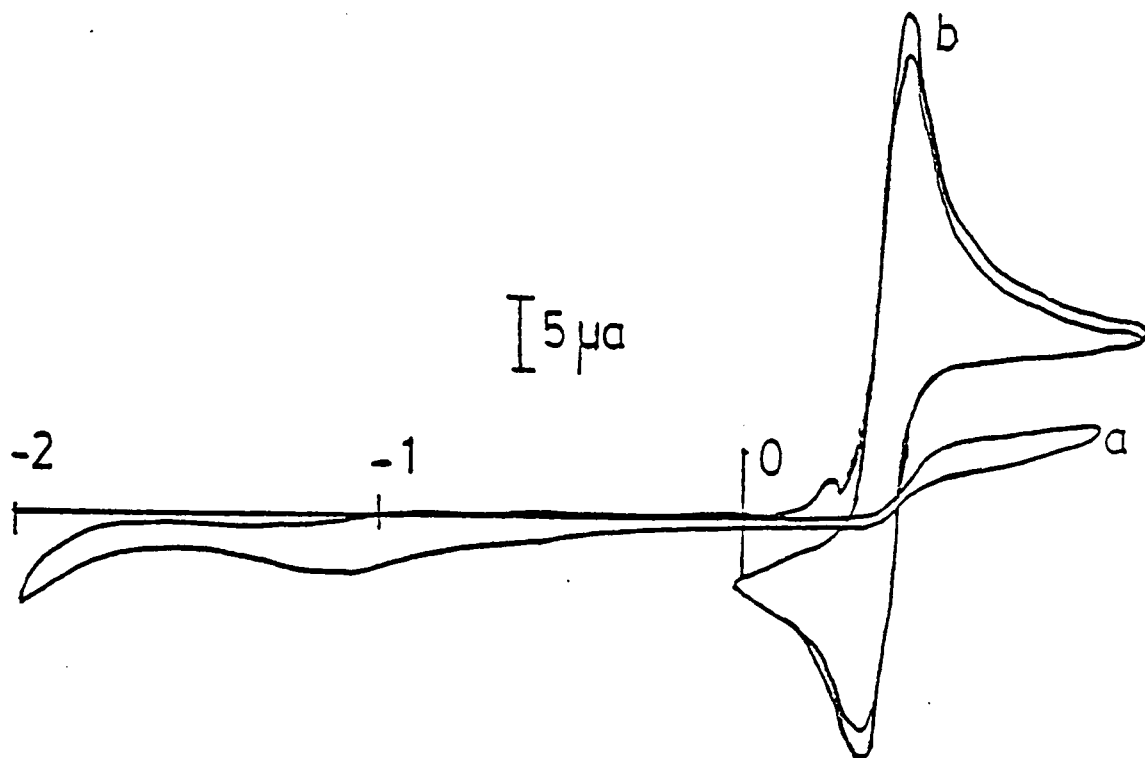


Figure 31: Cyclic voltammetry of a poly-DVB(100 nm) coated electrode in 1 mM ferrocene a) before negative scanning b) after negative scanning, electrolyte 0.1M TEAP.

Two anomalous phenomena are observed (Curve b, Figure 31) when the potential of the coated working electrode is scanned more negative than -1.0 V (vs SSCE):

a) a weak prewave appears prior to the oxidation wave of ferrocene (Figure 31),

b) the redox behavior of ferrocene is dramatically enhanced compared to the result before the negative potential scan is done.

The prewave phenomena has been observed with the other three derived polymers as well. It occurs only prior to the oxidation wave of ferrocene, and only when the coated electrode is subjected to potentials beyond -1 V (vs SSCE). The observed prewave was small in the cases of divinylbenzene, 4-vinylpyridine and N-methyl-4-vinylpyridinium derived polymers. In contrast phenol coated electrodes consistently show a strong pre-wave. Scan rate study of phenol derived pre-wave did not yield a linear relationship between peak intensity ( $i_p$ ) vs scan rate, indicating that the prewave is not due to ferrocene that is bound to the electrode surface. Similar pre-waves have been observed with both mono- and di-acetylferrocene on poly-DVB-coated electrodes.

This prewave may be explained by alterations of polymer structure due to potential scanning which generates deformed sites. Ferrocene may be trapped in these randomly deformed sites, which are away from the electrode surface, so that there is no direct electron transfer between the electrode surface and the trapped ferrocene. But when the electrode potential is scanned close to the oxidation potential of ferrocene, a minimal amount of ferrocenium ions is generated. The

small spike prior to the solution ferrocene oxidation may be due to the mediated electron transfer of the ferrocene trapped at the deformed polymer sites via the newly generated ferrocenium ions. It may be that we do not observe corresponding reduction peak due to the extrusion of charged ferrocenium ions from the neutral deformed polymer sites.

Further, the prewave phenomenon is consistently much more prominent with polyphenol coated electrodes than the other three types of polymer coated electrodes. Therefore it appears that entrapment of ferrocene during the potential induced polymer deformation/rearrangement is most prominent with poly-phenol coated electrodes. There is one remarkable difference in the phenol polymer and the three polymers which are from vinyl compounds. The vinyl polymers basically consisted of carbon/carbon bonds which were formed during the polymerization process. But, in the formation of poly-phenol polymers, the polymer chain formation occurs through carbon/oxygen/carbon [C-O-C] bonds. It may be that these C-O-C linkages are more susceptible to the immense potential gradient imposed upon the thin polymer film by potential scanning. Due to this reason it is possible that poly-phenol polymers trap more ferrocene at the deformed/rearranged pockets in the polymer network.

The second phenomenon (b) (Figure 31) is more complicated in nature and has not been previously reported in the literature. The following mechanism is hypothesized.

(i) During the deposition step, the electrode surface is positively charged (+1.6 V) and therefore, there are a considerable number of  $\text{ClO}_4^-$  ions migrating towards the electrode. During the

polymerization process it may be that intermolecular voids are formed in the polymer matrix so that it can accommodate species of the size of tetrahedral  $\text{ClO}_4^-$  ion. As the potential is scanned positively and back towards zero volts, the flow of  $\text{ClO}_4^-$  ions in and out of the polymer matrix should occur in order to neutralize the charge on the Pt electrode surface.

(ii) When the negative scanning is carried out, the electrode surface acquires a negative charge. Consequently, much larger tetraethylammonium ions should penetrate into the polymer matrix in order to neutralize the negative charge on the electrode surface. It may be that due to the larger size of the TEA cation compared to the  $\text{ClO}_4^-$  anion, the polymer film is being forced to expand. Upon reversing the scan towards zero volts, these bulky cations are gradually extruded from the polymer matrix, but the voids left by the accommodation of the larger cations may be returning to their equilibrium size at a much slower rate. This leaves large holes that ferrocene molecules can penetrate rapidly; hence, enhanced currents are observed. Holding the electrode at positive potentials after negative scanning shows decreasing redox currents, implying a collapse of the polymer. This is due to the fact that the polymer matrix is expanded to the extent more than necessary to hold  $\text{ClO}_4^-$  counter ions, therefore the slow contraction process continues at positive potentials. During the positive scanning, drastic changes of polymer behavior are not observed as they are in the negative scanning. It may be that the equilibrium structure of the polymer consists of voids that could easily accommodate  $\text{ClO}_4^-$  ions.

In the case of N-methyl-4-vinylpyridinium polymers, the collapsing process appears to be more rapid than all other cases. This may be attributed to more rapid expulsion of TEA cations due to positive charge present in this polymer coating. Similar behavior observed in KPF<sub>6</sub> may be due to distortion of the polymer matrix because of the movement of solvated K<sup>+</sup> ion in and out of the polymer matrix during the potential scanning.

The poly-DVB coated electrodes show similar blocking behavior in the aqueous media as well, which was even observed with ferrocene in acetonitrile solution. Due to the hydrocarbon nature of poly-DVB films, it is reasonable to expect that they be more contracted in the aqueous media than in the non-aqueous media. Compared to a clean electrode, the poly-DVB coated electrodes show blocking behavior towards Fe<sup>2+</sup>, Fe(CN)<sub>6</sub><sup>4-</sup> and hydroquinone. Figure 32 shows comparison of the behavior of poly-DVB coated electrode and a clean electrode towards Fe<sup>2+</sup> in 0.5M H<sub>2</sub>SO<sub>4</sub>. The clean electrode shows normal redox behavior of Fe<sup>2+</sup> ions, whereas the coated electrode shows tremendous hindrance of redox behavior of the same. In the XPS experiments of these films, we have not observed any evidence for the presence of either ClO<sub>4</sub><sup>-</sup> ion or N(Me)<sub>4</sub><sup>+</sup> ions. Therefore the polymer film appears to be neutral in nature and hence the hindrance of redox activity of Fe<sup>2+</sup> ions is very unlikely to be due to electrostatic reasons. Therefore, it appears that the greatly attenuated redox activity of Fe<sup>2+</sup> ions at the poly-DVB coated electrode is due to steric hindrance of the contracted film to the flow of Fe<sup>2+</sup> ions towards the electrode surface. Similar explanation can be given to the attenuated redox

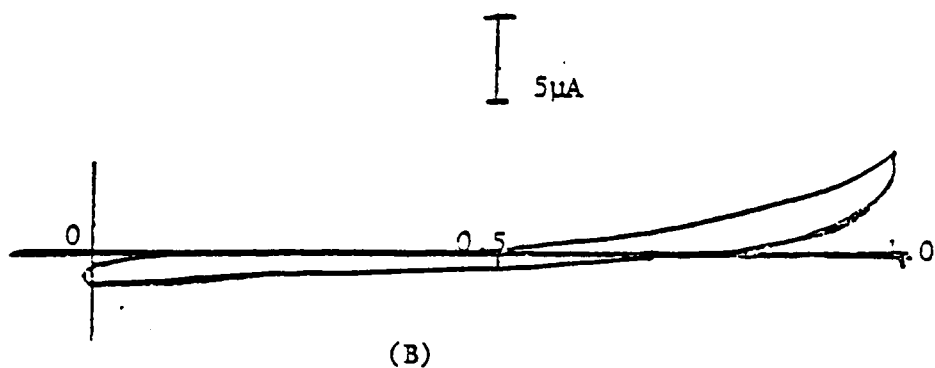
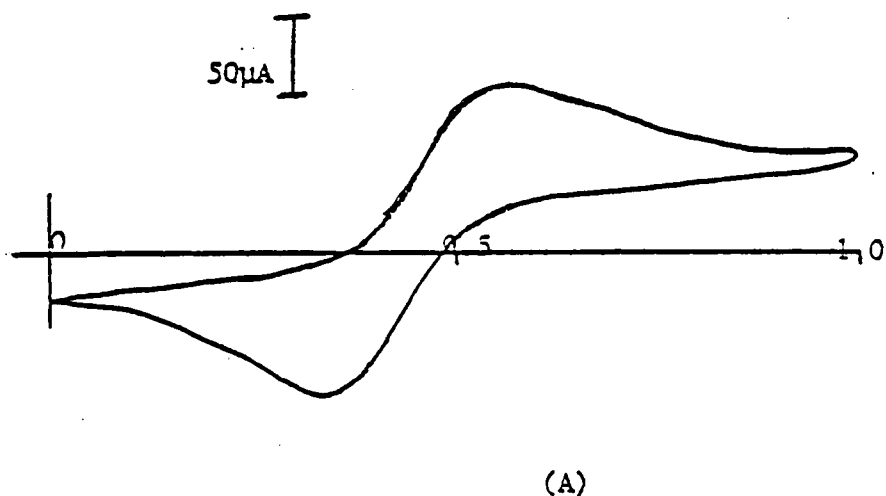


Figure 32: Cyclic voltammetric behavior of (a) a clean Pt electrode, (b) a Pt electrode coated in 100 nm DVB in 10mm ferrous sulphate/0.5M sulphuric acid.

behavior observed for hydroquinone and ferrocyanide ions.

In order to examine the redox trapping/adsorption properties of poly-DVB films, four coated electrodes as well as four clean electrodes were soaked (overnight) in ferrocene,  $\text{Fe}^{2+}$ ,  $\text{Fe}(\text{CN})_6^{4-}$  and KBr. The coated electrodes which were soaked in ferrocene,  $\text{Fe}^{2+}$  and  $\text{Fe}(\text{CN})_6^{4-}$  did not show the characteristic redox behavior of respective redox species when the electrodes were examined in a clean electrolyte. But the coated KBr soaked electrode showed a marked difference in behavior compared to the control electrode. In acetonitrile this electrode showed characteristic  $\text{Br}^-$  redox behavior (figure 33). Gradual decay of  $\text{Br}^-$  wave was observed.

Due to the apparent electro-neutral nature of the polymer films, it is difficult to believe that just  $\text{Br}^-$  is being adsorbed into the polymer film. It is more likely that  $\text{K}^+\text{Br}^-$  partitions into the polymer film as an ion pair. In later studies similar behavior was observed with coated electrodes soaked in aqueous KI as well.

The coatings exhibit good stability. The coated electrodes retain their characteristic behavior after use in acidic and neutral aqueous solutions. Further attempts to recoat the electrodes in fresh DVB electrolytes produce no significant deposition currents. Repeated scanning in 0.5 M  $\text{H}_2\text{SO}_4$  between the oxidation and reduction waves of the Pt electrode gradually destroys the polymer.

XPS- experiments have shown that electropolymerization in 10 mm DVB yields about 4 - 5 nm thick poly-DVB films.

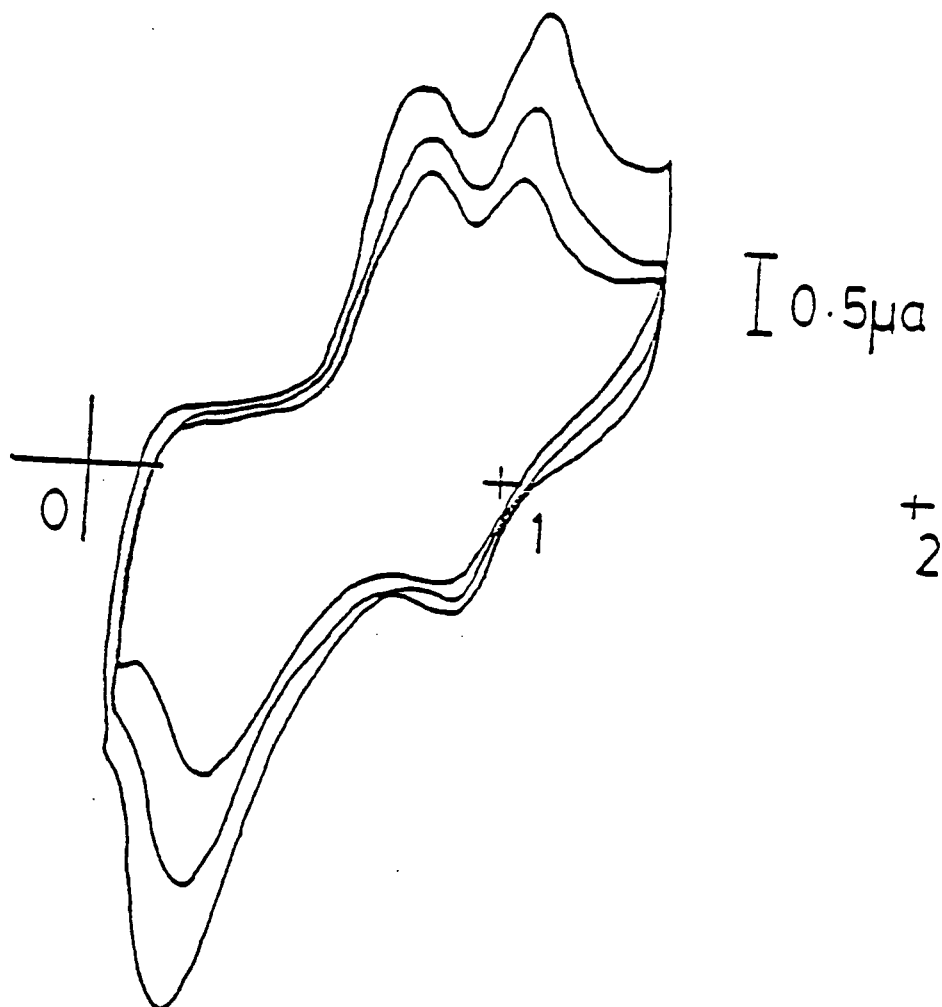


Figure 33: Cyclic voltammetry of bromide ions trapped in poly-DVB coated Pt electrode, in 0.1M TEAP.



#### 4.IV.F 4-Vinylpyridine

4-Vinylpyridine, like DVB, forms a coating on a Pt electrode upon scanning across its oxidation potential 1.3 V (vs SSCE) (Figure 34). At higher concentrations (e.g. 100 mM) of 4-vinylpyridine, the deposition current ( $i_p^{OX}$ ) observed is much smaller than that observed at lower concentrations (10 mM), and the coatings formed are thicker, similar to DVB. As in the case of 100 mM DVB coated electrodes 4-vinylpyridine coated electrodes also show strong attenuation of ferrocene redox chemistry. Electrodes coated in 10 mM solutions of 4-vinylpyridine, yield assymmetric redox waves as observed for DVB coated electrodes (10 mM concentration). Therefore, these poly-4-vinylpyridine films also appear to be neutral. XPS- depth profiling experiments have not been carried out on these coatings. The coatings also show strong blocking behavior towards  $Fe^{2+}$  in 0.5 M  $H_2SO_4$  and  $Fe(CN)_6^{4-}$  in pH = 7 buffer. In the case of  $Fe^{2+}$  the protonation of 4-vinylpyridine may preclude the diffusion of  $Fe^{2+}$  ions through the polymer film. But in the case of  $Fe(CN)_6^{4-}$  the inhibition of redox chemistry may be mainly due to steric factors. In pH 7 buffer, the hydroquinone is permeable through the coating (Figure 35). Protonation of the N atom of pyridine moiety is excluded as the  $H_2Q$  redox waves have shapes corresponding to a diffusion controlled process rather than surface bound species. At this point this behaviour is a mystery. Similar to DVB coatings, these coatings derived from 4-vinylpyridine also adsorb  $Br^-$  from KBr solution.

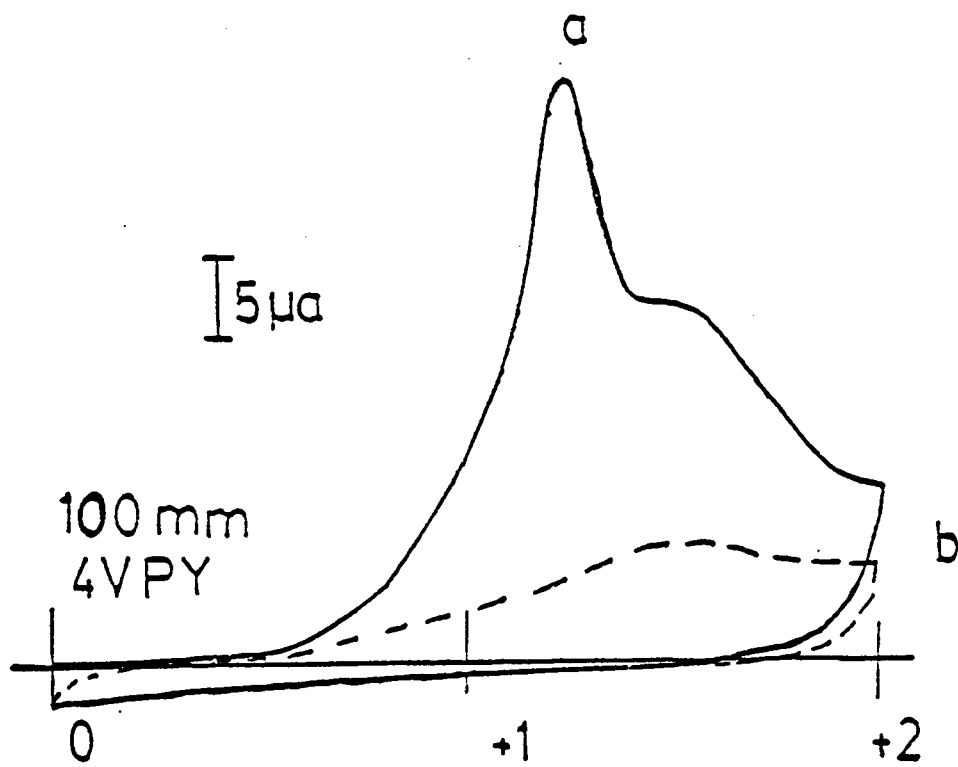


Figure 34: Electrochemical deposition of 100mm 4-vinylpyridine  
(a) scan 1, (b) scan 2 in 0.1M TEAP.

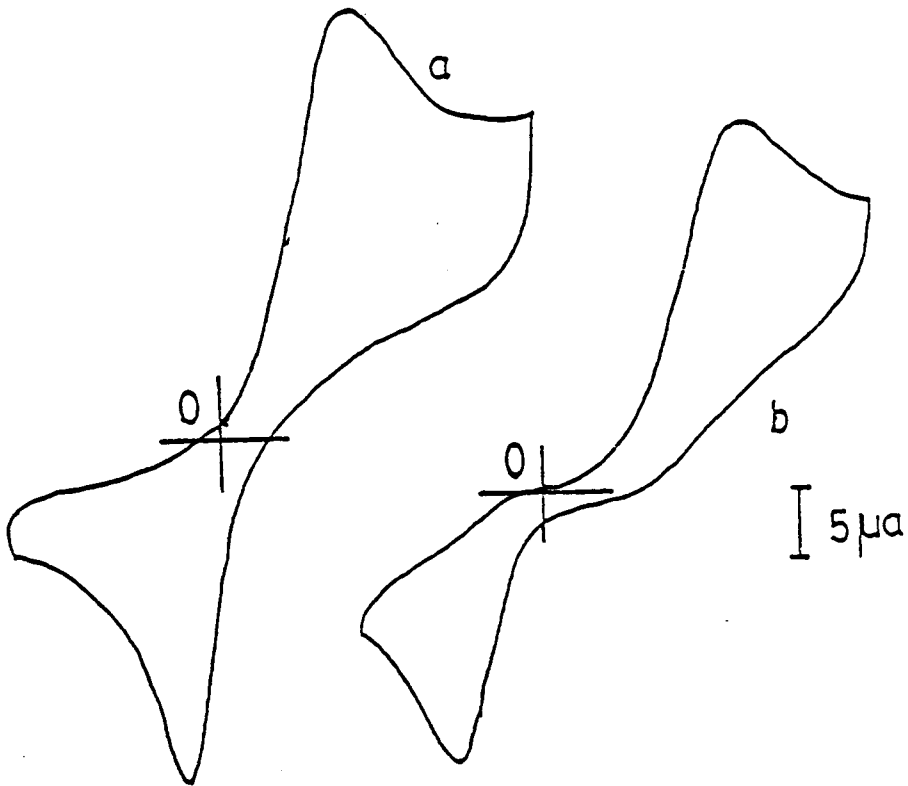


Figure 35: Cyclic voltammetry of poly-4-vinylpyridine coated electrode in 1mm hydroquinone, (a) clean electrode (b) coated electrode in 0.1M TEAP.

#### 4.IV.G Phenol

Pham and DuBois (81) have shown oxidation of 0.1 M phenol in aqueous alkaline solutions form (50 - 200 nm) films of polyphenylene oxide. In acetonitrile, concentrations of phenol as low as 0.4 mM form coatings during multiple potential scans through the oxidation wave. The passivation of the electrode is not as rapid as that of DVB or 4-vinylpyridine (Figure 36) probably because of the lower concentration of phenol that was employed. The most notable feature of a phenol-coated electrode is a prominent prewave for ferrocene, which is several times stronger (Figure 37) than that observed for either DVB or 4-vinylpyridine. The polymer deformation during the negative potential scans may be larger than the previous two cases, trapping larger amounts of ferrocene at deformed sites. Attenuation of the ferrocene peak is never as strong as in the previous two cases, which may be due to smaller thickness of the polymer layer.

#### 4.IV.H N-methyl-4-vinylpyridinium salts

N-methyl-4-vinylpyridinium salts form polymer coatings upon scanning across the first reduction potential -1.1 V (vs SSCE). During this process, a gradual decrease of the reduction wave is evident. This negative shift may be due to the film resistance of the coated electrode (Figure 38). A large reduction peak is evident after holding the potential of the coated electrode at 0 V (vs SSCE). The peak current ( $i_p^{\text{red}}$ ) is much larger than that during the first potential scan. Both the pyridinium salt and 4-vinylpyridine show a weak oxidation wave near 0 V (vs SSCE). It may be that by holding the

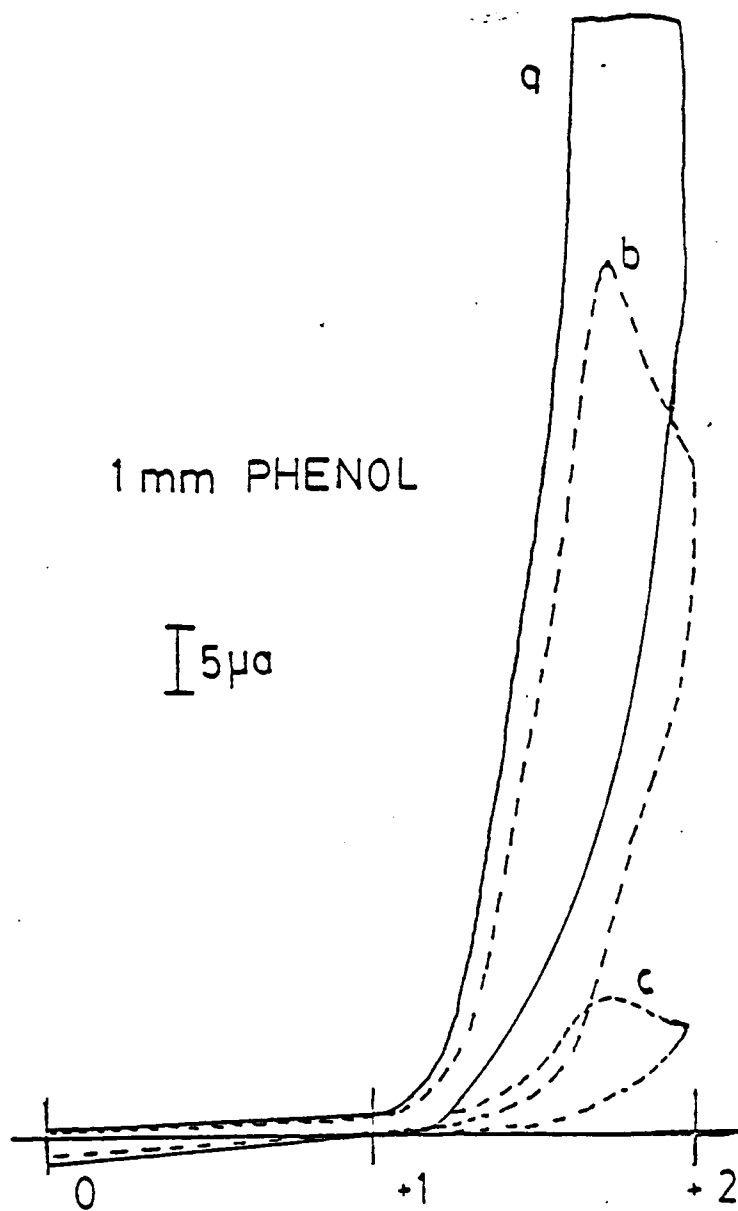


Figure 36: Electrochemical deposition of phenol (a) scan 1 (b) scan 15 (c) scan 30, electrolyte 0.1M TEAP.

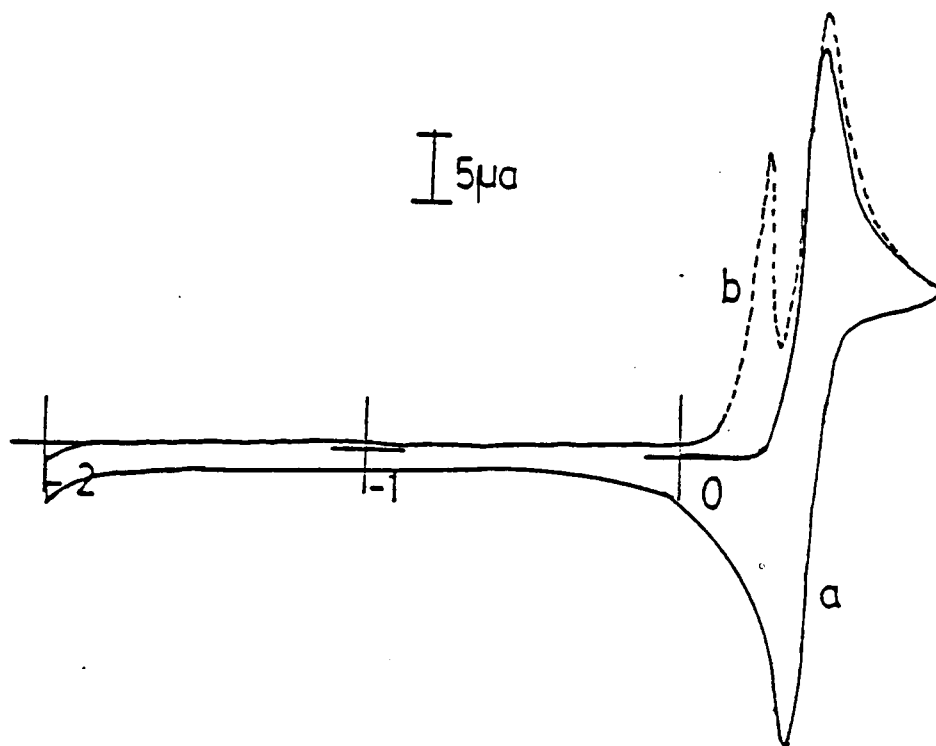


Figure 37: Poly-phenol coated electrode in 2 mm ferrocene, (a) before negative scanning (solid line), (b) after negative scanning (dashed line).

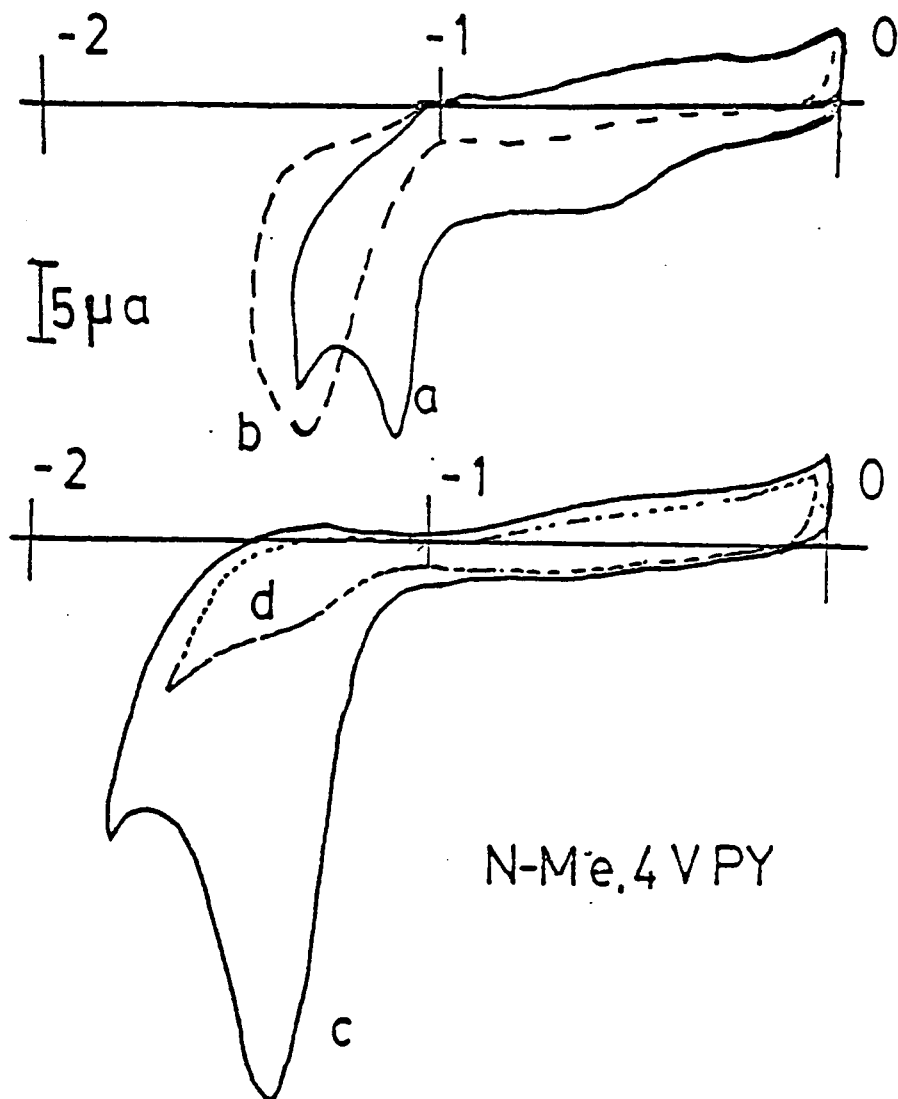


Figure 38: Electrochemical deposition of N-methyl-4-vinylpyridinium tetrafluoroborate, (a) scan 1 (b) scan 15 (c) scan 16 (after holding at 0 volts), (d) scan 17.

potential at 0 V (vs SSCE), the film is being oxidized. Alkylpyridiniums rapidly dimerize upon reduction; the dimer can be reoxidized to the monomer near 0 V. Thus, we attribute the observed behavior to dimerization occurring simultaneously with deposition.

Compared to the previous three polymer coatings, the coatings derived from the pyridinium salt are known to be positively charged. Upon soaking in a solution of  $K_4Fe(CN)_6$ , [pH = 7.0], the coated electrodes exhibit a surface-bound electrochemical wave (Figure 39), with  $\Delta E_p = 25$  mV and  $i_p$  proportional to scan rate (Figure 40). Electrostatic trapping of an anion confirms the positive charge associated with the polymer coatings. Similar ferrocyanide trapping has been reported by Oyama and Anson (104) for protonated polyvinylpyridine-coated electrodes. There may be other anionic species that can be trapped in a similar manner in the polymer matrix with potential applications in electrocatalysis (104).

#### 4.IV.I Diffusion of Solute at Rotating Disk Electrode

Rotating disk voltammetry which has been extensively employed in the electrochemical mechanistic studies, also can be used in the investigations of diffusion of solute through thin films. The limiting current observed for an oxidation/reduction process takes place at rotating disk electrodes (RDE) is given by the equation (21,105):

$$i_L = 0.62 n F A C_s D_s^{2/3} \nu^{-1/6} \omega^{1/2} \quad (40)$$

D = diffusion coefficient of solute

$\omega$  = angular velocity of disk given by  $\omega = 2\pi N$



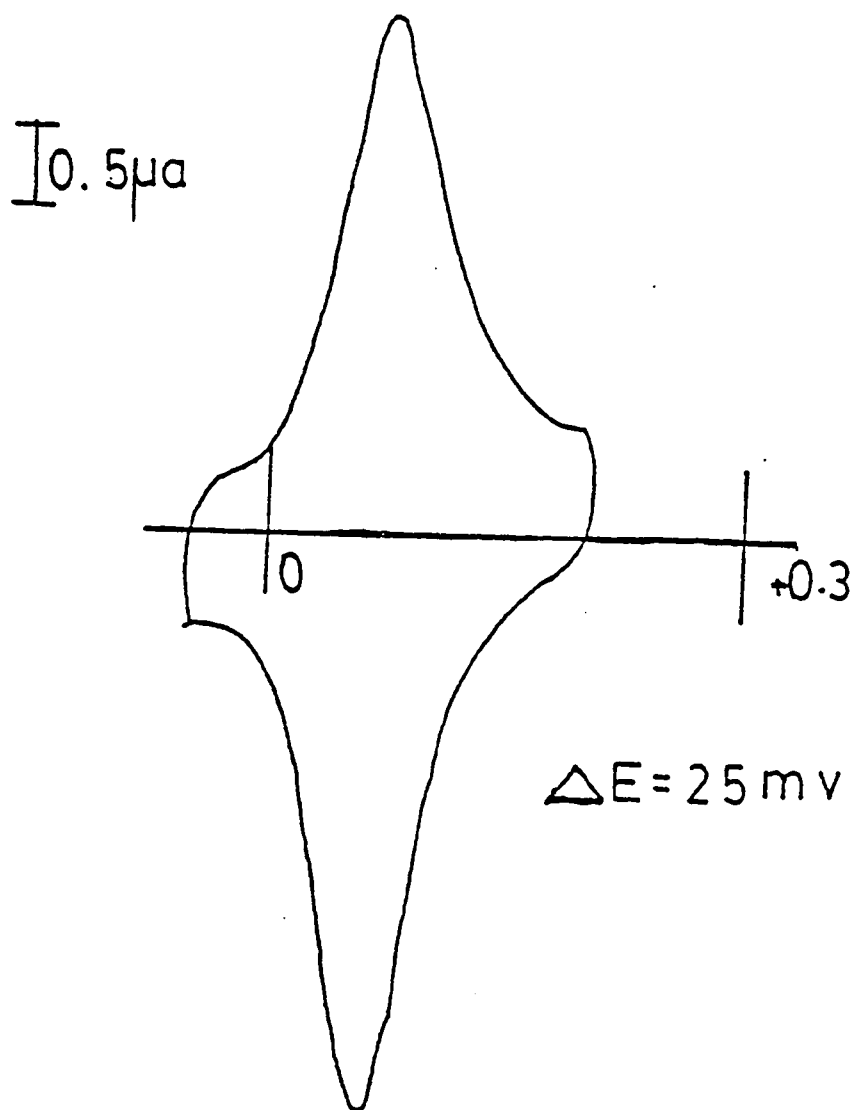


Figure 39: Cyclic voltammetry of electrostatically bound ferrocyanide on poly-N-methyl-4-vinylpyridinium tetrafluoroborate coated electrode.

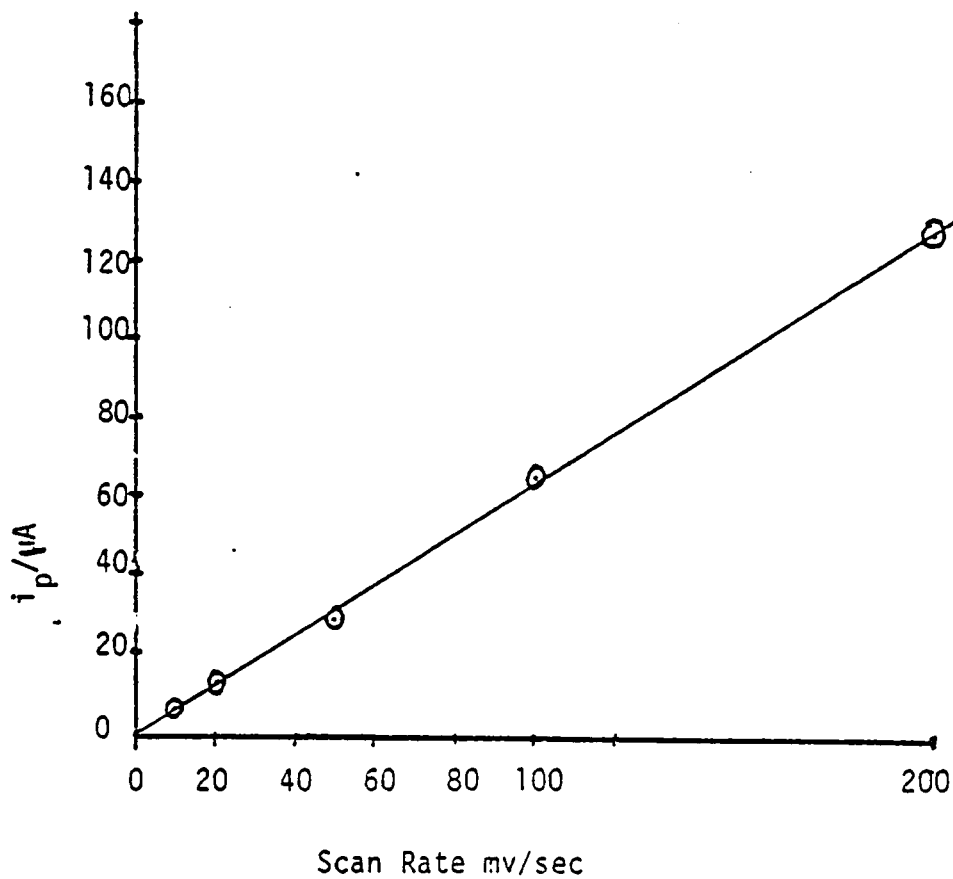


Figure 40: Scan rate of electrostatically bound ferrocyanide on poly-N-methyl-4-vinylpyridinium tetrafluoroborate coated electrode.

$N = \text{rps}$

$\nu = \text{kinematic viscosity, cm}^2/\text{sec.}$

This equation is especially useful in the evaluations of diffusion coefficients of redox species.

In the event the RDE is coated with a thin film, the solute has to be passed through the membrane prior to the redox process at the electrode surface. Therefore the limiting current ( $i_L$ ) depends on the partition coefficient ( $P$ ) of the solute into the membrane, and the diffusion coefficient ( $D_{S,Pol}$ ) of the solute through the membrane barrier. The limiting current is membrane permeable species is given by inverse Levich relationship (106):

$$\frac{1}{i_L} = \frac{1}{nFAD_{S,Pol} \cdot PC_{S/d}} + \frac{1}{0.62 nFA D_S^{2/3} \nu^{-1/6} \omega^{1/2} C_S} \quad (41)$$

$d = \text{membrane thickness.}$

The two terms in the right hand side represent the diffusion rates of solute through the membrane and Levich depletion layer in solution, respectively. If the diffusion through the membrane is very rapid due to very thin film ( $d$  very small) or very large  $P \cdot d_{S,Pol}$ ,  $i_L^{-1}$  vs  $\omega^{1/2}$  is linear with zero intercept (ie  $D_S^{2/3} \nu^{-1/6} \omega^{1/2} \ll P \cdot D_{S,Pol}/d$ ). If the diffusion through the membrane is slower,  $i_L^{-1}$  vs  $\omega^{-1/2}$  is linear and  $P \cdot D_{S,Pol}/d$  can be evaluated from the intercept. In addition to that the following features are observed in the inverse Levich plots.

(a) Its slope should yield the same  $D_S$  as at a naked rotated disc electrode independent of  $C_S$  or  $d$ .

(b) The intercept should be inversely proportional to  $C_S$ .

(c) The intercept should be proportional to  $d$ .

The parameter  $P \cdot D_{S,Pol}/d$ , which can be evaluated for a redox species, is useful to understand the properties such as the film homogeneity or the absence of pin-holes or cracks in the polymer film. In the event of the former situation, one should be able to observe dramatic changes of the  $P \cdot D_{S,Pol}/d$  parameter as the molecular size of the diffusing species is gradually increased.

With this objective in mind, we have investigated RDE behavior of poly-DVB coated electrodes. Figure (41) shows inverse Levich plots of clean Pt electrode (curve a) and a (10 mM) poly-DVB coated electrode (curves b, c, d). The curve a shows ideal RDE behavior in 2 mM ferrocene. In fact the calculated value for  $D_S$  ( $= 2.38 \times 10^{-5}$  cm<sup>2</sup>/sec) is comparable with the values reported in the literature (106). Ideally, the slopes of the clean Pt electrode and the coated electrodes should be identical (equation 22). As it is shown even the slopes of the same coated electrodes do not agree with each other in three different measurements when:

- (i) randomly changing the rotation speed,
- (ii) increasing the rotation speed gradually,
- (iii) decreasing the rotation speed gradually.

Also they are different from the slope that is observed for the clean electrode. Further, the reproducibility of limiting current of the same coated electrode is extremely poor. The limiting current would either increase or decrease, depending on the prior potential history of the coated electrode.

This poor reproducibility and the random variation of the limiting

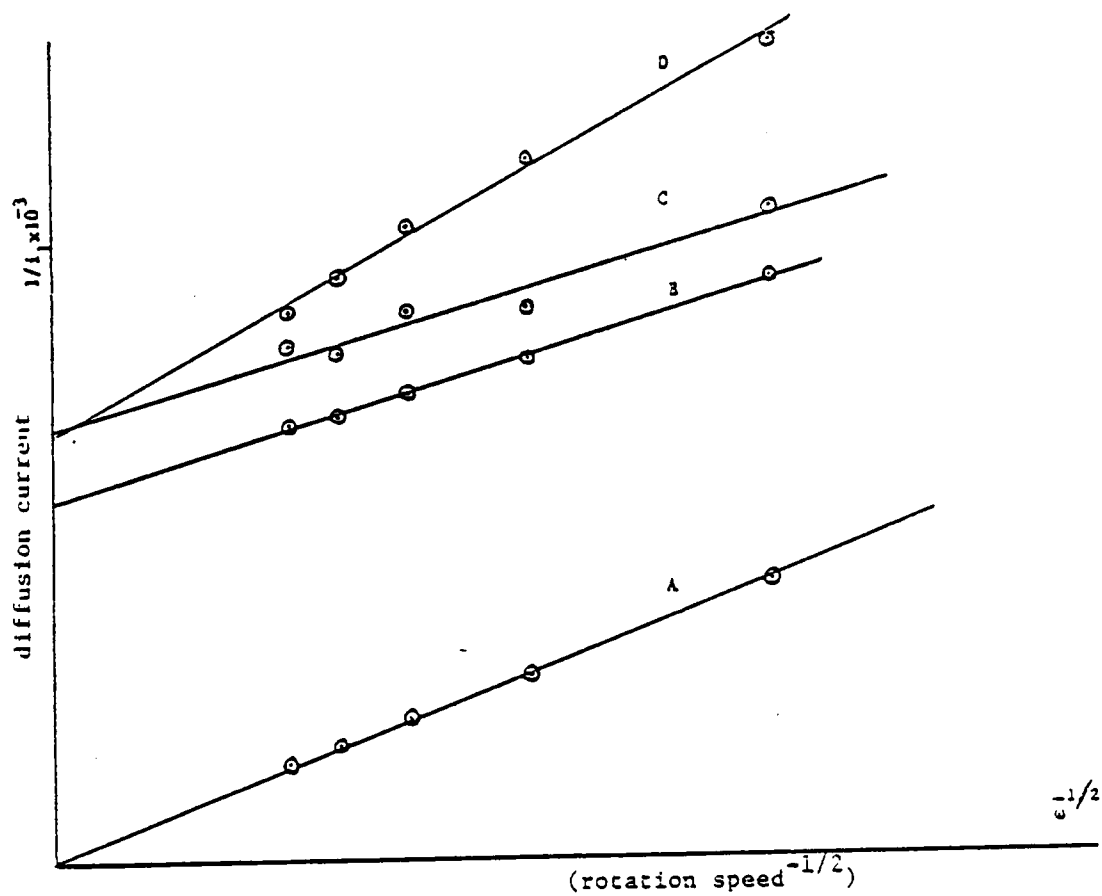


Figure 41: Rotating disk voltammetric plots of (a) clean Pt electrode and a poly-DVB coated electrode, in (b) random, (c) gradually increasing (d) gradually decreasing order, of the rotation speed.

currents observed, believed to be due to the morphological changes in the nature of the polymer films, did not permit reliable evaluations of  $P \cdot D_{S, Pol} / d$  parameters and in turn failed to yield any information on size discriminating nature of permeating molecules and information on the nature of film homogeneity.

#### 4.V Conclusion

Four surface coatings have been synthesized by electrochemical polymerization using the monomers divinylbenzene, phenol, 4-vinylpyridine, and N-methyl-4-vinylpyridinium salts. The first three coatings are neutral and the fourth is positively charged, as shown by its ability to electrostatically trap anions. These coatings cause considerable attenuation of redox chemistry of redox couples such as  $Fe^{2+}$ ,  $Fe(CN)_6^{4-}$ , hydroquinone, ferrocene, and nitrobenzene. The anomalous pre-wave phenomena observed in these coatings may be due to trapping of ferrocene in the deformed polymer matrix during potential scanning. The observed film opening and closing phenomena may be due to partitioning of bulky tetraethylammonium ions into the polymer matrix during the negative potential scanning. Further, these electrochemically formed films appear to be very homogeneous and free of pinholes.

## Chapter 5

### CONCLUSION

Due to the presence of several different mechanisms which cause attenuation of both bridging and terminal OH groups, it is difficult to assess the reactivity of OH groups on the basis of peak attenuation. The surface coverage calculation based on the Si-C absorbance data indicates the presence of approximately monolayer coverage of silane on a modified TiO<sub>2</sub> surface. The photocurrent generation experiments of modified TiO<sub>2</sub> indicate that the hydrophobicity of the modified layer plays an important role towards stability of the modified layer. Further, it may be that the inhomogeneity of the modified layer due to the presence of different attenuating mechanisms (OH groups) partly contributes to the instability of the modified layer, during photocurrent generation.

The electrochemical polymerization experiments have shown the feasibility of synthesis of polymer coatings from divinylbenzene, 4-vinylpyridine, phenol, and N-methyl 4-vinylpyridinium salts. All four coatings show good blocking characteristics towards electroactive species. This further indicates superior homogeneity of the modified layers synthesized in this manner, over similar layers synthesized by covalent attachments.

Electrochemical as well as XPS- data indicate that the first three coatings are neutral whereas the fourth indicates its positively charged nature by trapping ferrocyanide anions. Further, the DVB

derived polymers have shown specific adsorption characteristics towards  $\text{Br}^-$ , which may have useful applications as ion-selective membrane.

Electrochemical polymerization is very likely to lead to the synthesis of polymer films with very interesting properties such as ion selective membranes and modified surfaces suitable for specific electro-catalysis. The modification by covalent bonding of non-electroactive species of small band gap n-type semiconductors does not seem to yield substantial improvements in photoelectrochemical devices. This is mainly due to the difficulty in forming very homogeneous modified surfaces by this approach, which is essential for the stabilization of n-type small band-gap semiconductors. The electrochemical polymerization seems to produce more homogeneous films which are suitable for this purpose. But the homogeneity of these films itself is not adequate for the success of the photoelectrochemical systems. They should be rugged enough to resist and survive the reactive intermediates which are produced during this process. Until such developments are made it is quite unlikely that the photoelectrochemical systems will live up to the expectation as a viable and reliable alternative source of energy.



## REFERENCES

- (1) Bard, A.J., *J. Chem. Ed.* 1983, 60, 302-304.
- (2a) Moses, P.R., Wier, L., Murray, R.W., *Anal. Chem.* 1975, 47, 1882-1886.
- (2b) Murray, R.W., *Accts. Chem. Res.* 1980, 13, 135-141.
- (3) Hair, M.L., "Infra-red Spectroscopy in Surface Chemistry", Mercel Dekker, NY, 1967.
- (4) Little, L.H., "Infra-red Spectroscopy of Adsorbed Species", Academic Press, London, 1966.
- (5) Kiselev, A.V., Lygin, V.I., "Infra-red Spectroscopy of Surface Compounds", Wiley, NY, 1975.
- (6) Ishida, H., Koenig, J.L., *Amer. Lab.* 1978, 10, 33-42.
- (7) Bell, A.T., Hair, M.L., "Vibrational Spectroscopy of Adsorbed Species", ACS, Washington, D.C., 1980.
- (8) Jackson, P., Parfitt, A.D., *Trans. Faraday. Soc.* 1971, 67, 2469-2483.
- (9) Jones, P., Hockey, J.A., *Trans. Faraday Soc.* 1971, 67, 2669-2678.
- (10) Jones, P., Hockey, J.A., *Trans. Faraday Soc.* 1971, 67, 2679-2685.
- (11) Read, H.H., (Ed.), "Rutleys' Elements of Mineralogy", George Allen & Unwin Ltd., London, 1962.
- (12) Yates, D.J.C., *J. Phys. Chem.* 1961, 65, 746-763.
- (13) Primet, M., Pichat, P., Mathien, M.V., *J. Phys. Chem.* 1971, 75, 1216-1220.
- (14) Griffiths, D.M., Rochester, C.H., *J. Chem. Soc., Faraday Trans.* 1977, 1, 73, 1510-1529.
- (15) Parfitt, A.D., Ramsbotham, J., Rochester, C.H., *Trans. Faraday Soc.* 1971, 67, 841-847.
- (16) Parfitt, A.D., Ramsbotham, J., Rochester, C.H., *Trans. Faraday Soc.* 1971, 67, 1500-1506.
- (17) Herrmann, M., Boehm, H.P., *Z. anorg. Chem.* 1969, 368, 73.

- (18) Finklea, H.O., Murray, R.W., J. Phys. Chem. 1979, 83, 353-358.
- (19a) Finklea, H.O., Vithanage, R., J. Phys. Chem. 1982, 86, 3621-3626.
- (19b) Finklea, H.O., Vithanage, R., "Chemically Modified TiO<sub>2</sub> Surfaces with Methylsilanes and Characterization by IR Absorption Spectroscopy" Chap. 10 in, Chemically Modified Surfaces in Catalysis and Electrocatalysis, ACS. Symp. Ser. 192, Ed. J.S. Miller, AC, 1981, Wash.
- (20) Hertl, W., J. Phys. Chem. 1968, 72, 1248.
- (21) Hertl, W., J. Phys. Chem. 1968, 72, 3993-3997.
- (22) Hair, M.L., Hertl, W., J. Phys. Chem. 1969, 73, 2372-2378.
- (23) Hertl, W., Hair, M.L.; J. Phys. Chem. 1971, 75, 2181-2185.
- (24) Peri, J.B., J. Phys. Chem. 1966, 70, 2937-2945.
- (25) Little, L.H., "Infrared Spectroscopy of Adsorbed Species", p. 1-21, Academic Press, London, 1966.
- (26) Yolman, M., Yates, D.J.C., J. Phys. Chem. 1959, 63, 183-187.
- (27) Hoffmann, R.W., Brindley, J., J. Phys. Chem. 1961, 65, 443-449.
- (28) Little, L.H., J. Phys. Chem. 1956, 60, 194-198.
- (29) Williams, J.R., "Solar Energy", Rev. Ed., Ann Arbor Science, Michigan, 1977.
- (30) Messel, H., Butler, S.T., Solar Energy, Pergamon Press, Oxford, U.K. 1977.
- (31) Nozik, A.J., Ann. Rev. Phys. Chem. 1978, 29, 189-221.
- (32) Bard, A.J., Faulkner, L.R., "Electrochemical Methods", 1st Ed., John Wiley & Sons, Inc., NY, 1980.
- (33) Hemming, R., Electrochimica Acta, 1980, 25, 77-78.
- (34) Harris, L.A., Wilson, R.H., Ann. Rev. Mater. Sci. 1978, 8, 99-134.
- (35) Gerisher, H., J. Electro. Chem. 1975, 68, 263-274.
- (36) Bolton, J.R., in Chemistry for Energy, Ed. by Tomlinson, M., ACS, Washington, D.C. 1979.

- (37) Nozik, A.J., Phil. Trans. R. Chem. Soc. Lond., A, 1980, 295, 453-470.
- (38a) Bard, A.J., Wrighton M.S., J. Electro. Chem. Soc. 1977, 124, 1706-1710.
- (38b) Gerisher, H., J. Electroanal. Chem. 1977, 82, 133-143.
- (39) Finklea, H.O., Murray R.W., J. Phys. Chem. 1979, 83, 353-358.
- (40) Grushka, E., Ed. "Bonded Phases in Chromatography", Ann Arber Science Pub., Ann Arbor, Michigan, 1974.
- (41) Hercules, D.M., Cox, L.E., Onisick, O., Nichols, A.D., Anal. Chem. 1973, 45, 832.
- (42) Harper, Bruce, Anal. Chem. 1975, 47, 348-351.
- (43) Murray, R.W., Acc. Chem. Res. 1980, 13, 135.
- (44) Oyama, N., Anson, F.C., Anal. Chem. 1980, 52, 1192.
- (45) Moses, P.R., Wier, L., Murray, R.W., Anal. Chem. 1975, 47, 1882-1886.
- (46) Elliott, C.M., Murray, R.W., Anal. Chem. 1976, 48, 1247-1254.
- (47) Moses, P.R., Murray, R.W. JACS, 1976, 98, 7435-7436.
- (48) Lenhard, J.R., Murray, R.W., J. Electroanal. Chem. 1977, 78, 195-210.
- (49) Moses, P.R., Murray, R.W., J. Electroanal. Chem. 1977, 77, 393-399.
- (50) Finklea, H.O., Murray, R.W., J. Phys. Chem. 1979, 83, 353-358.
- (51) Finklea, H.O., Abruna, H., Murray, R.W., "Interfacial processes of energy conversion and synthesis", Ed. M.S. Wrighton, ACS, Washington, D.C., 1980.
- (52) Moses, P.R., Wier, L.M., Lennox, J.C. Finklea, H.O., Lenhard, J.R., Murray, R.W., Anal. Chem. 1978, 50, 576-585.
- (53a) Vithanage, R., Finklea, H.O., submitted for publication.
- (53b) Finklea, H.O., Mott-Schotky, ., J. Electrochem. Soc. 1982, 129, 2003-2008.
- (54) Yoneyama, H., Murao, F., Tamura, H., J. Electroanal. Chem. 1980, 108, 87-96.

- (55) Canfield, D., Parkinson, B.A., JACS, 1981, 103, 1279-1281.
- (56) White, H.S., Abruna, H.D., Bard, A.J., J. Electrochem. Soc. 1982, 129, 265-271.
- (57) Wrighton, M.S., Austin, R.G., Bocarsley, A.B., Bolts, J.M., Hass, O., Legg, K.D., Nadjo, L., Palazzotto, M.S. JACS, 1978, 100, 1602-1603.
- (58a) Legg, K.D., Ellis, A.B., Bolts, J.M., Wrighton, M.S., Proc. Natl. Acad. Sci., U.S.A., 1977, 74, 4116-4120.
- (58b) Wrighton, M.S., Ginley, D.S., Wakzank, P.T., Ellis, A.B., Morse, D.C., Lewis, A., Proc. Acad. Sci., U.S.A., 1975, 72, 1515-1522.
- (58c) Bolts, J.M., Wrighton, M.S., JACS, 1978, 100, 5257-5262.
- (59) Bolts, J.M., Wrighton, M.S., JACS, 1979, 101, 6179-6184.
- (60) Stirn, R.J., Yeh, Y.C.M., Appl. Phys. Lett. 1975, 27, 95-98.
- (61) Parkinson, B.A., Heller, A., Miller, B. Appl. Phys. Lett. 1978, 33, 521.
- (62) Bocarsley, A.B., Walton, E.G., Wrighton, M.S., JACS, 1980, 102, 3390-3398.
- (63) Bookbinder, D.C., Lewis, N.S., Bradley, M.G., Bocarsley, A.B., Wrighton, M.S., JACS, 1979, 101, 7721-7723.
- (64) Bookbinder, D.C., Wrighton, M.S., JACS, 1980, 102, 5123-5125.
- (65) Dominey, R.N., Lewis, N.S., Bruce, J.A., Bookbinder, D.C., Wrighton, M.S., JACS, 1982, 104, 467-482.
- (66) Abruna, H.D., Denisevich, P., Umana, M., Meyers, T.J., Murray, R.W., JACS, 1981, 103, 1-5.
- (67a) Untereker, D.F., Lennox, J.C., Wier, L.M., Moses, P.R., Murray, R.W., J. Electroanal. Chem. 1977, 81, 309-320.
- (68) Ferrer, S., Somarjai, G.A., Surface Sci. 1980, 94, 41-56.
- (69a) Harris, L.A., Wilson, R.H., J. Electrochem. Soc. 1976, 123, 1010-1015.
- (69b) Harris, L.A., Cross, D.R., Gerstner, M.G. J. Electrochem. Soc. 1977, 124, 839.
- (70) Moses, P.R., Wier, L.M., Murray, R.W., Anal. Chem. 1975, 47, 1882-1892.

- (71) Weinberg, N.L., "Techniques of Chemistry", Vol. V, Part I, II. Ed., John Wiley & Sons, NY, 1944.
- (72) Fry, Albert. "Synthetic Organic Electrochemistry", Harper & Row Publishers, NY, 1972.
- (72b) Baizer, M.M., "Organic Electrochemistry", Marcel Dekker, Inc., NY, 1973.
- (73) Teng, F.S., Mahlingan, R., Subramaniam, R.V., Raff, R.A.V., J. Electrochem. Soc. 1977, 124, 995-1006.
- (74) Subramaniam, R.V., pp. 34-56 in "Advances in Polymer Series", Vol. 33, Springer-Verlag, NY, 1979.
- (75) Murray, R.W., ACC. Chem. Res. 1980, 13, 135-141.
- (76a) Abruna, H.D., Denisevich, P., Umana, M., Meyer, T.J., Murray, R.W., JACS, 1980, 103, 1-5.
- (76b) Denisevich, P., Abruna, H.D., Leidner, C.R., Meyer, T.J., Murray, R.W., Inorg. Chem. 1982, 21, 2153-2161.
- (77a) Diaz, A.F., Kanazawa, K.K., Gardini, A.P., JCS. Chem. Comm. 1979, 635-636.
- (77b) Kanazawa, K.K., Diaz, A.F., Geiss, R.H., Gill, W.D. Kwak, J.F., Logan, J.A., J.C.S. Chem. Comm. 1979, 854-855.
- (77c) Diaz, A.F., Castillo, J., J.C.S. Chem. Comm. 1980, 397-398.
- (77d) Diaz, A.F., Vollejo, J.M.V., Duran, A.M., I.B.M. J. Res. Develop. 1981, 25, 42-50.
- (78) Diaz, A.F., Logan, J.A., J. Electroanal. Chem. 1980, 111, 111-114.
- (79) Waltman, R.J., Bargon, J., Diaz, A.F., J. Phys. Chem. 1983, 87, 1459-1463.
- (80) Tourillon, A., Garnier, F., J. Electroanal. Chem. 1982, 135, 173-178.
- (81a) Bruno, F., Pham, M.C., DuBois, J.E., Electrochimica Acta, 1977, 22, 451-457.
- (81b) Pham, M.C., Pierre, C.L., DuBois, J.M., J. Electroanal. Chem. 1978, 86, 147-157.
- (81c) Pham, M.C., Dubois, J.E., Lacaze, P.C., J. Electroanal. Chem. 1979, 99, 331-340.

- (81d) DuBois, J.E., Lacaze, P.C., Pham, M.C., J. Electroanal. Chem. 1981, 117, 233.
- (82) Volkov, A., Tourillon, A., Lacaze, P.C., DuBois, J.E., J. Electroanal. Chem. 1980, 115, 279-291.
- (83a) Pham, M.C., Tourillon, A., Lacaze, P.C., DuBois, J.E., J. Electroanal. Chem. 1980, 111, 385-390.
- (83b) Pham, M.C., DuBois, J.E., Lacaze, P.C., J. Electrochem. Soc. 1983, 130, 346-351.
- (84) Lapowsky, M., Zak, J., Strojak, J.W., J. Electroanal. Chem. 1983, 145, 173.
- (85) Hnil, C.Z., Kova, M., Sommer, L., J. Electroanal. Chem. 1983, 193, 171-174.
- (86) LeBerre, V., Carlier, R., Tallec, A., Simonet, J., J. Electroanal. Chem. 1982, 143, 425-432.
- (87) Landrum, H.L., Salmon, R.T., Hawkridge, F.M., JACS, 1977, 99, 3154-3158.
- (88) Simon, M.S., Moore, P.J., J. Poly. Sci. 1975, 13, 1-17.
- (89) Elliott, C.M., Martin, W.S., J. Electroanal. Chem. 1982, 137, 377-385.
- (90) Shaw, B.R., Haigh, G.P., Falkner, C.R., J. Electroanal. Chem. 1982, 140, 147-153.
- (91) Spiro, T.A., Ghosh, P.K., JACS, 1980, 102, 5543-5549.
- (91b) Ghosh, P.K., Spiro, T.A., J. Electrochem. Soc. 1981, 128, 1281-1287.
- (92) Abruna, H.D., Denisevich, P., Umana, M., Meyer, T.J., Murray, R.W., JACS, 1981, 103, 1-5.
- (93) Willman, K.W., Murray, R.W., J. Electroanal. Chem. 1982, 133, 211-231.
- (94) Denisevich, P., Abruna, H.D., Leidner, C.R., Meyer, T.J., Murray, R.W., Inorg. Chem. 1982, 21, 2153-2161.
- (95) Braddock, J.W., Meyer, T.J., JACS, 1973, 95, 3158-3162.
- (96) Sullivan, B.P., Salmon, D.J., Meyer, T.J., J. Inorg. Chem. 1978, 17, 3334-3341.

- (97) Denisevich, P., Willman, K.W., Murray, R.W., JACS, 1981, 103, 4727-4737.
- (98) Oyama, N., Anson, F.C., J. Electrochem. Soc. 1980, 127, 247-250.
- (99) Finklea, H.U., Vithanage, R.S., "Non-electroactive polymer coatings formed by electrochemical polymerization" accepted for publication (J. Electroanal. Chem.).
- (100) Heinemann, W.R., Wieck, H.J., Yacynych, A.M., Anal. Chem. 1980, 52, 345-346.
- (101) Cheek, A., Wales, C.P., Nowak, R.J., Anal. Chem. 1983, 55, 380-381.
- (102) Bard, A.J., J. Chem. Ed. 1983, 60, 302-304.
- (103a) Kauffmann, F.B., Engler, E.M., JACS, 1979, 101, 547-549.
- (103b) Kauffmann, F.B., Schroeder, A.H., Engler, E.M., Kraner, S.R., Chambers, C.Q., JACS, 1980, 102, 483-488.
- (104) Oyama, N., Anson, F.C., Anal. Chem. 1980, 52, 1192-1198.
- (105) Adams, R.N., "Electrochemistry at Solid Electrodes", Marcel Dekker, Inc., NY, 1969.
- (106) Ikelda, T., Schmehl, R., Denesevich, P., Willman, K., Murray, R.W., JACS, 1982, 104, 2683-2692.

APPENDIX 1

$$\Gamma = \frac{\text{total sample on the surface}}{\text{total surface area}} \left( \frac{\mu\text{moles}}{\text{m}^2} \right)$$

$\Gamma$  = surface concentration.

If the concentration of the sample is  $c$  and total volume of the disc is

$v$

total sample =  $c.v.$  mols  $\text{lt}^{-1} \text{cm}^{-3}$  if the weight of the pellet is  $\omega$  (in grams) and the surface area of the powder is " $a$ " (in  $\text{m}^2/\text{g}$ )

total surface area =  $\omega.a.$  ( $\text{m}^2$ )

$$\therefore \Gamma = \frac{C (\text{mol lt}^{-1}) V (\text{cm}^3)}{a (\text{m}^2 \text{g}^{-1}) \omega (\text{g})} \quad (1)$$

if the adsorbed sample obeys Beers' Law

$$A = \epsilon . c . d . \quad (2)$$

$d$  = thickness

Volume of the pellet

$$V = \pi r^2 d \quad (3)$$

Substitute (2) and (3) into (1)

$$\therefore \Gamma = \frac{C . \pi r^2 d}{a . \omega} \frac{\text{mol lt}^{-1} \text{cm}^3}{\text{m}^2}$$



$$\therefore \Gamma = \left(\frac{A}{\epsilon}\right) \cdot \frac{\pi r^2}{W \cdot a} \frac{\text{mol lt}^{-1} \text{ cm}^3}{\text{m}^2} \quad (4)$$

$$\Gamma = \left(\frac{A}{\epsilon}\right) \frac{\pi r^2}{W \cdot a} \cdot \frac{\text{mol}}{10^3} \cdot \frac{\text{cm}^{-3} \cdot \text{cm}^3}{\text{m}^2}$$

$$= 10^3 \left(\frac{A}{\epsilon}\right) \frac{\pi r}{W \cdot a} \mu\text{mol m}^{-2} .$$

**The vita has been removed from  
the scanned document**